Pergamon

Chemical Engineering Science, Vol. 52, No. 6, pp. 861–911, 1997

0009–2509/97 $17.00 + 0.00

PII: S0009–2509(96)00458–7

REVIEW ARTICLE NUMBER 50

The Maxwell–Stefan approach to mass transfer

R. Krishna*,† and J. A. Wesselingh‡

†Department of Chemical Engineering, University of Amsterdam, Nieuwe Achtergracht 166, 1018 WV Amsterdam, The Netherlands; ‡Department of Chemical Engineering, University of Groningen, Nijenborgh 4, 9747 AG Groningen, The Netherlands

(Received 7 May 1996; in revised form 27 September 1996; accepted 4 October 1996)

Abstract—The limitations of the Fick's law for describing diffusion are discussed. It is argued that the Maxwell–Stefan formulation provides the most general, and convenient, approach for describing mass transport which takes proper account of thermodynamic non-idealities and influence of external force fields. Furthermore, the Maxwell–Stefan approach can be extended to handle diffusion in macro- and microporous catalysts, adsorbents and membranes. © 1997 Elsevier Science Ltd. All rights reserved

Keywords: Multicomponent diffusion; porous media; membrane separations; Fick's law; ionic diffusion; zeolities.

CONTENTS

* Corresponding author. Fax: + 31 20 5255604; e-mail: krishna@chemeng.chem.uva.nl.

INTRODUCTION

Chemical engineers need to describe diffusion within fluid phases, across phase interfaces, within gels, porous catalysts and adsorbents, and across porous membranes; see Fig. 1. As portrayed in Fig. 2, a variety of species transport mechanisms are involved: bulk gas diffusion, bulk liquid diffusion, Knudsen diffusion inside pores, solid-phase diffusion and diffusion inside pores of molecular dimensions (Xiao and Wei, 1992). Traditionally chemical engineers have developed their design procedures for separation and

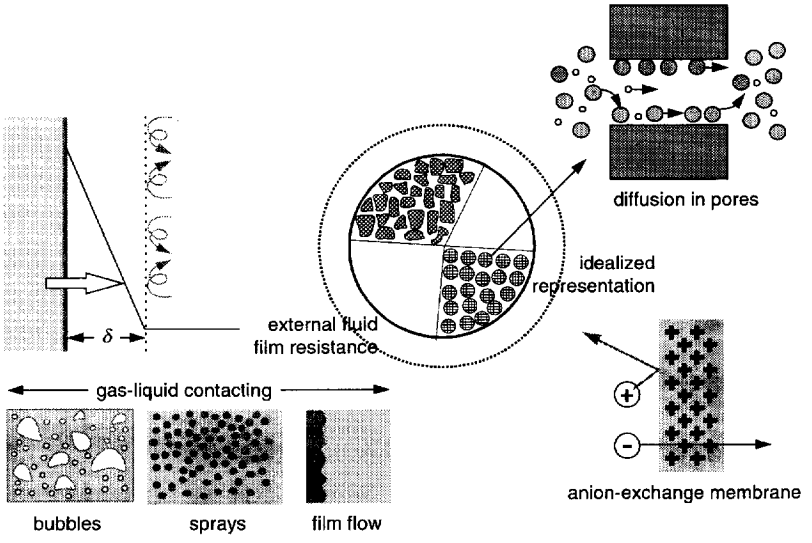

Fig. 1. Typical mass transfer situations.

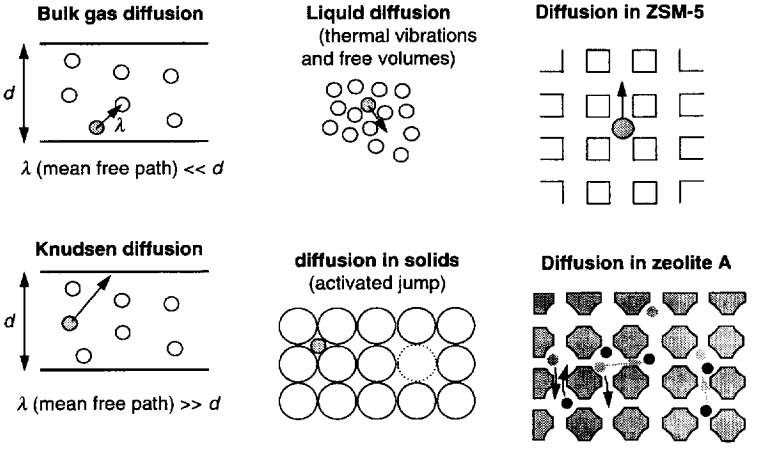

Fig. 2. Various diffusion mechanisms. Adapted from Xiao and Wei (1992).

reaction equipment using Fick's law of diffusion as a basis. Fick's law postulates a linear dependence of the flux $\mathbf{J}_i$, with respect to the molar average mixture velocity $\mathbf{u}$, and its composition gradient ∇x_i:

$$\mathbf{J}_i \equiv c_i(\mathbf{u}_i - \mathbf{u}) = -c_i D_i \nabla x_i. \tag{1}$$

The molar flux $\mathbf{N}_i$ with respect to a laboratory-fixed coordinate reference frame is given by

$$\mathbf{N}_i \equiv c_i \mathbf{u}_i = ctx_i \mathbf{u}_i = \mathbf{J}_i + x_i \mathbf{N}_t = -c_t D_i \nabla x_i + x_i \mathbf{N}_t,$$

$$\mathbf{N}_t = \sum_{i=1}^{n} N_i. \tag{2}$$

The constitutive relation (1) is strictly valid only under the following set of conditions: (i) for binary mixtures or (ii) for diffusion of dilute species i in a multicomponent mixture, and (iii) in the absence of electrostatic or centrifugal force fields. If one takes the view that eq. (1) provides a definition of the effective Fick diffusivity of component i in a multicomponent mixture, then this parameter shows a complicated, often unpredictable, behaviour; this is illustrated by means of four examples.

Diffusion in an ideal ternary gas mixture

Let us first consider a simple and illuminating set of experiments conducted by Duncan and Toor (1962). These authors examined diffusion in an ideal ternary gas mixture hydrogen (1)–nitrogen (2)–carbon dioxide (3). The experimental set-up consisted of two-bulb diffusion cells, pictured in Fig. 3. In an experiment that we shall highlight here the two bulbs, bulb 1 and bulb 2, had the initial compositions (mole fractions) given below:

$$\begin{aligned} &\text{Bulb 1:} \quad x_1 = 0.00000, \quad x_2 = 0.50086, \quad x_3 = 0.49914 \\ &\text{Bulb 2:} \quad x_1 = 0.50121, \quad x_2 = 0.49879, \quad x_3 = 0.00000. \end{aligned} \tag{3}$$

The two bulbs were connected by means of a 86 mm long capillary tube. At time $t = 0$, the stopcock separating the two composition environments at the centre of the capillary was opened and diffusion of the three species was allowed to take place. From the information given in the paper by Duncan and Toor it is verifiable that the diffusion in the capillary is in the bulk diffusion regime. Further, the pressure differences between the two bulbs are negligibly small implying the absence of viscous flow. Since the two bulbs are sealed there is no net transfer flux out of or into the system, i.e. we have conditions corresponding to equimolar diffusion:

$$\mathbf{u} = 0, \quad \mathbf{N}_1 + \mathbf{N}_2 + \mathbf{N}_3 = 0. \tag{4}$$

The composition–time trajectories for each of the three diffusing species in either bulb has been presented in Fig. 3. Let us first examine what happens to hydrogen (1) and carbon dioxide (3). The composition–time trajectories are as we should expect; hydrogen diffuses from bulb 2 to bulb 1 and the two compositions approach each other, albeit slowly. Carbon dioxide diffuses from bulb 1 to bulb 2 in the expected normal fashion. The diffusion behaviour of these two species hydrogen and carbon dioxide may be termed to be Fickian, i.e. down their respective composition gradients; there is nothing extraordinary here.

If we examine the composition–time trajectory of nitrogen (2) we see several curious phenomena. Initially, the compositions of nitrogen in the two bulbs are almost identical and therefore at this point the composition gradient driving force for nitrogen must vanish. However, it was observed experimentally by Duncan and Toor that the diffusion of nitrogen does take place decreasing the composition of bulb 1 at the expense of bulb 2; this is contrary to the Fickian expectations for we have

$$\nabla x_2 = 0, \quad \mathbf{J}_2 \neq 0, \quad t \approx 0. \tag{5}$$

The bulb 1 composition continues to decrease at the expense of bulb 2 composition of nitrogen between $t = 0$ and $t = t_1$; this diffusion of nitrogen is in an up-hill direction, i.e.

$$\frac{\mathbf{J}_2}{-\nabla x_2} < 0, \qquad 0 < t < t_1. \tag{6}$$

Up-hill diffusion of nitrogen continued to take place until the time $t = t_1$ is reached when the composition profiles in either bulb tend to plateau. This plateau implies that the diffusion flux of nitrogen is zero at this point despite the fact that there is a large driving

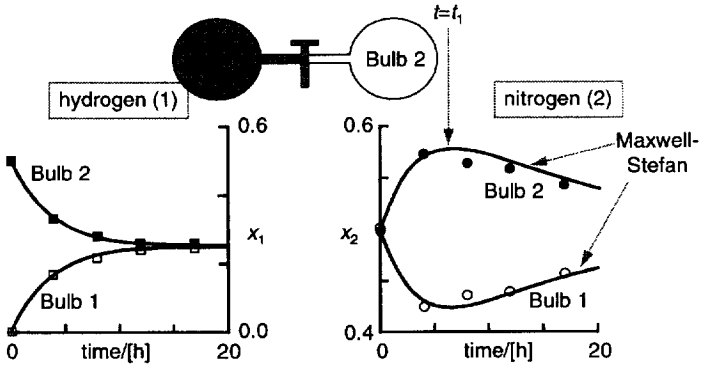

Fig. 3. The two-bulb diffusion experiment with the system hydrogen (1)–nitrogen (2)–carbon dioxide (3). Adapted from Duncan and Toor (1962) and Taylor and Krishna (1993).

force existing. At $t = t_1$ we have

$$\nabla x_2 \neq 0, \quad \mathbf{J}_2 = 0, \quad t = t_1. \tag{7}$$

Beyond the point $t = t_1$, the diffusion behaviour of nitrogen is 'normal', i.e. the composition of nitrogen in bulb 2 with a higher concentration decreases while the composition of nitrogen in bulb 1 with the lower concentration increases.

Toor (1957) in a classic paper had anticipated these curious phenomena and assigned the following names to them:

Osmotic diffusion: This is the phenomenon observed at $t = 0$ and described by eq. (5), namely diffusion of a component despite the absence of a driving force.

Reverse diffusion: This phenomenon is observed for nitrogen in the time interval $0 < t < t_1$ and described by eq. (6): diffusion of a component in a direction opposite to that dictated by its driving force.

Diffusion barrier: This phenomenon is observed at $t = t_1$ and is described by eq. (7): here a component diffusion flux is zero despite a large driving force.

The above three phenomena are pictorially represented in Fig. 4, which sharply contrasts the diffusion behaviour of a binary mixture from a ternary mixture.

It should be clear that the use of the Fick formulation, eq. (1), will be totally inadequate to describe these anomalies described above because in order to rationalize the experimental observations we must demand the following behaviour of the Fick diffusivity for nitrogen:

- $D_2 \to \infty$ at the osmotic diffusion point; cf. eq. (5)
- $D_2 < 0$ in the region where reverse diffusion occurs, cf. eq. (6) and
- $D_2 = 0$ at the diffusion barrier; cf. eq. (7).

It must be emphasized that this strange behaviour of the Fick diffusivity for nitrogen has been observed experimentally for an *ideal gas mixture* at constant temperature and pressure conditions and for a situation corresponding to *equimolar diffusion*.

Diffusion in mixed ion system

Let us now consider diffusion of ionic species. Vinograd and McBain (1941) investigated the diffusion of electrolytes and using a two-compartment diffusion cell, shown schematically in Fig. 5. The top compartment contained pure water while the bottom one contained an aqueous electrolyte solution. Diffusion takes place through the pores of a sintered glass disk that separated the two compartments. In one set of experiments the top compartment contained an aqueous solution of HCl and $BaCl_2$, the composition of which was varied. On complete ionization the mixture consists of the ionic species H^+, Cl^-, Ba^{2+} and unionized H_2O. By monitoring the concentrations of the three ionic species as a function of time, Vinograd and McBain obtained the effective ionic diffusivities D_i for H^+, Cl^- and Ba^{2+}. The experimentally observed ionic diffusivities are shown in Fig. 5 as function of the square root of the ratio of the initial ionic concentrations of H^+ and Ba^{2+} in the top compartment $\sqrt{c_{H^+}/c_{Ba^{2+}}}$. With increasing values of $\sqrt{c_{H^+}/c_{Ba^{2+}}}$, it is observed that both D_{H^+} and $D_{Ba^{2+}}$ decrease while D_{Cl^-} increases. During the start of the diffusion process, the highly mobile H^+ diffuses ahead of its companion ions into the pure water compartment, creating an excess of positive charge. This induces an electrical potential which acts in such a way as to maintain electro-neutrality. The consequence of this is that the Cl^- experiences an extra electrostatic 'pull', enhancing its effective diffusivity value. The electrical potential gradient also serves to retard the motion of the positive ions H^+ and Ba^{2+} or in other words these ions experience a 'push' in a direction opposite to that dictated by their composition gradient driving forces. For $\sqrt{c_{H^+}/c_{Ba^{2+}}} = 2$ the electrostatic 'push' on Ba^{2+} is such as to result in a vanishing value for $D_{Ba^{2+}}$. For $\sqrt{c_{H^+}/c_{Ba^{2+}}} > 2$, negative values of $D_{Ba^{2+}}$ can be expected, as predicted by simplified Maxwell–Stefan diffusion model to be discussed later. The Fick diffusivity concept breaks down for describing transport of individual ionic species.

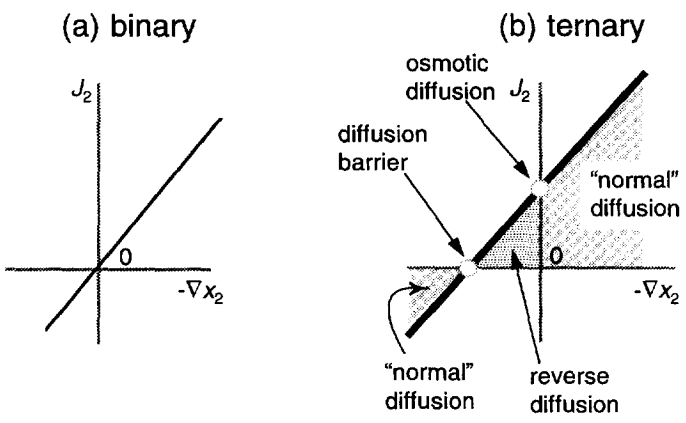

Fig. 4. The diffusion flux as a function of the composition gradient for (a) binary system and (b) ternary system. Adapted from Taylor and Krishna (1993).

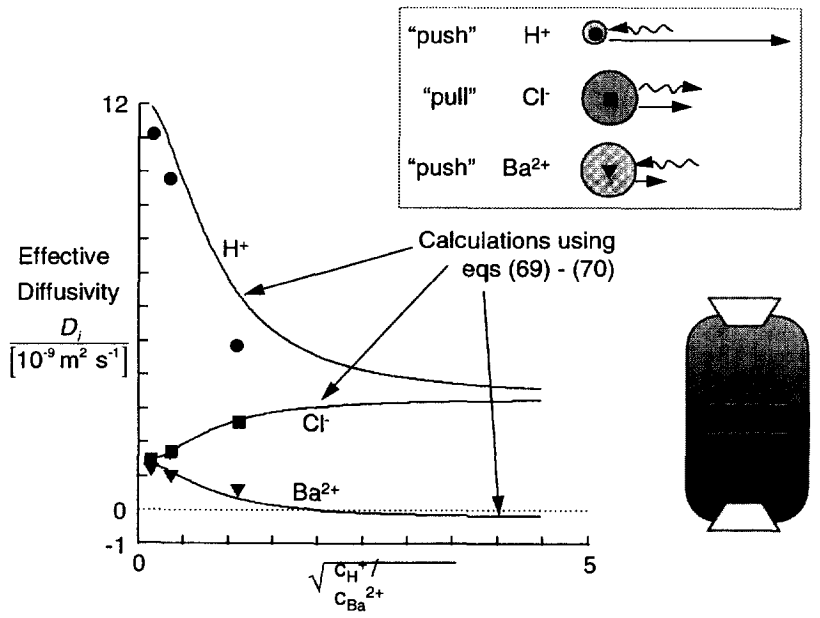

Fig. 5. Effective ionic diffusivity in the mixed ion system. Data from Vinograd and McBain (1941). Adapted from Taylor and Krishna (1993)

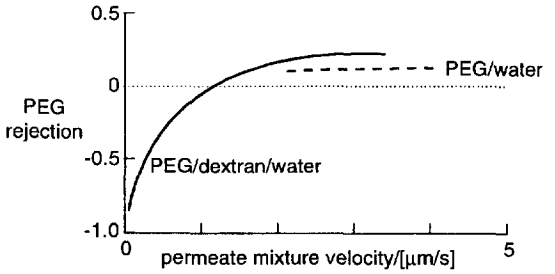

Fig. 6. Polyethylene glycol (PEG) rejection from PEG/water and PEG/dextran/water solutions. Adapted from Van Oers (1994).

Ultrafiltration of an aqueous solution of polyethylene glycol and dextran

Let us look at a study by Van Oers (1994) of the ultrafiltration of polyethylene glycol (PEG)/water mixtures in the presence of varying concentration of dextran; see Fig. 6. In the absence of dextran the rejection of PEG, defined on a dextran-free concentration basis, is always positive and practically constant. Addition of dextran to the solution influences the rejection of PEG significantly and negative rejections are observed! Negative values for the rejection imply that the permeate concentration is larger than the bulk concentration. Clearly, the mutual interaction of dextran and PEG needs to be accounted for in the modelling of membrane transport.

Transport of n-butane and hydrogen across zeolite membrane

As the last example demonstrating the inadequacy of the Fick constitutive relation (1), let us consider diffusion of a mixture of *n*-butane and hydrogen across a silicalite-1 membrane separating two well-mixed compartments (Kapteijn *et al.*, 1995). Figure 7(a) presents the development of single-component fluxes of hydrogen and *n*-butane at room temperature at 95 and 5 kPa partial pressure, respectively, as a function of time upon switching the feed gas from helium to the feed mixture. Figure 7(b) contains the results of a 95 : 5 feed mixture. In the single-component experiments the steady-state hydrogen permeation flux is about 20 times larger than that of the *n*-butane at the applied conditions, whereas in the binary experiments the hydrogen flux drops by a factor of more than a 100 while the *n*-butane flux remained unaltered. In the binary experiments hydrogen permeates first and appears at the same time as in the single-component experiment, but then drops quickly and reaches its final, low value as the *n*-butane appears. An *n*-butane selectivity of more than 100 over hydrogen is found (Kapteijn *et al.*, 1995). The selectivity-reversal phenomena when moving from single component to binary mixtures cannot be simply modelled on the basis of eq. (1).

The four examples presented above serve to underline the shortcomings of the Fick constitutive relation (1). It is clearly necessary to adopt a more general constitutive relation. The essential concepts behind such a general constitutive relation were already available more than a century ago following the pioneering works of James Clerk Maxwell (1866) and Josef Stefan (1871). Maxwell preceded Stefan in his analysis of multicomponent diffusion and the formulation should properly be termed the Maxwell–Stefan instead of Stefan–Maxwell formulation as it is sometimes referred to in the literature (see e.g. Lightfoot,

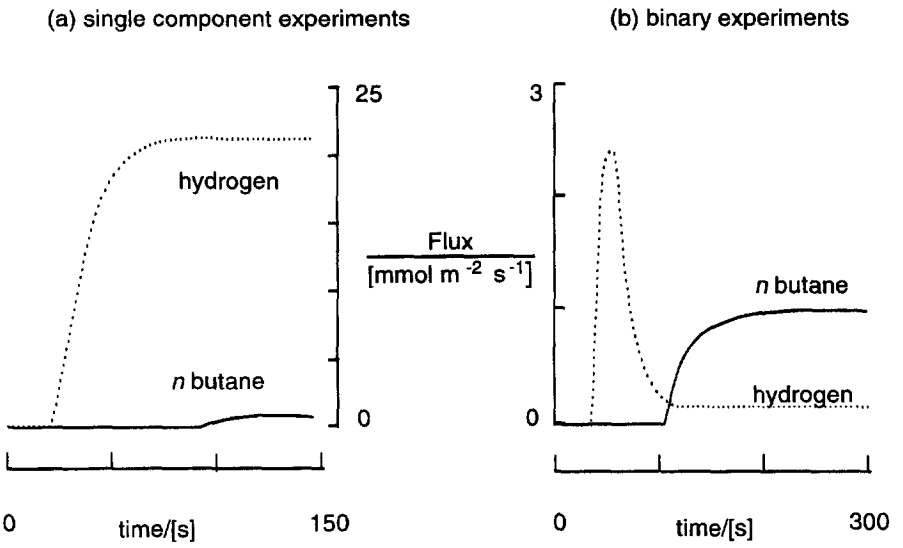

Fig. 7. Transport of n-butane and hydrogen across a silicalite membrane on stainless steel support; adapted from Kapteijn *et al.* (1995). (a) Single-component permeation fluxes for hydrogen (95 kPa upstream partial pressure) and n-butane (5 kPa). (b) Transient permeation flux development for a mixture of hydrogen (95 kPa) and n-butane (5 kPa). The downstream pressure was maintainted at $p_\delta = 100$ kPa and a sweep gas was used. The membrane thickness was $\delta = 40$ μm. The temperature was maintained at 300 K.

1974). It is interesting to note that Stefan was aware of Maxwell's work but apparently found it difficult to follow (*Das Studium der Maxwell'schen Abhandlung ist nicht leicht*)!

In this paper the Maxwell–Stefan diffusion formulation is developed and its superiority to the Fick formulation underlined with the aid of several examples.

ISOTHERMAL DIFFUSION WITHIN AND ACROSS BULK FLUID PHASES

Diffusion in binary mixtures

Before proceeding to the general multicomponent case, let us start with a simple two-component system, made up of species denoted by 1 and 2. To effect relative motion between the molecular species 1 and 2 in the mixture we must exert a force on each of the two species. To calculate this force that is exerted on any molecular species i, let us consider z-directional diffusion in the system and write down the force balances for the control volume shown in Fig. 8. The cross-sectional area available for diffusion is 1 m^2 and the length of the diffusion path is dz. If the change in the partial pressure of component i across the diffusion distance dz is $-\mathrm{d}p_i$, the force acting per m^3 is $-\mathrm{d}p_i/\mathrm{d}z$. The concentration of species i in the mixture is c_i and therefore the force acting per mole of species i is $(1/c_i)(-\mathrm{d}p_i/\mathrm{d}z)$. For an ideal gas mixture we have $c_i = p_i/RT$ and therefore the force per mole of species i can be written as $(RT/p_i)\ (-\mathrm{d}p_i/\mathrm{d}z) = RT\ (-\mathrm{d}\ln p_i/\mathrm{d}z)$ or expressed in terms of the chemical potential gradient, at constant temperature and pressure, of species i, this force is $-\mathrm{d}\mu_i/\mathrm{d}z$. This force is balanced by friction between the diffusing species 1 and 2 in the binary mixture; see the pictorial representation in Fig. 9. The force balance on the species 1 takes the form

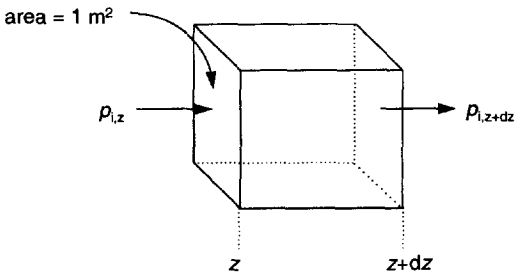

Fig. 8. A simple force balance on a control volume containing an ideal gas mixture.

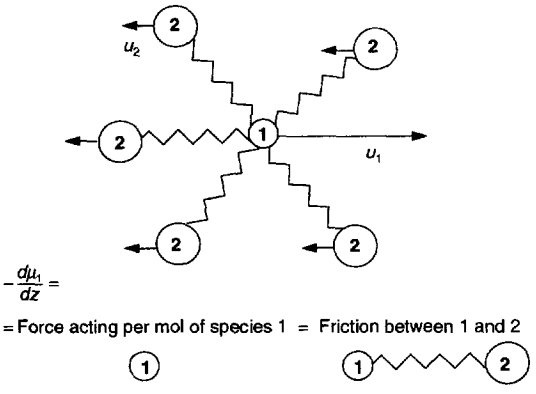

Fig. 9. Relative motion between species 1 and 2 is caused by exertion of a force on each of the species. This force is balanced by inter-species friction.

$$-\frac{\mathrm{d}\mu_1}{\mathrm{d}z} = \frac{RT}{Đ}x_2(u_1 - u_2). \tag{8}$$

For transport of species 1 in the positive z direction, i.e. positive velocity u_1, we must have a positive value for $(-\mathrm{d}\mu_1/\mathrm{d}z)$ and therefore the left member of eq. (8) must be viewed as the driving force for transport in the positive z-direction. This force is balanced by the friction experienced between the species 1 and 2. We may expect that the frictional drag will be proportional to the velocity difference $(u_1 - u_2)$ and to the concentration of the mixture, expressed in eq. (8) as the mole fraction of component 2, x_2. The term $RT/Đ$ on the right-hand side of eq. (8) may be interpreted to be the drag coefficient. With this definition, the Maxwell–Stefan diffusivity $Đ$ has the units $(\mathrm{m^2\,s^{-1}})$ and the physical significance of an *inverse* drag coefficient.

Multiplying both sides of eq. (8) by x_1/RT we get

$$-\frac{x_1}{RT}\frac{\mathrm{d}\mu_1}{\mathrm{d}z} = \frac{x_1x_2u_1 - x_1x_2u_2}{Đ}. \tag{9}$$

Rearranging eq. (9) using the definition for the fluxes $N_1 = \mathrm{c_t}x_1u_1$ [cf. eq. (2)] we obtain after vector generalization

$$-\frac{x_1}{RT}\nabla_{T,p}\mu_1 = \frac{x_2\mathbf{N}_1 - x_1\mathbf{N}_2}{c_tĐ}. \tag{10}$$

For a non-ideal fluid mixture we may introduce the component activity coefficients to express the left member of eq. (10) as

$$-\frac{x_1}{RT}\nabla_{T,p}\mu_1 = -\left(1 + x_1\frac{\partial \ln\gamma_1}{\partial x_1}\right)\nabla x_1 = -\Gamma\nabla x_1 \tag{11}$$

where Γ is the thermodynamic correction factor portraying the non-ideal behaviour. For highly non-ideal mixtures the thermodynamic factor Γ is usually a strong function of the mixture composition and vanishes in the region of the critical point. This behaviour has been illustrated in Fig. 10 for the system methanol (1)–*n*-hexane (2). For the temperature under consideration the system tends to undergo phase splitting at $x_1 \approx 0.5$; at this mole fraction we note that Γ tends to vanishingly low values. Combining eqs (2), (10) and (11) after introducing $x_2 = (1 - x_1)$ we obtain

$$\mathbf{J}_1 \equiv \mathbf{N}_1 - x_1\mathbf{N}_t = -c_tĐ\Gamma\nabla x_1. \tag{12}$$

Comparison of eq. (12) with Fick's law, eq. (1) applied to the binary system of 1 and 2 yields the following relationship between the Fick diffusivity D and the Maxwell–Stefan diffusivity $Đ$:

$$D = Đ\Gamma. \tag{13}$$

For gaseous mixtures at low to moderate pressures and for thermodynamically ideal liquid mixtures, the thermodynamic factor $\Gamma = 1$ and, furthermore, the Maxwell–Stefan diffusivity is independent of composition; for this limiting case the Fick and Maxwell–Stefan diffusivity are identical to each other. The Maxwell–Stefan diffusivity has the physical significance of an inverse drag coefficient and is more easily interpretable and predictable than the Fick diffusivity; the latter parameter is a conglomerate of two separate concepts: drag effects and thermodynamic non-ideality effects.

For highly non-ideal liquid mixtures, because of the strong composition dependence of the thermodynamic factor Γ, we should expect the Fick diffusivity to also exhibit a corresponding strong composition dependence; this is indeed borne out by experimental evidence available in the literature and is illustrated in Fig. 11 for the system methanol (1)–*n*-hexane for which we note that the Fick diffusivity tends to approach zero in the region of the phase transition point near $x_1 \approx 0.5$ (Clark and Rowley, 1986). The Maxwell–Stefan diffusivity, calculated from the Fick diffusivity and thermodynamic data, shows only a mild composition dependence. An empirical formula for the composition dependence is due to Vignes (1966):

$$Đ = (Đ_{(x_1\to 1)})^{x_1}(Đ_{(x_1\to 0)})^{1-x_1} \tag{14}$$

where the bracketed terms are, respectively, the infinite dilution values of the Maxwell–Stefan diffusivity at either ends of the composition range. The Vignes relation (14) implies that the logarithm of $Đ$ should be linear in the mole fraction x_1. From the data in Fig. 11

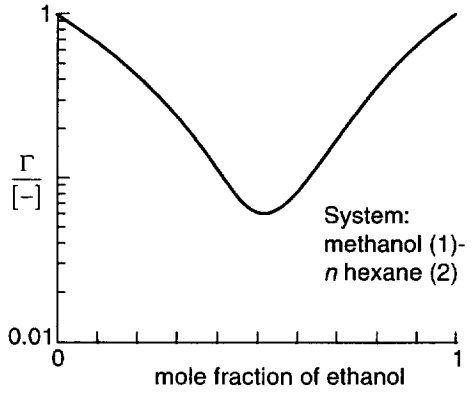

Fig. 10. Thermodynamic factor for the system methanol–*n*-hexane. Adapted from Taylor and Krishna (1993).

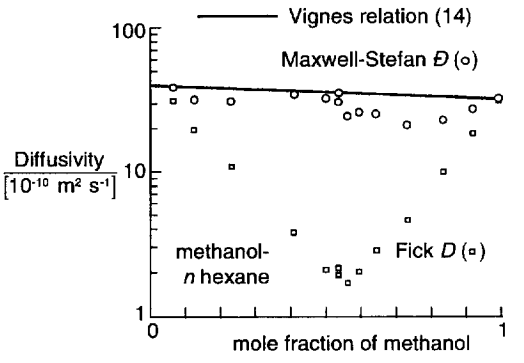

Fig. 11. Experimental data for the Fick and Maxwell–Stefan diffusivity for the system methanol–*n*-hexane. Data from Clark and Rowley (1986).

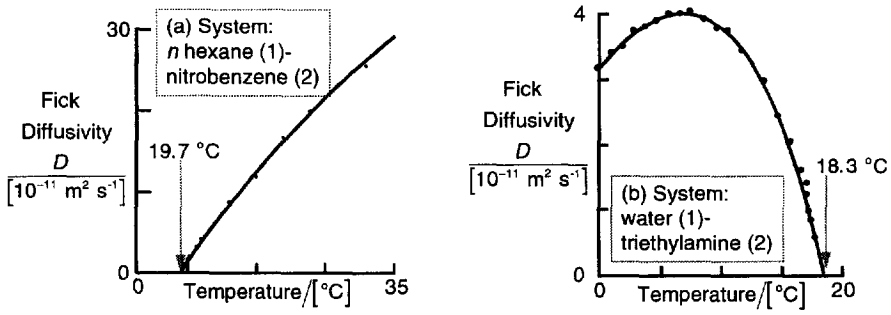

Fig. 12. Fick diffusivity as a function of temperature tends to vanish as the (a) upper and (b) lower critical solution temperature is approached. Data from Haase and Siry (1968).

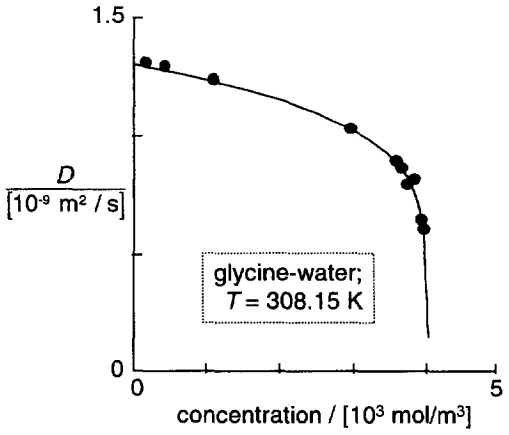

Fig. 13. Fick diffusivity for the system glycine–water as a function of concentration. Data from Chang and Myerson (1986).

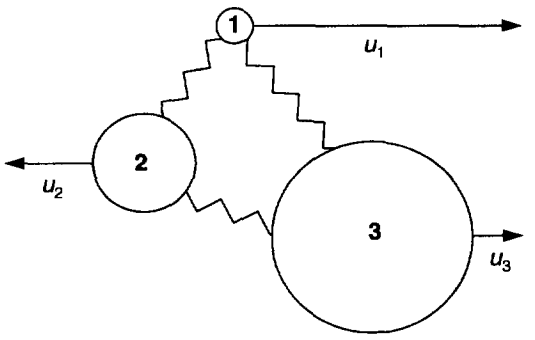

Fig. 14. The Maxwell–Stefan diffusion equations for ternary mixtures. The force exerted on 1 is balanced by friction between species 1 and 2 and the friction between species 1 and 3.

we see that this empirical model of Vignes holds remarkably well, considering the large variation of the Fick diffusivity. For further information regarding the prediction of the Maxwell–Stefan diffusivity for gaseous and liquid mixtures the reader is referred to Taylor and Krishna (1993) and Wesselingh and Krishna (1990).

Binary liquid mixtures are thermodynamically stable provided $\partial\mu_i/\partial x_1 > 0$ and the thermodynamic stability bounds are given by the spinodal curve for which $\partial\mu_i/\partial x_1 = 0$. From eqs (11) and (13) we may see that the Fick diffusivity $D = 0$ at the spinodal curve. The only points of this curve that are accessible to experiment are critical (consolute) points. Experimental data for water–triethylamine and *n*-hexane–nitrobenzene do indeed show that the Fick D vanishes as the critical solution temperatures are approached (Haase and Siry, 1968; Pertler *et al.*, 1996); see Fig. 12. The diffusivity of glycine in water plummets to vanishingly low values as supersaturation concentration values are reached (Chang and Myerson, 1986); see Fig. 13. A lucid discussion on diffusion near critical or consolute points is given by Cussler (1984). The proper driving force for the description of crystallization kinetics is the chemical potential difference between the supersaturated solution (the transferring state) and the crystal (the transferred state) and Garside (1985) has shown that this difference can be simply related to the more commonly used 'supersaturation' driving force.

Generalization to multicomponent mixtures

The mechanistic picture developed above for diffusion in a two-component system can be extended to the general multicomponent cases quite easily. The force exerted on species 1 is balanced by the friction between species 1 and each of the other species in the mixture, pictured in Fig. 14 for a ternary mixture. The generalization of eq. (8) for multicomponent mixtures is thus

$$-\frac{d\mu_1}{dz} = RTx_2\frac{(u_1-u_2)}{Đ_{12}} + RTx_3\frac{(u_1-u_3)}{Đ_{13}} + RTx_4\frac{(u_1-u_4)}{Đ_{14}} + \cdots . \quad (15)$$

The terms on the right-hand side of eq. (15) represent, respectively, the friction between 1–2, 1–3, 1–4 and so on. Expressed in vector notation, eq. (15) is

$$-\nabla_T\mu_i = RT\sum_{\substack{j=1\\ j\neq 1}}^{n}\frac{x_j(\mathbf{u}_i-\mathbf{u}_j)}{Đ_{ij}}, \quad i = 1,2,\ldots,n. \quad (16)$$

By multiplying both sides of eq. (16) by x_i/RT and introducing the definition of the molar fluxes $\mathbf{N}_i$ [cf. eq. (2)] we obtain the following equation, analogous to eq. (9), for the binary case:

$$-\frac{x_i}{RT}\nabla_T\mu_i = \sum_{\substack{j=1\\ j\neq 1}}^{n} \frac{x_j\mathbf{N}_i - x_i\mathbf{N}_j}{c_t\mathcal{D}_{ij}}$$

$$= \sum_{\substack{j=1\\ j\neq 1}}^{n} \frac{x_j\mathbf{J}_i - x_i\mathbf{J}_j}{c_t\mathcal{D}_{ij}}, \quad i = 1,2,\ldots,n, \tag{17}$$

where the second equality holds irrespective of the reference velocity frame chosen for the diffusion process. Let us define a quantity $\mathbf{d}_i$:

$$\mathbf{d}_i \equiv -\frac{x_i}{RT}\nabla_T\mu_i. \tag{18}$$

We note that $c_tRT\mathbf{d}_i$ is the force acting per volume of the mixture and that $(\mathbf{d}_i/x_i)$ is the force acting per mole of component i. Only $n-1$ of the eqs (17) are independent because of the Gibbs–Duhem restriction

$$\sum_{i=1}^{n} c_i\nabla_T\mu_i = \nabla p. \tag{19}$$

Constraints imposed by the second law

The occurrence of the phenomena of reverse or uphill diffusion observed in the experiments of Duncan and Toor (1962) is not in violation of the second law of thermodynamics; the second law requires that the total rate of entropy produced by all diffusing species should be positive-definite (Standart *et al.*, 1979):

$$\sigma = (1/T)\sum_{i=1}^{n} \mathbf{J}_i\cdot(-\nabla_T\mu_i) \geqslant 0 \tag{20}$$

which for ideal gas mixtures simplifies to

$$\sigma = R\sum_{i=1}^{n} \mathbf{J}_i\cdot(-\nabla x_i/x_i) \geqslant 0 \quad \text{(ideal gas mixtures)}. \tag{21}$$

Equation (21) allows a component k in the multicomponent mixture to consume entropy by undergoing uphill diffusion, i.e. $\mathbf{J}_k/(-\nabla x_k) < 0$, provided the other components produce entropy at such a rate that the overall rate of entropy production σ remains positive definite. Put another way, the other components ($i \neq k$) pump component k uphill.

Insertion of the Maxwell–Stefan diffusion (16) into eq. (20) we obtain on re-arrangement (Standart *et al.*, 1979)

$$\sigma = \frac{1}{2}c_tR\sum_{i=1}^{n}\sum_{j=1}^{n}\frac{x_ix_j}{\mathcal{D}_{ij}}|\mathbf{u}_i - \mathbf{u}_j|^2 \geqslant 0. \tag{22}$$

For mixtures of ideal gases for which the $\mathcal{D}_{ij}$ are independent of composition the positive-definite condition (22) can only be satisfied if

$$\mathcal{D}_{ij} \geqslant 0 \quad \text{(ideal gas mixtures)}. \tag{23}$$

Equation (23) was first derived by Hirschfelder *et al.* (1964). For non-ideal liquid mixtures the $\mathcal{D}_{ij}$ are composition dependent in general and a result analogous to eq. (23) cannot be derived.

Generalized Fick's law

It is helpful to express the left member of eq. (17) in terms of the mole fraction gradients by introducing an $(n-1)\times(n-1)$ matrix of thermodynamic factors $[\Gamma]$:

$$\frac{x_i}{RT}\nabla_T\mu_i = \sum_{j=1}^{n-1}\Gamma_{ij}\nabla x_j, \quad \Gamma_{ij} = \delta_{ij} + x_i\frac{\partial\ln\gamma_i}{\partial x_j},$$

$$i,j = 1,2,\ldots,n-1. \tag{24}$$

Combining eqs (17) and (24) we obtain the multicomponent analog of eq. (12),

$$-c_t[\Gamma](\nabla x) = [B](\mathbf{J}) \text{ or } (\mathbf{J}) = -c_t[B]^{-1}[\Gamma](\nabla x) \tag{25}$$

where we use $(n-1)$-dimensional matrix notation; $(\mathbf{J})$ represents the column vector of $(n-1)$ diffusion fluxes defined by the first equality in eq. (1). The elements of the matrix $[B]$ can be derived from eq. (17) in terms of the Maxwell–Stefan diffusivities $\mathcal{D}_{ij}$ as follows:

$$B_{ii} = \frac{x_i}{\mathcal{D}_{in}} + \sum_{\substack{k=1\\ k\neq i}}^{n}\frac{x_k}{\mathcal{D}_{ik}}, \quad B_{ij(i\neq j)} = -x_i\left(\frac{1}{\mathcal{D}_{ij}} - \frac{1}{\mathcal{D}_{in}}\right),$$

$$i,j = 1,2,\ldots,n-1. \tag{26}$$

It is common to define a matrix of Fick diffusivities $[D]$ analogous to the binary case [cf. eqs (1) and (12)] by using $(n-1)\times(n-1)$ matrix notation:

$$[D] = [B]^{-1}[\Gamma]. \tag{27}$$

For the general multicomponent mixture it is difficult to ascribe simple physical interpretations to the elements of $[D]$; it is for this reason we prefer the Maxwell–Stefan formulation that also aids in the prediction of the elements of $[D]$. Specifically, the advantage of the M–S formulation is that the we decouple the drag effects (portrayed by $[B]$) from thermodynamic effects (portrayed by $[\Gamma]$). Comparing eq. (25) with eq. (27) we see

$$(\mathbf{J}) = -c_t[D](\nabla x) \tag{28}$$

which is the proper generalization of the Fick formulation (1) to multicomponent mixtures. There are a few limiting cases in which the use of the simplified formulation (1) with a constant value for the effective Fick diffusivity D_i is justified; these are discussed below.

Limiting and special cases

When (i) the binary pair Maxwell–Stefan diffusivities $\mathcal{D}_{ij}$ are equal to one another ($=\mathcal{D}$) and (ii) the mixture is thermodynamically ideal, i.e. $\Gamma_{ij} = 1$, we obtain the simplification

$$\mathbf{J}_i = -c_t\mathcal{D}\nabla x_i \quad (\mathcal{D}_{ij} = \mathcal{D}, \quad \Gamma_{ij} = 1) \tag{29}$$

and each of the species in the mixture has the same transfer mobility.

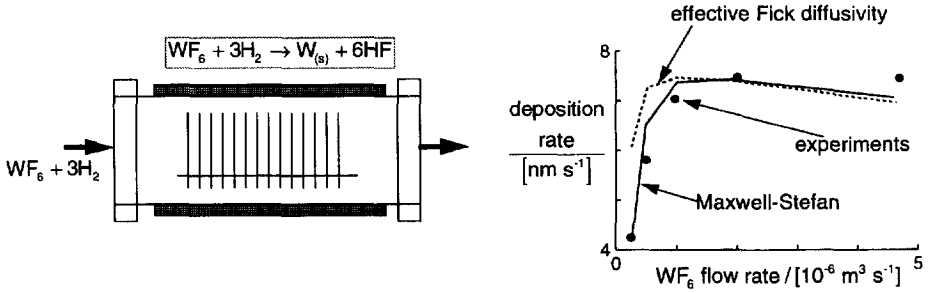

Fig. 15. Comparison of the chemical vapour deposition rate predicted by the Maxwell–Stefan and effective Fick diffusivity formulations with experimental data. Adapted from Kuijlaars (1996).

When the components $1, 2, 3, \ldots, n-1$ are all present in small amounts in excess of a 'solvent' species n (i.e. $x_i \to 0$, $x_n \to 1$), we see from eqs (24) and (26) that $\Gamma_{ij} = 1$ and $B_{ij} = 1/Đ_{in}$ and therefore eq. (28) collapses to

$$\mathbf{J}_i = -cĐ_{in}\nabla x_i \quad (x_i \to 0,\ x_n \to 1) \quad i = 1, 2, \ldots, n-1 \tag{30}$$

and each of the $(n-1)$ species 'sees' only the solvent species n during its transport. Equation (30) is useful in e.g. absorption of dilute gaseous components in a solvent liquid.

Traditionally, in chemical engineering operations the concept of what constitutes a 'dilute' species is based on the species mole fraction in the mixture. For chemical vapour deposition processes, in which the proper description of diffusional transport in multicomponent gaseous mixtures is vital, there could be significant differences between the species mole fractions and the species mass fractions. For example, for deposition of tungsten, by surface reaction on a wafer

$$WF_6 + 3H_2 \to W_{(s)} + 6HF \tag{31}$$

the gaseous system consists of three species WF_6, H_2 and HF, whose molar masses are in the ratio 300:2:20. If the H_2 inlet mole fraction to the CVD reactor in a WF_6–H_2 mixture is 90%, its mass fraction is only about 5%. In other words, from a mole fraction point of view WF_6 and HF are to be considered 'dilute', whereas from a mass fraction point of view H_2 and HF are to be considered dilute and there is no consistent procedure for calculation of the Fick effective diffusivity D_i in such cases (Kuijlaars *et al.*, 1995). The deposition rate predicted by the Fick effective diffusivity approach is significantly poorer than that predicted by the Maxwell–Stefan model; see Fig. 15 (Kuijlaars, 1996).

The Wilke formula (Wilke, 1950)

$$D_i = (1 - x_i) \Big/ \sum_{\substack{k=1 \\ k \neq i}}^{n} (x_k/Đ_{ik}) \tag{32}$$

is often used to calculate the effective diffusivity of component i in a multicomponent mixture, even

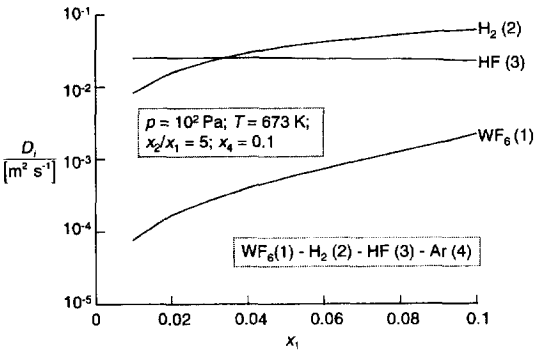

Fig. 16. Calculation of the effective diffusivities in the gaseous mixture WF_6, –H_2–HF–Ar at a temperature of 673 K and pressure 100 Pa. Data from Kuijlaars *et al.* (1995).

though its general validity is restricted to the situation wherein the species i diffuses in a mixture of stagnant, non-transferring, species, i.e. when N_j $(j \neq i) = 0$ (Elnashaie *et al.*, 1989; Krishna, 1989).

For diffusion with a heterogeneous reaction

$$\nu_1 A_1 + \nu_2 A_2 + \nu_3 A_3 + \cdots + \nu_n A_n = 0 \tag{33}$$

the flux ratios are fixed by the reaction stoichiometry and so

$$\frac{\mathbf{N}_1}{\nu_1} = \frac{\mathbf{N}_2}{\nu_2} = \frac{\mathbf{N}_3}{\nu_3} = \cdots = \frac{\mathbf{N}_n}{\nu_n}. \tag{34}$$

An effective diffusivity can be defined for component i,

$$\mathbf{N}_i = -c_t D_i \left(\frac{x_i}{RT} \nabla_T \mu_i \right), \quad \frac{1}{D_i} = \sum_{\substack{j=1 \\ j \neq i}}^{n} \frac{x_j}{Đ_{ij}} \left(1 - \frac{x_i \mathbf{N}_j}{x_j \mathbf{N}_i} \right)$$

$$= \sum_{\substack{j=1 \\ j \neq i}}^{n} \frac{x_j}{Đ_{ij}} \left(1 - \frac{x_i \nu_j}{x_j \nu_i} \right), \quad i = 1, 2, \ldots, n. \tag{35}$$

In a tungsten CVD reactor, for example, with the species WF_6 (1), H_2 (2), HF (3) and inert Ar (4) the flux ratios are $\nu_2/\nu_1 = 3$, $\nu_3/\nu_1 = -6$, $\nu_4/n_1 = 0$. Calculations of the effective diffusivities according to eq. (35) are illustrated in Fig. 16 for typical conditions. Interestingly, the effective diffusivity of HF in the

mixture can even exceed that of hydrogen for a certain composition range.

When none of the above four special situations apply and the multicomponent mixture is made up of molecular species of different sizes, shape and polarity we have to reckon with the complete form of the Maxwell–Stefan relations (17), (24)–(28). To illustrate the importance of adopting the complete Maxwell–Stefan formulation for bulk fluid diffusion we consider some examples below.

Non-ideal ternary mixtures

Firstly, let us consider bulk diffusion in a non-ideal liquid mixture made up of the components acetone (1)–benzene (2)–carbon tetrachloride (3) at a temperature of 25°C. At the composition of $x_1 = 0.35$, $x_2 = 0.35$ and $x_3 = 0.3$, the Maxwell–Stefan diffusivities $Đ_{ij}$ are estimated to be $Đ_{12} = 3.4 \times 10^{-9}$, $Đ_{13} = 2.5 \times 10^{-9}$ and $Đ_{23} = 1.7 \times 10^{-9}\ \mathrm{m^2\,s^{-1}}$, respectively. The matrix $[B]$ can be calculated from the pair Maxwell–Stefan diffusivities using eq. (26):

$$[B] = \begin{bmatrix} 0.363 & -0.036 \\ 0.107 & 0.495 \end{bmatrix} \times 10^9.$$

The matrix of thermodynamic factors is estimated from activity coefficient data to be

$$[\Gamma] = \begin{bmatrix} 0.69 & -0.13 \\ 0.07 & 1.05 \end{bmatrix}.$$

The matrix of Fick diffusivities can then be calculated as

$$[D] = \begin{bmatrix} 1.92 & -0.58 \\ -0.28 & 2.25 \end{bmatrix} \times 10^{-9}.$$

The two independent diffusion fluxes $\mathbf{J}_i$ for components 1 and 2 can now be expressed explicitly in terms of the composition gradient driving forces using eq. (28) as

$$\begin{pmatrix} \mathbf{J}_1 \\ \mathbf{J}_2 \end{pmatrix} = -c_t \begin{bmatrix} 1.92 & -0.58 \\ -0.28 & 2.25 \end{bmatrix} \times 10^{-9} \begin{pmatrix} \nabla x_1 \\ \nabla x_2 \end{pmatrix}$$

which shows that there is a strong influence of the driving force of component 2 on the flux of component 1. This *coupling* is caused by two effects: (i) the thermodynamic non-idealities in the system (note that $[\Gamma]$ is significantly non-diagonal) and (ii) the differences in the Maxwell–Stefan diffusivities (this implies that the frictional drag of the pairs 1–2, 1–3 and 2–3 are all significantly different from one another).

A positive value of the off-diagonal coefficient D_{12} implies that the flux of component 1 will be enhanced if the composition gradients of components and 2 are of the same sign. Cussler and Breuer (1972) discuss techniques for such flux enhancement by deliberate addition of a third component to a binary mixture.

At the critical point or at the spinodal curve the determinant of the Fick diffusivity matrix vanishes, i.e. $|D| = 0$, which implies that one of the eigenvalues of $[D]$ has a zero value (Taylor and Krishna, 1993); this has interesting consequences for the composition trajectory in e.g. liquid extraction (Krishna *et al.*, 1985). Lo and Myerson (1989) and Vitagliano *et al.* (1978) have experimentally demonstrated the rapid decline of $|D|$ as the critical solution concentration is approached.

In highly non-ideal liquid mixtures, the effective Fick diffusivity D_i can be expected to be a function not only of the composition but also of the composition gradients of the various species in the mixture. The strong composition dependence of the effective Fick diffusivity D_i in a non-ideal ternary mixture is the basis of a commercial process for spray drying of food liquids such as orange juice while retaining the aroma compounds. A food liquid typically consists of aroma, water and sugar. Consider acetone to represent a model aroma compound with malto dextrin representing the sugar compound. Analogous to Fig. 13, we note that with decreasing water concentrations there is a strong decrease in the diffusion coefficients both for acetone and water, with a much stronger decrease of acetone diffusivity; see Fig. 17. At water concentrations lower than 15 wt% the ratio $D_{\mathrm{acetone}}/D_{\mathrm{water}}$ becomes so small that the system can be considered

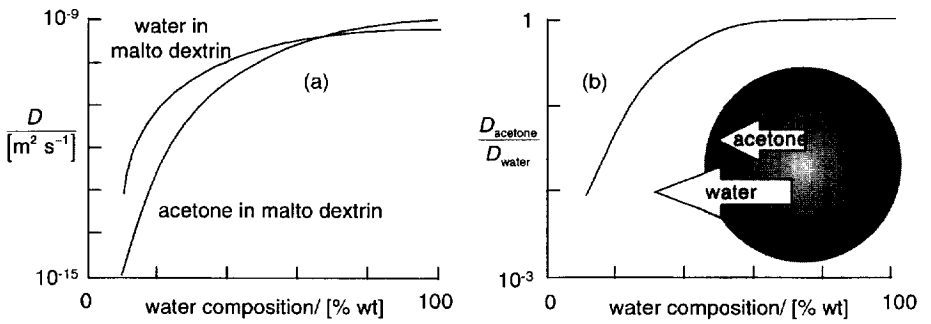

Fig. 17. (a) Effective Fick diffusivity of water and acetone in aqueous malto dextrin solutions as a function of water content. (b) Ratio of diffusivities of acetone and water in aqueous malto dextrin solutions as a function of water content. Adapted from Coumans *et al.* (1994).

impermeable to acetone. In spray drying operation it is essential to ensure a rapid decrease of water concentration at the outer surface of the food liquid droplet (see Fig. 17) and if the surface water is very quickly lowered to below 15 wt%, aroma retentions up to 100% are possible (Coumans *et al.*, 1994). For rigorous modelling of the transport processes during the drying process, see Chandrasekaran and King (1972), Coumans *et al.* (1994) and Etzel (1993).

Meerdink and van 't Riet (1993) have modelled the drying of a liquid food mixture containing water, sucrose and sodium caseinate by making use of eq. (26) for estimation of the matrix $[D]$. The experimentally observed segregation of solute material during drying could be modelled successfully.

The solution to eq. (17) in combination with homogeneous chemical reactions can lead to negative values for the enhancement factors (Sentarli and Hortaçsu, 1987) and exhibit complex spatiotemporal behaviour (Othmer and Scriven, 1969). Strong liquid-phase thermodynamic non-idealities could have a significant effect on mass transfer with chemical reaction (Frank *et al.*, 1995a; Valerio and Vanni, 1994; Vanni *et al.*, 1995).

Diffusional coupling effects can be expected to be particularly strong for mixtures of polymers and monomers (Sundelöf, 1979). Cussler and Lightfoot (1965) found that for the ternary system consisting of two monodisperse polystyrenes in toluene the four elements D_{ij} of the matrix $[D]$ can be of the same order of magnitude! Curtiss and Bird (1996) have developed the Maxwell–Stefan description of diffusion in polymeric liquids by modelling the polymer molecules as bead-spring structures. To obtain the Maxwell–Stefan equations explicit account must be taken of bead–bead interactions between different molecules.

The generalized Fick formulation (28) has been applied to the describe diffusion of particles in a fluid, i.e. diffusiophoresis (Shaeiwitz, 1984; Shaeiwitz and Lechnick, 1984).

Ideal ternary gas mixtures revisited

Let us now consider the case of an ideal gas mixture for which the matrix of thermodynamic factors $[\Gamma] \rightarrow [I]$, the identity matrix; eq. (17) simplifies in this case to

$$-\nabla x_i = \sum_{\substack{j=1 \\ j \neq i}}^{n} \frac{x_j \mathbf{N}_i - x_i \mathbf{N}_j}{c_t \mathcal{D}_{ij}}, \quad i = 1, 2, \ldots, n. \quad (36)$$

With the aid of eq. (36) we shall explain the curious diffusion phenomena observed by Duncan and Toor (1962) for the system hydrogen (1)–nitrogen (2)–carbon dioxide (3); cf. Fig. 3. For this ternary mixture the Maxwell–Stefan diffusivities of the three binary pairs can be estimated from the kinetic gas theory to be $\mathcal{D}_{12} = 8.33 \times 10^{-5}$, $\mathcal{D}_{13} = 6.8 \times 10^{-5}$, $\mathcal{D}_{23} = 1.68 \times 10^{-5}$ m^2 s^{-1}. The compositions in the two bulbs equilibrate after several hours to $x_1 = 0.25$, $x_2 = 0.5$ and $x_3 = 0.25$. At this equilibrium composition the elements of the matrix $[B]$ can be estimated from eq. (26):

$$[B] = \begin{bmatrix} 0.134 & 0.007 \\ 0.237 & 0.476 \end{bmatrix} \times 10^5$$

and the matrix of Fick diffusivities is therefore

$$[D] = \begin{bmatrix} 7.68 & -0.11 \\ -3.832 & 2.16 \end{bmatrix} \times 10^{-5}.$$

Let us estimate the flux of nitrogen $\mathbf{J}_2 = -c_t D_{21} \nabla x_1 - c_t D_{22} \nabla x_2$ in bulb 1 during the initial stages of the experiment. The composition gradients ∇x_i can be calculated from the differences between the equilibrium composition and the initial bulb 1 composition, $\nabla x_i = \Delta x_i / \ell$, where ℓ is the length of the capillary tube connecting the two bulbs and so $\mathbf{J}_2 = -(c_t/\ell)(D_{21}\Delta x_1 + D_{22}\Delta x_2) = -(c_t/\ell)(-3.83 \times \Delta x_1 + 2.16 \times \Delta x_2) \times 10^{-5}$. Initially $\Delta x_2 = 0$ (cf. Fig. 18), but the nitrogen flux remains non-zero and equals $\mathbf{J}_2 = -(c_t/\ell)(-3.83 \times \Delta x_1) \times 10^{-5}$. Since the driving force $\Delta x_1 = -0.25$, this causes a large positive flux for nitrogen, directed from bulb 1 to 2, causing its composition in bulb 1 to decrease. Between $t = 0$ and $t = t_1$ the direction of nitrogen transport is against its intrinsic gradient; this is reverse or uphill diffusion; notice in Fig. 18 that the signs of $\mathbf{J}_2$ and Δx_2 are the same! At the point $t = t_1$ we have $\mathbf{J}_2 = -(c_t/\ell)(-3.83 \times \Delta x_1 + 2.16 \times \Delta x_2) \times 10^{-5} = 0$ despite the existence of a significant driving force Δx_2; nitrogen experiences a diffusion 'barrier'. Beyond the point $t = t_1$, the diffusion behaviour of nitrogen is 'normal', directed from bulb 2 to bulb 1.

As an alternative to the matrix algebra development, the Maxwell–Stefan diffusion concept, pictorially represented in Fig. 14, can be used to provide a rationalization of the 'curious' behaviour of nitrogen in Figs 3 and 18. Firstly we note that in the initial

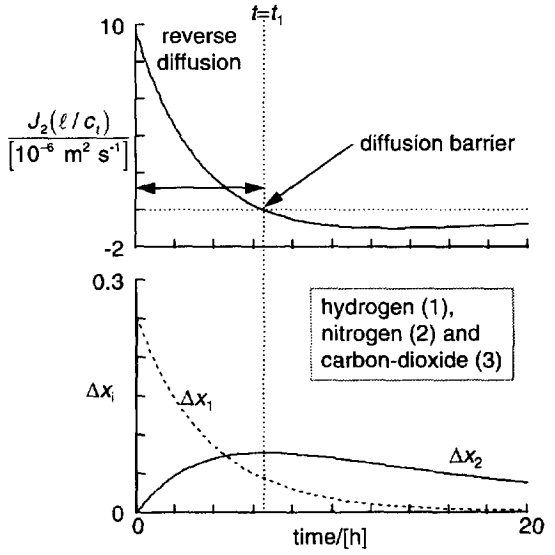

Fig. 18. Maxwell–Stefan calculations of the (a) flux of nitrogen and (b) driving forces as a function of time for the two-bulb diffusion experiment of Duncan and Toor (1962).

stages the driving force of nitrogen is much smaller compared with that of hydrogen and carbon dioxide: $\Delta x_1 = -0.25$, $\Delta x_2 = 0$, $\Delta x_3 = 0.25$. The frictional drag exerted by carbon dioxide (3) on nitrogen (2) transport is considerably larger than the frictional drag exerted by hydrogen (1) on nitrogen (2) transport; this can be seen from the fact that $(1/\mathcal{D}_{23}) \gg (1/\mathcal{D}_{12})$. During the time interval $t = 0$ and $t = t_1$ the direction in which the driving force of carbon dioxide acts is opposite to that in which the driving force of nitrogen acts. The much larger flux of carbon dioxide drags nitrogen against its intrinsic gradient, i.e. uphill. On a triangular composition diagram, the phenomenon of uphill diffusion manifests itself by causing a non-monotonous equilibration path; examine the equilibration paths for N_2 in bulbs 1 and 2; cf. Fig. 19.

In diffusion processes in lung airways normally at least four gases are involved O_2, CO_2, N_2 and H_2O vapour and the Maxwell–Stefan eqs (36) are commonly used to model pulmonary gas transport (Bres and Hatzfeld, 1977; Chang and Farhi, 1973; Chang *et al.*, 1975; Gibbs *et al.*, 1973; Modell and Farhi, 1976; Tai and Chang, 1979; Worth and Piiper, 1978).

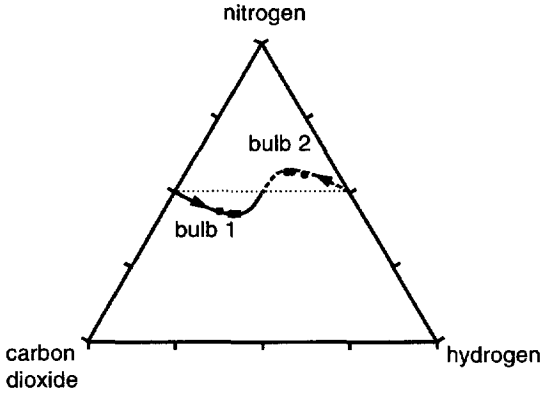

Fig. 19. Triangular diagram representation of the composition profiles in the two-bulb diffusion experiment of Duncan and Toor (1962).

For diffusion with a heterogeneous surface reaction, Löwe and Bub (1976) have shown that the solution of eq. (36), when coupled with the stoichiometric constraints (34), can yield multiple steady states.

Curvilinear composition trajectories

For diffusion in glasses, Varshneya and Cooper (1968) have experimentally verified the phenomena of uphill diffusion. Two 'semi-infinite' glass slabs with different compositions of K_2O–SrO–SiO_2 were brought into contact at time $t = 0$ and the transient compositions distributions determined. The non-monotonous equilibration trajectory observed for SrO in Fig. 20 in either slab signifies the occurrence of uphill diffusion; such phenomena are of importance in the processing of ceramics, cements and liquid metals (Christensen, 1977; Cooper, 1974; Johansen *et al.*, 1978). Analogous results have been observed by Krishna *et al.* (1985) for interphase mass transfer in a stirred cell with the liquid–liquid system glycerol (1)–water (2) and acetone (3). As seen in Fig. 21 the equilibration trajectory within the glycerol-rich phase is non-monotonous and a non-diagonal matrix of intraphase transport coefficients is required to successfully model the diffusion process (Krishna *et al.*, 1985; Taylor and Krishna, 1993). The correct description of the mass transfer trajectories in a ternary mixture of polymer/solvent/non-solvent is of the essence in the phase-inversion technique for membrane formation (Van den Berg and Smolders, 1992; Mulder, 1991).

Interphase mass transfer

For transfer within a fluid phase in practical operations such as distillation, extraction and drying the

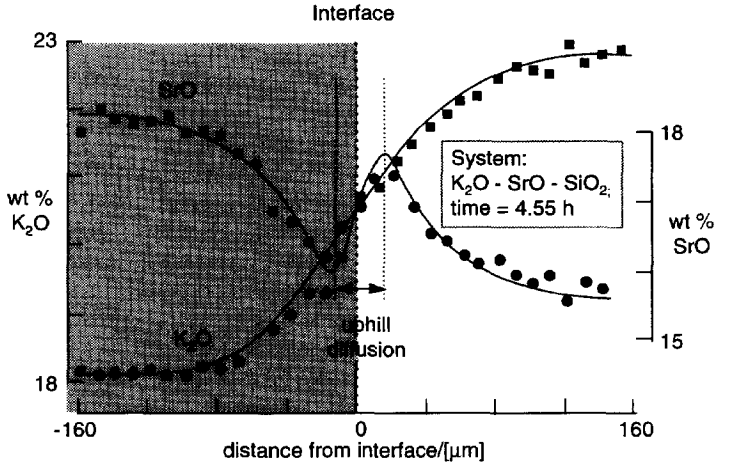

Fig. 20. Spatial composition profiles for the system K_2O–SrO–SiO_2 when two 6 mm thick glass samples of different compositions are brought into contact with each other. Adapted from Varsheya and Cooper (1972).

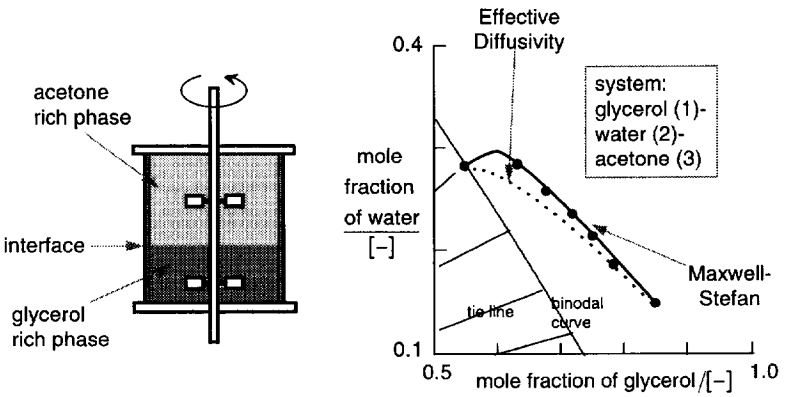

Fig. 21. Equilibration paths in the glycerol-rich phase for the system glycerol (1)–water (2)–acetone (3) measured in a stirred cell by Krishna *et al.* (1985). Adapted from Taylor and Krishna (1993).

Maxwell–Stefan diffusion equations need to be solved along with the equations of continuity (Bird *et al.*, 1960)

$$\frac{\partial c_i}{\partial t} + \nabla \cdot \mathbf{N}_i = \mathscr{R}_i, \quad i = 1, 2, \ldots, n-1. \tag{37}$$

Solutions to eq. (37), in combination with eq. (17), are available for a variety of models describing the phase hydrodynamics: e.g. film model (Krishna and Standart, 1976; Krishna, 1977a), penetration model (Krishna, 1978a), film-penetration model (Krishna, 1978b), turbulent boundary layer model (Krishna, 1982). The solution for the interphase molar transfer fluxes N_i can be expressed in $(n-1)$-dimensional matrix notation as

$$(N) = -c_t[k](\Delta x) + (x)N_t \tag{38}$$

where the composition difference driving forces are defined as (cf. Fig. 22)

$$\Delta x_i \equiv x_{ib} - x_{iI}, \quad i = 1, 2, \ldots, n-1. \tag{39}$$

The $(n-1)\times(n-1)$-dimensional matrix of multicomponent mass transfer coefficients $[k]$ is expressible in the same form as the corresponding matrix of Fick diffusivities

$$[k] = [R]^{-1}[\Gamma] \tag{40}$$

where the matrix $[R]$ is

$$R_{ii} = \frac{x_i}{\kappa_{in}} + \sum_{\substack{k=1 \\ k \neq i}}^{n} \frac{x_k}{\kappa_{ik}}, \quad R_{ij} = -x_i\left(\frac{1}{\kappa_{ij}} - \frac{1}{\kappa_{in}}\right), \quad i \neq j \tag{41}$$

in which κ_{ij} represent the mass transfer coefficients of the binary pairs in the multicomponent mixture; these coefficients can be estimated using the methods found in standard texts such King (1980) and Sherwood *et al.* (1975). Use of the bulk phase mole fractions x_{ib} in eq. (41) is sufficiently accurate for most engineering purposes (Krishna, 1979). Equations (38)–(41) provide a procedure for predicting interphase mass transfer in multicomponent mixtures on the basis of information on the transport coefficients of the corresponding binary pairs in both phases. This procedure has been experimentally verified by Tuohey *et al.* (1982) to be of reasonable accuracy for vapour–liquid transfer in the system methanol–2-propanol–ethanol in a stirred cell. The applicability of the suggested procedure has also been demonstrated for multicomponent distillation in a wetted-wall column by Dribika and Sandall (1979) and Krishna *et al.* (1981b).

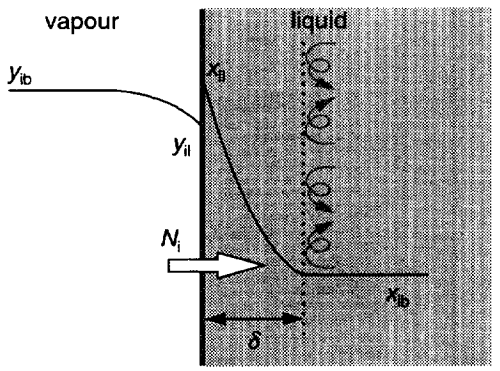

Fig. 22. Interphase mass transfer in vapour–liquid system.

Diffusional coupling effects in distillation

When the matrix of diffusivities within a phase $[D]$ is strongly non-diagonal, $[k]$ will also be strongly non-diagonal and phenomena such as osmotic transfer, reverse transfer and transfer barrier can be expected to occur. For distillation of methanol (1)–2-propanol (2)–water (3) in a packed column, Gorak (1991) has provided data on the vapour-phase driving force for 2-propanol, Δy_2, along with the corresponding interphase molar flux N_2; see Fig. 23. It is seen that the driving force of 2-propanol Δy_2 changes sign along the packing height, typical for a component with intermediate volatility. Even when $\Delta y_2 = 0$, the corresponding flux of 2-propanol is non-zero; this is osmotic transport. The system also exhibits the

phenomena of transport barrier and reverse transport. These phenomena occur routinely in multicomponent distillation. As a consequence, in tray columns, the component point Murphree efficiencies are unbounded and could have values ranging from $-\infty$ to $+\infty$. Figure 24 shows the experimental results obtained by Vogelpohl (1979) for the system acetone–methanol–water in a sieve tray column. We note that the component Murphree efficiency of water on tray 10 is -150%. Such 'odd' behaviours as negative efficiencies are quite common in multicomponent distillation, especially for components which have intermediate volatility; for such components the driving force Δy_i changes sign along the column, and, consequently should assume vanishingly small values at some location, i.e. $\Delta y_i \to 0$. When this is the case, its flux will be influenced strongly by the other components, leading to component efficiency values greater than 100% and of either sign. Usually, a high negative efficiency value will follow a high positive efficiency value; these values should also necessarily pass through zero. The experimentally measured column composition profiles are more accurately simulated allowing for unequal component efficiencies (calculated using the Maxwell–Stefan model) than by the more commonly used approach in which component Murphree efficiencies are assumed to be all equal to one another; see Fig. 24.

For total reflux distillation in a packed column, Ronge (1995) has shown that the Maxwell–Stefan mass transfer model is able to simulate the measured composition trajectory quite accurately, whereas the equilibrium stage model follows a significantly different trajectory; see Fig. 25. This implies that the values of the individual height of a theoretical plate (HETP) or height of a transfer unit (HTU) are all different from one another (Krishna *et al.*, 1981b). Heights of transfer units for individual components are unbounded (Olano *et al.*, 1995). The use of the classical HETP–NTP method for packed-column design could

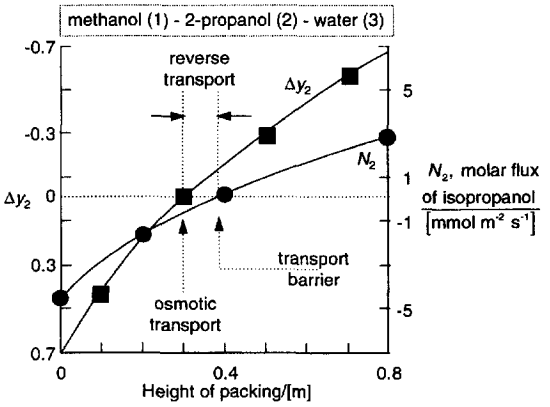

Fig. 23. Driving force for 2-propanol and its corresponding flux during distillation of methanol (1)–2-propanol (2)–water (3) in a packed column. Data from Gorak (1991).

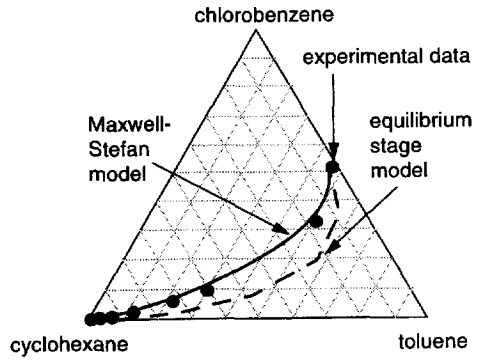

Fig. 25. Comparison of measured composition profiles with simulations for distillation in the system chlorobenzene–cyclohexane–toluene in a packed column. Adapted from Ronge (1994).

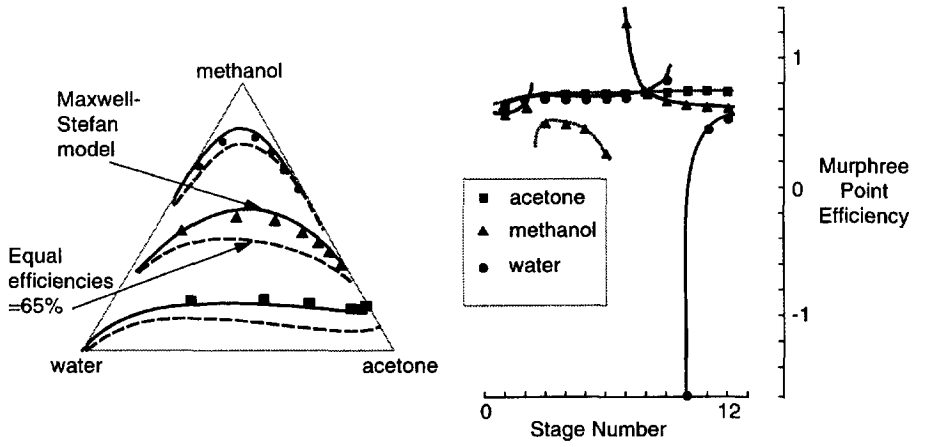

Fig. 24. Composition profiles and component efficiencies for distillation in the system acetone–methanol–water. Data from Vogelpohl (1979).

lead to poorer results than a more rigorous approach using the complete Maxwell–Stefan model for interphase mass transfer (Gorak, 1995). Accurate prediction of column composition profiles are essential in complex distillation column design involving multiple feeds and side streams.

Zimmerman *et al.* (1995) have shown how the Maxwell–Stefan formulations for liquid–liquid mass transfer can be incorporated into a rigorous model for an extractor taking due account of drop size distributions, axial mixing, drop breakage and coalescence. The important and challenging problem of modelling mass transfer in distillation columns operating with two liquid phases is considered by Lao and Taylor (1994).

SIMULTANEOUS HEAT AND MASS TRANSFER

Perfectly isothermal systems are rare in chemical engineering practice and many processes such as distillation, absorption, condensation, evaporation and drying involve the simultaneous transfer of mass and energy across phase interfaces. Representative temperature profiles in some non-isothermal processes are shown in Fig. 26.

Mass transfer affects heat transfer in two ways. Firstly, due to the species fluxes there is an additional enthalpy transport in addition to the conductive heat flux $\mathbf{q}$:

$$\mathbf{E} = \mathbf{q} + \sum_{i=1}^{n} \mathbf{N}_i \bar{H}_i. \tag{42}$$

Secondly, there is a direct contribution to the heat flux induced by species diffusion; this is termed the Dufour effect (Kuiken, 1994). The Dufour effect is usually not of importance in chemical engineering applications.

Heat transfer affects mass transfer in a variety of ways. Temperature gradients in the region of the phase interface affect phase equilibria and chemical reaction rates. Enthalpy changes accompanying the mass transfer process can have profound effects as illustrated in below.

Non-isothermal gas absorption

Consider the absorption of ammonia from air into water in a packed column (von Stockar and Wilke, 1977). We assume counter-current operation, with fresh water entering at the top (Fig. 27). The rich ammonia/air mixture enters at the bottom where the ammonia is absorbed. The enthalpy change due to absorption causes a rise in temperature of the liquid. As a result, water vaporizes. The mass transfer process in the vapour phase therefore involves three species: ammonia, water and (stagnant) air. Ammonia and water vapour diffuse against each other at the bottom of the column (Grenier, 1966). Towards the top of the column the vapour encounters cold incoming water. Therefore, water vapour condenses near the top of the column and we have co-diffusion of ammonia and water vapour through air towards the liquid phase. Water vaporization at the bottom and vapour condensation at the top cannot be ignored in the analysis. The resulting temperature profiles along the column show a pronounced bulge towards the bottom of the column (Raal and Khurana, 1973). Such temperature bulges are common in absorption of CO_2 and H_2S in amine solutions (Kohl and Riesenfeld, 1985; Yu and Astarita, 1987).

The need for a proper simultaneous heat and mass transfer analysis, incorporating the Maxwell–Stefan mass transfer model, has been dramatically emphasized by Krishna (1981a) by reanalysing the published experimental results of Modine (1963). Modine measured vapour–liquid mass transfer rates in a wetted-wall column for the system acetone–benzene–helium; see Fig. 28. The Maxwell–Stefan mass transfer

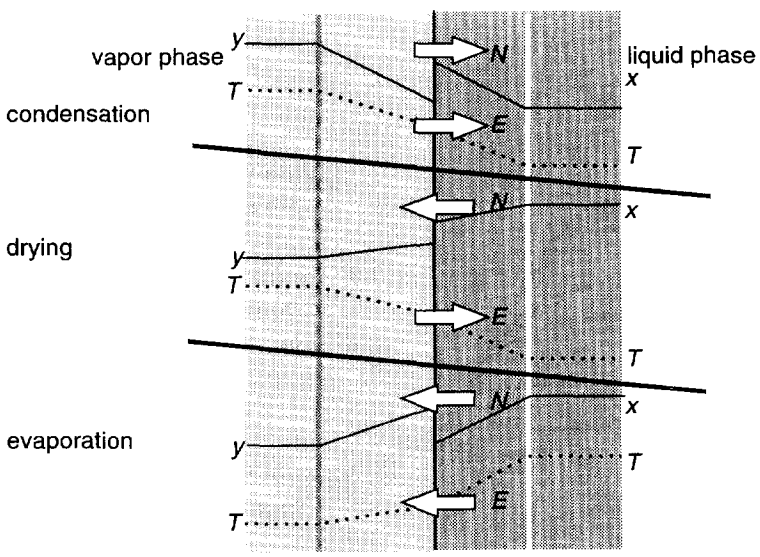

Fig. 26. Typical temperature and composition profiles in simultaneous heat and mass transfer processes.

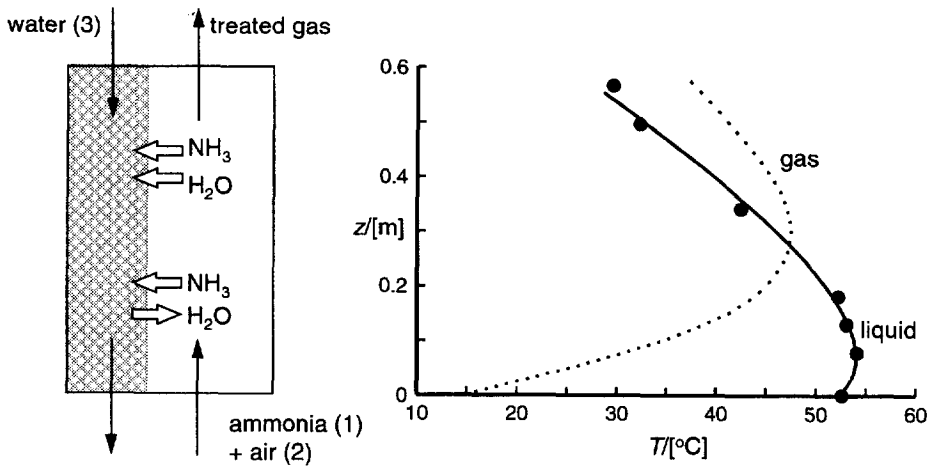

Fig. 27. Absorption of ammonia from air into water in a packed column. Data from Raal and Khurana (1973).

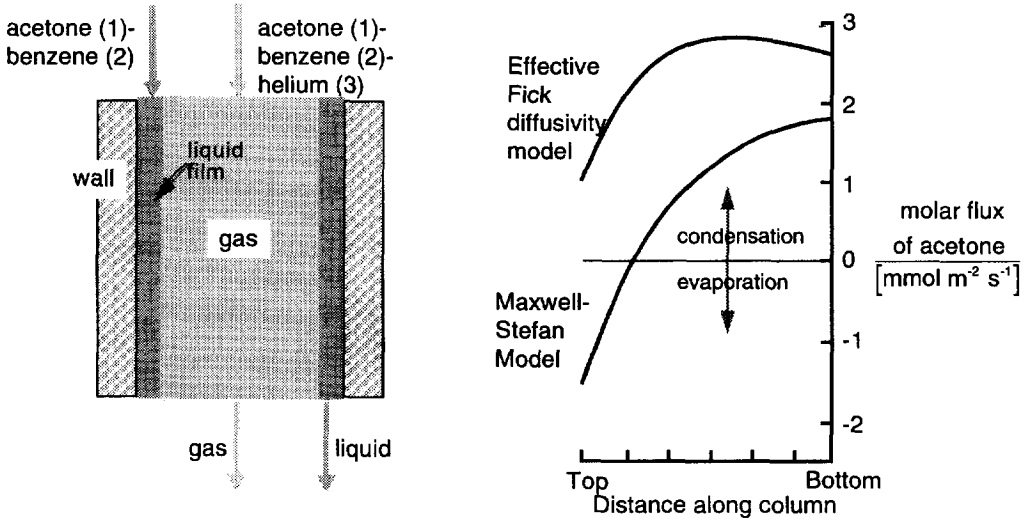

Fig. 28. Mass transfer in a wetted-wall column. The vapour phase consists of acetone–benzene–helium and this phase is brought into contact with a downward flowing liquid film of acetone and benzene. The Maxwell–Stefan diffusion model predicts condensation of acetone at the bottom of the column and vaporization at the top of the column. A pseudo-binary diffusion model based on effective diffusivities predicts that acetone will condense everywhere in the column. Experiments of Modine (1963) showed that for these conditions net vaporization of acetone occurs, validating the Maxwell–Stefan model. Adapted from Taylor and Krishna (1993).

approach predicts that the flux of acetone should change sign along the height of the column, whereas the conventionally used Wilke effective diffusivity model predicts that the acetone flux is always positive (i.e. condensation of acetone everywhere along the height). Experimentally, for the particular run, net *evaporation* of acetone was observed. This means that the effective diffusivity approach fails even at the qualitative level to describe the mass transfer process.

Rigorous design procedures for the design of mixed-vapour condensers incorporating the Maxwell–Stefan mass transfer formulations are available (Furno *et al.*, 1986; Taylor *et al.*, 1986). Conlisk (1996) has modelled absorption heat pumps using such an approach.

In a computational study of non-isothermal mass transfer across a vapour/liquid interface, followed by exothermic liquid-phase chemical reaction, Frank *et al.* (1995b) have demonstrated the importance of proper coupled heat and mass transfer modelling using the Maxwell–Stefan formulation. It is now commonly accepted that for design of sour gas absorption units involving concentrated gas mixtures such approaches are essential (Al-Ghawas and Sandall, 1991; Katti, 1995).

Breaking azeotropes with an inert gas

Multicomponent 'interaction' effects can be used to devise novel separation techniques. Condensation of an azeotropic mixture of 2-propanol (1) and water vapour (3) in the presence of air (3) will lead to a condensate composition which is richer in the faster diffusing species water vapour; see Fig. 29. The fluxes of 2-propanol and water are unequal due primarily to the differences in the values of the pair diffusivities: $Đ_{13} = 1.05 \times 10^{-9}$; $Đ_{23} = 2.6 \times 10^{-9}\ m^2\ s^{-1}$ and since the condensate composition $x_1 = N_1/(N_1 + N_2)$, the condensate will be richer in water. There is thus a possibility of 'breaking' azeotropes by deliberate introduction of an inert gas. This diffusion selective separation concept has been verified experimentally by Fullarton and Schlunder (1986) and the process aspects have been investigated by McDowell and Davis (1988). Conceptually speaking the function of the inert gas in this separation process is analogous to that of an 'inert' membrane and this phenomenon has been termed sweep diffusion in the literature (Cichelli *et al.*, 1951). Indeed, we shall see a bit later that the most convenient way of modelling membrane transport is to view the membrane as a pseudo-species.

Drying, crystallization

In drying operations the selectivity of the process can be significantly influenced by appropriate adjustment of the temperature and the humidity of the air used. Riede and Schlünder (1990a, b) and Martinez and Setterwal (1991) underline the need for using the Maxwell–Stefan approach in gas-phase controlled convective drying of solids wetted with multicomponent liquid mixtures.

Matsuoka and Garside (1991) emphasize the need for a proper simultaneous heat and mass transfer analysis of crystallization operations; the enthalpy changes accompanying crystallization have a significant influence on the rate of crystal growth.

Heat and mass transfer in distillation

Traditionally, in distillation operations the interphase mass transfer is assumed to be equimolar. Application of the proper energy balances to the vapour and liquid phases, it can be shown that the proper constraint on the interfacial molar fluxes is (Krishna, 1977b)

$$\sum_{i=1}^{n} \mathbf{N}_i(\overline{H_i^V} - \overline{H_i^L}) = 0. \tag{43}$$

Only when the molar enthalpies of vaporization of the individual species are equal to one another does eq. (43) reduce to the requirement of equimolar transport across the vapour–liquid interface

$$\sum_{i=1}^{n} \mathbf{N}_i = 0 \quad \text{(equimolar transport)}. \tag{44}$$

Consider the reactive distillation process for the manufacture of methyl tert-butyl ether (MTBE) by heterogeneously catalysed reaction of isobutene with methanol. The molar heats of vaporization of the species involved are (at 40°C): isobutene: 19.6 kJ/mol; methanol: 36.5 kJ/mol; MTBE: 29.5 kJ/mol. In the mass transfer modelling of this process a proper account is to be taken of these differences (Sundmacher and Hoffmann, 1994b).

Rigorous stagewise design software for multicomponent distillation columns incorporating eqs (38)–(41), along with the interfacial energy balance (43), are available (RATEFRAC™ from ASPEN Technology, Boston, U.S.A.; ChemSep from CACHE Corporation, U.S.A.); see Seader (1989) and Taylor

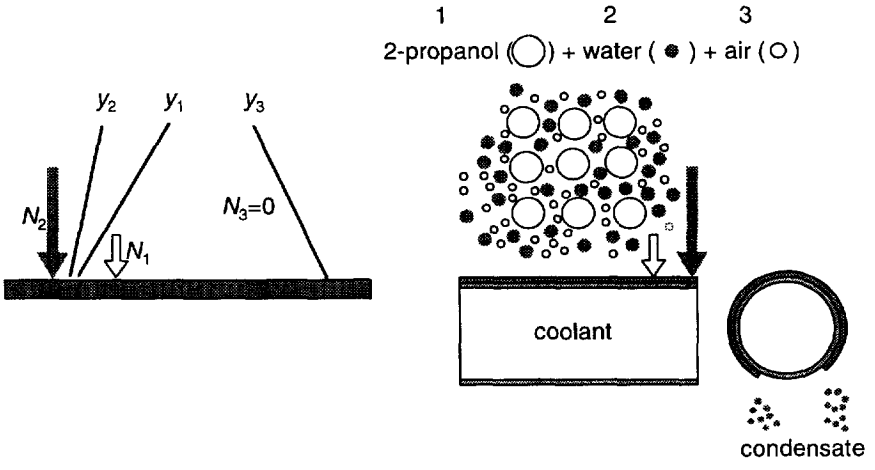

Fig. 29. Condensation of an azeotropic mixture of 2-propanol (1)–water (2) in the presence of air (3) results in a condensate which is richer in water. This is due to the fact that water vapour molecules diffuse faster in the ternary vapour–gas mixture. Experimental confirmation of this separation idea was obtained by Fullarton and Schlunder (1986).

and Lucia (1995) for a brief introduction and to Krishnamurthy and Taylor (1985a, b) and Taylor and Krishna (1993) for further details.

Thermal diffusion

When steep temperature gradients are encountered, such as in chemical vapour deposition processes, we need additionally to take account of the thermal diffusion (Soret effect) contribution to the molar fluxes. Equations (16) can be augmented in the following form (see Kuiken, 1994 for detailed derivations):

$$-\frac{x_i}{RT}\nabla_T\mu_i = \sum_{\substack{j=1\\ j\neq i}}^{n}\frac{x_i x_j(\mathbf{u}_i^T - \mathbf{u}_j^T)}{\mathcal{D}_{ij}}, \quad i = 1,2,\ldots,n \tag{45}$$

where $\mathbf{u}_i^T$ is the augmented species velocity incorporating the thermal diffusion contribution

$$\mathbf{u}_i^T = \mathbf{u}_i + \left(\frac{D_i^T}{\rho_i}\right)\frac{\nabla T}{T}, \quad i = 1,2,\ldots,n. \tag{46}$$

The thermal diffusion coefficients D_i^T have been defined in the manner of Hirschfelder *et al.* (1964) and have the units $\mathrm{kg^{-1}\,m^5\,s^{-1}}$. In CVD processes, thermal diffusion causes large, heavy gas molecules like WF_6, whose $D_i^T > 0$, to concentrate in cold regions whereas small, light molecules like H_2, whose $D_i^T < 0$, concentrate in hot regions. Kleijn and Hoogendoorn (1991) have demonstrated the importance of the thermal diffusion contribution in the modelling of CVD processes.

Wong and Denny (1975) have shown that thermal diffusion effects can be important for transport and reaction of gaseous mixtures inside catalyst particles and the importance of this increases when there is a large difference in the molar masses of the component species.

DIFFUSION UNDER THE INFLUENCE OF EXTERNAL BODY FORCES

Generalized driving force

When the system is subject to external body forces such as electrostatic potential gradients and centrifugal forces we need to extend the Maxwell–Stefan relations to take these into account. Let $\tilde{\mathbf{F}}_i$ represent the force acting per kg of species i. Expressed per volume of mixture the driving force $\mathbf{d}_i$ for diffusion is to be extended as follows [cf. eq. (18)]:

$$c_t RT d_i \equiv -c_i\nabla_T\mu_i + \rho_i\tilde{\mathbf{F}}_i. \tag{47}$$

Under the action of external body forces, linear momentum will be conserved

$$-\frac{1}{\rho}\nabla p + \sum_{i=1}^{n}\omega_i\tilde{\mathbf{F}}_i = \frac{\mathrm{d}\mathbf{v}}{\mathrm{d}t} + \nabla\cdot\boldsymbol{\tau} \tag{48}$$

where $\mathbf{v}$ is the mass average mixture velocity, $\boldsymbol{\tau}$ is the stress tensor and ω_i is the mass fraction of species i. In diffusion processes of relevance to chemical engineering mechanical equilibrium is established far quicker than thermodynamic equilibrium and we may safely assume

$$\frac{\mathrm{d}\mathbf{v}}{\mathrm{d}t} + \nabla\cdot\boldsymbol{\tau} \approx 0 = -\frac{1}{\rho}\nabla p + \sum_{i=1}^{n}\omega_i\tilde{\mathbf{F}}_i. \tag{49}$$

It is convenient to incorporate the mechanical equilibrium constraint (49) by redefining the generalized driving force in eq. (47) as follows:

$$c_t RT\mathbf{d}_i \equiv -c_i\nabla_T\mu_i + \rho_i\tilde{\mathbf{F}}_i + \rho_i\left(\frac{1}{\rho}\nabla p - \sum_{k=1}^{n}\omega_k\tilde{\mathbf{F}}_k\right) \tag{50}$$

where we add a vanishing vector (Lightfoot, 1974; Taylor and Krishna, 1993) to the driving force defined by eq. (47). The chemical potential gradient term may be expanded to explicitly include the contribution of the pressure gradient

$$\nabla_T\mu_i = \nabla_{T,p}\mu_i + \bar{V}_i\nabla p. \tag{51}$$

Inserting eq. (51) into eq. (50) and rearranging we obtain

$$c_t RT\mathbf{d}_i \equiv -c_i\nabla_{T,p}\mu_i - (c_i\bar{V}_i - \omega_i)\nabla p + \rho_i\left(\tilde{\mathbf{F}}_i - \sum_{k=1}^{n}\omega_k\tilde{\mathbf{F}}_k\right) \tag{52}$$

where we note that $c_i\bar{V}_i$ is the volume fraction of species i. The Maxwell–Stefan equations (17) can be generalized as follows:

$$\mathbf{d}_i \equiv -\frac{x_i}{RT}\nabla_{T,p}\mu_i - \frac{1}{c_t RT}(c_i\bar{V}_i - \omega_i)\nabla p + \frac{\rho_i}{c_t RT}\left(\tilde{\mathbf{F}}_i - \sum_{k=1}^{n}\omega_k\tilde{\mathbf{F}}_k\right) \tag{53}$$

$$= \sum_{\substack{j=1\\ j\neq i}}^{n}\frac{x_j\mathbf{N}_i - x_i\mathbf{N}_j}{c_t\mathcal{D}_{ij}} = \sum_{\substack{j=1\\ j\neq i}}^{n}\frac{x_j\mathbf{J}_i - x_i\mathbf{J}_j}{c_t\mathcal{D}_{ij}}, \quad i = 1,2,\ldots,n.$$

For ideal gas mixtures eqs (53) reduce to

$$-\nabla x_i - \frac{1}{p}(x_i - \omega_i)\nabla p + \frac{\rho_i}{p}\left(\tilde{\mathbf{F}}_i - \sum_{k=1}^{n}\omega_k\tilde{\mathbf{F}}_k\right) = \sum_{\substack{j=1\\ j\neq i}}^{n}\frac{x_j\mathbf{N}_i - x_i\mathbf{N}_j}{c_t\mathcal{D}_{ij}}, \quad i = 1,2,\ldots,n. \tag{54}$$

If the body forces $\mathbf{F}_i$ represent the force acting per mole of species i, the corresponding relations are

$$\mathbf{d}_i \equiv -\frac{x_i}{RT}\nabla_{T,p}\mu_i - \frac{1}{c_t RT}(c_i\bar{V}_i - \omega_i)\nabla p + \frac{1}{c_t RT}\left(c_i\mathbf{F}_i - \omega_i\sum_{k=1}^{n}c_k\mathbf{F}_k\right) \tag{55}$$

$$= \sum_{\substack{j=1\\ j\neq i}}^{n}\frac{x_j\mathbf{N}_i - x_i\mathbf{N}_j}{c_t\mathcal{D}_{ij}}, \quad i = 1,2,\ldots,n.$$

and

$$-\nabla x_i - \frac{1}{p}(x_i - \omega_i)\nabla p + \frac{1}{p}\left(c_i\mathbf{F}_i - \omega_i \sum_{k=1}^{n} c_k\mathbf{F}_k\right) = \sum_{\substack{j=1 \\ j\neq i}}^{n} \frac{x_j\mathbf{N}_i - x_i\mathbf{N}_j}{c_t\mathcal{D}_{ij}}, \quad i = 1,2,\ldots,n. \tag{56}$$

Diffusion under the influence of two important body forces: electrostatic potentials and centrifugal forces are discussed below.

Transport in ionic systems

For isothermal, isobaric transport in electrolyte systems we must reckon with an additional force caused by the electrostatic potential gradient $\nabla\Phi$

$$\mathbf{F}_i = -z_i\mathcal{F}\nabla\Phi \tag{57}$$

where z_i is the ionic charge of species i and $\mathcal{F}$ is the Faraday constant. Except in regions close to electrode surfaces, where there will be charge separation (the double-layer phenomena), the condition of electroneutrality is met

$$\sum_{i=1}^{n} c_i z_i = 0 \tag{58}$$

and therefore

$$\sum_{k-1}^{n} c_k\mathbf{F}_k = \left(\sum_{k=1}^{n} c_k z_k\right)\mathcal{F}\nabla\Phi = 0. \tag{59}$$

Incorporating eqs (57)–(59) into eq. (55) yields

$$-\frac{x_i}{RT}\nabla_T\mu_i - x_i z_i\frac{\mathcal{F}}{RT}\nabla\Phi = \sum_{\substack{j=1 \\ j\neq i}}^{n} \frac{x_i x_j(\mathbf{u}_i - \mathbf{u}_j)}{\mathcal{D}_{ij}} = \sum_{\substack{j=1 \\ j\neq i}}^{n} \frac{x_j\mathbf{N}_i - x_i\mathbf{N}_j}{c_t\mathcal{D}_{ij}}, \quad i = 1,2,\ldots,n. \tag{60}$$

For aqueous electrolyte solutions the nth component is usually taken to be water (subscript w). Equations (60) can also be expressed in terms of the diffusion fluxes relative to the neutral solvent water

$$-\frac{x_i}{RT}\nabla_T\mu_i - x_i z_i\frac{\mathcal{F}}{RT}\nabla\Phi = \sum_{\substack{j=1 \\ j\neq i}}^{n} \frac{x_j\mathbf{J}_i^n - x_i\mathbf{J}_j^n}{c_t\mathcal{D}_{ij}}, \quad i = 1,2,\ldots,n-1. \tag{61}$$

The total current carried by the electrolyte is

$$\mathbf{i} = \mathcal{F}\sum_{i=1}^{n} z_i\mathbf{N}_i. \tag{62}$$

In many chemical engineering applications such as ion exchange, no external electrical field is imposed on the system and also there is no flow of current, i.e.

$$\sum_{i=1}^{n} z_i N_i = 0, \qquad \sum_{i=1}^{n} z_i\mathbf{J}_i^n = 0. \tag{63}$$

Krishna (1987) has discussed a simple matrix method for calculation of the diffusion fluxes in such cases.

As an illustration let us consider diffusion in an aqueous solution of H_2SO_4; the transport properties for this system have been collected by Umino and Newman (1993). The system consists of three species: H^+ (= '+'), SO_4^{2-} (= '−') and H_2O (= 'w'). The charges are $z_+ = 1$, $z_- = -2$ and $z_w = 0$. Let c_s represent the concentration of the electrolyte or 'salt' in the aqueous solution and c_w the molar concentration of water. The concentrations of the ions are $c_+ = 2c_s$; $c_- = c_s$ and the corresponding mole fractions are $x_+ = 2c_s/(3c_s + c_w)$; $x_- = c_s/(3c_s + c_w)$. Equation (60) can be written explicitly for the ionic species in the system as follows:

$$x_+ = 2c_s/(3c_s + c_w); \quad x_- = c_s/(3c_s + c_w)$$

$$-\frac{x_+}{RT}\nabla_T\mu_+ - x_+ z_+\frac{\mathcal{F}}{RT}\nabla\Phi = \frac{x_+x_-(\mathbf{u}_+ - \mathbf{u}_-)}{\mathcal{D}_{+-}} + \frac{x_+x_w(\mathbf{u}_+ - \mathbf{u}_w)}{\mathcal{D}_{+w}}$$

$$-\frac{x_-}{RT}\nabla_T\mu_- - x_- z_-\frac{\mathcal{F}}{RT}\nabla\Phi = \frac{x_-x_+(\mathbf{u}_- - \mathbf{u}_+)}{\mathcal{D}_{+-}} + \frac{x_-x_w(\mathbf{u}_- - \mathbf{u}_w)}{\mathcal{D}_{-w}}. \tag{64}$$

The values of the three Maxwell–Stefan diffusivities $\mathcal{D}_{+w}$, $\mathcal{D}_{-w}$ and $\mathcal{D}_{+-}$ as functions of the sulfuric acid concentrations are shown in Fig. 30. The diffusivity of H^+ ion in water, $\mathcal{D}_{+w}$, is about 10 times higher than that of the SO_4^{2-} ion, $\mathcal{D}_{-w}$. However, due to the requirement of electroneutrality (58), an electric field ϕ is set up, called the diffusion potential, which tends to slow down the H^+ ions and accelerate the SO_4^{2-} ions so that they move in unison. The effective Maxwell–Stefan diffusivity of H_2SO_4, considered as a whole, can be defined by

$$-\frac{1}{RT}\nabla_T\mu_s = \frac{x_w(\mathbf{u}_s - \mathbf{u}_w)}{\mathcal{D}_{sw}} \tag{65}$$

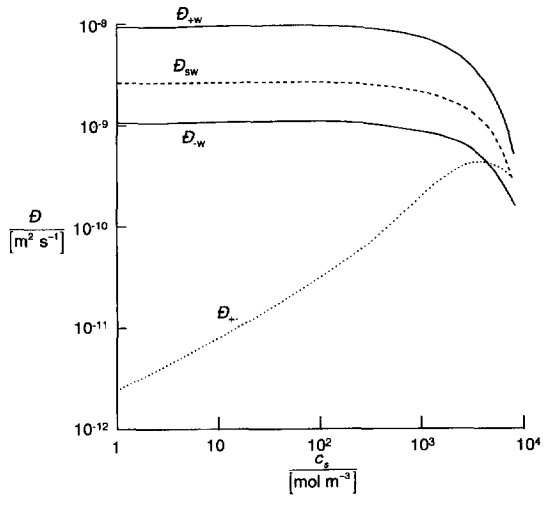

Fig. 30. Maxwell–Stefan diffusivities in the aqueous sulfuric acid system. Data from Umino and Newman (1993).

where the chemical potential of the 'salt' is

$$\mu_s = (2)\mu_+ + (1)\mu_- \tag{66}$$

where the individual ionic chemical potentials have been multiplied by the corresponding stoichiometric coefficients for the H^+ and SO_4^{2-} ions, respectively. Combining eqs (64)–(66) allows us to obtain the following expression for the Maxwell–Stefan diffusivity $Đ_{sw}$:

$$Đ_{sw} = \frac{Đ_{+w}Đ_{-w}(z_+ - z_-)}{z_+Đ_{+w} - z_-Đ_{-w}} \tag{67}$$

whose value lies between $Đ_{+w}$ and $Đ_{-w}$; see Fig. 30.

It is interesting to note from eq. (67) that the ion–ion interaction coefficient $Đ_{+-}$ has no influence on the diffusivity of the neutral electrolyte. The values of $Đ_{+-}$, which represents the long-range cation–anion interaction, are typically one or two orders of magnitude lower than the ion–water diffusivities (cf. Fig. 30) and vanish as the concentration approaches zero with a $\sqrt{c_s}$ dependence in accordance with Debye–Hückel–Onsager theory for ion–ion interactions in dilute solution (see Newman, 1991). The diffusivity $Đ_{+-}$ value decreases strongly with increasing charge numbers of the ions (Kraaijeveld and Wesselingh, 1993b); see Fig. 31. Estimation procedures for the $Đ_{ij}$ are discussed by Pinto and Graham (1986, 1987a) and Wesselingh *et al.* (1995).

For aqueous solutions of two electrolytes with a common anion we have to additionally reckon with the coefficient $Đ_{++}$. The behaviour of the $Đ_{++}$ coefficients in solutions of chloride salts is shown in Fig. 32 and it is observed that these coefficients are *negative*! This is not in violation of the second law of thermodynamics, eq. (22), as has been argued by Kraaijeveld *et al.* (1994) and Kuiken (1994). The absolute values of the $Đ_{++}$ coefficients roughly follow those of the $Đ_{+-}$ coefficients; they also increase as the inverse of the square root of the electrolyte concentration and decrease strongly with higher charge numbers. Wesselingh *et al.* (1995) have presented a tentative physical

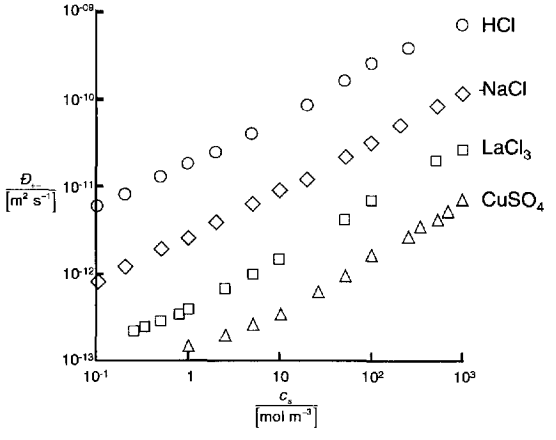

Fig. 31. Maxwell–Stefan plus–minus diffusivities for various electrolyte systems. Data from Wesselingh *et al.* (1995).

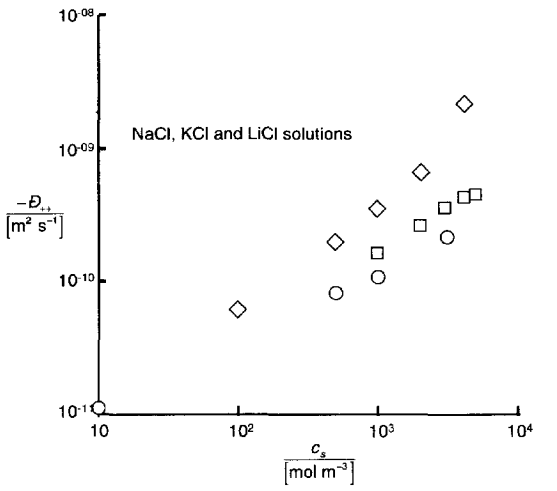

Fig. 32. Maxwell–Stefan plus–plus diffusivities for various electrolyte systems. Data from Wesselingh *et al.* (1995).

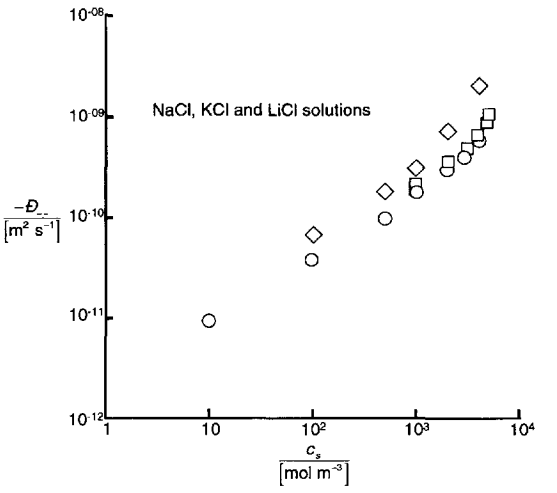

Fig. 33. Maxwell–Stefan minus–minus diffusivities of chloride ion in solutions of different salts. Data from Wesselingh *et al.* (1995).

argument to rationalize the negative $Đ_{++}$. At high salt concentrations, the $Đ_{++}$ may become positive. The hydrogen ion is an exception; in all cases that have been examined by Wesselingh *et al.* (1995) it has a positive $Đ_{++}$ coefficient. Available data on the $Đ_{--}$ coefficients also indicate negative values; see Fig. 33.

For hydrogen ion in aqueous sulfuric acid solutions, the relative friction experienced with the sulfate ions to that with water is $(x_-/Đ_{+-})/(x_w/Đ_{+w})$; similarly, for the sulfate ion the relative friction experienced with the hydrogen ion to that with water is $(x_+/Đ_{+-})/(x_w/Đ_{-w})$. These relative values have been calculated using the data of Umino and Newman (1993) and presented in Fig. 34. We see that for electrolyte concentrations smaller than about 2 mol/m^3 the cation–anion friction is less than 10% of

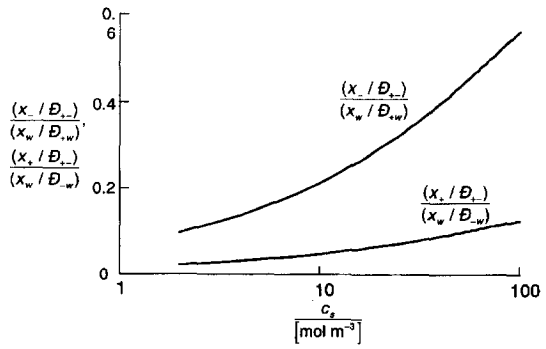

Fig. 34. Relative contributions of ion–ion friction and ion–water friction in aqueous solution of sulfuric acid. Calculations using data from Umino and Chapman (1993).

the ion–water friction and the first right members of eq. (64) can be ignored giving for ionic species i:

$$\mathbf{N}_i = -\mathcal{D}_{iw}\nabla c_i - c_i z_i \mathcal{D}_{iw}\frac{\mathcal{F}}{RT}\nabla\Phi + c_i \mathbf{u}_n, \quad i = 1,2,\ldots,n-1 \tag{68}$$

which is the Nernst–Planck equation and the three contributions to the molar flux of ionic species i are usually termed 'diffusion', 'migration' and 'convection'. In deriving eq. (68) we additionally assume that the ionic activity coefficients are unity. The ion–water diffusivities are practically independent of electrolyte concentration for dilute solutions.

For diffusion in mixtures of HCl and $BaCl_2$, discussed earlier, the Nernst–Plank equations (68) for the three ionic species can be combined with the no-current relation (63) to calculate the individual fluxes $\mathbf{J}_i^n$:

$$\begin{pmatrix} \mathbf{J}^n_{H^+} \\ \mathbf{J}^n_{Cl^-} \\ \mathbf{J}^n_{Ba^{2+}} \\ (\mathcal{F}/RT)\nabla\Phi \end{pmatrix} = -\begin{bmatrix} 1/\mathcal{D}_{H^+,w} & 0 & 0 & c_{H^+}z_{H^+} \\ 0 & 1/\mathcal{D}_{Cl^-,w} & 0 & c_{Cl^-}z_{Cl^-} \\ 0 & 0 & 1/\mathcal{D}_{Ba^{2+},w} & c_{Ba^{2+}}z_{Ba^{2+}} \\ z_{H^+} & z_{Cl^-} & z_{Ba^{2+}} & 0 \end{bmatrix}^{-1} \begin{pmatrix} \nabla c_{H^+} \\ \nabla c_{Cl^-} \\ \nabla c_{Ba^{2+}} \\ 0 \end{pmatrix}$$

$$= -[B]^{-1}\begin{pmatrix} \nabla c_{H^+} \\ \nabla c_{Cl^-} \\ \nabla c_{Ba^{2+}} \\ 0 \end{pmatrix} \tag{69}$$

where $[B]$ is an augmented coefficient matrix. Equation (69) can be used to calculate the Fick effective diffusivity of an individual ion D_i

$$-\nabla c_i = \frac{\mathbf{J}_i^n}{D_i}, \quad i = 1,2,\ldots,n-1 \tag{70}$$

and these values are plotted in Fig. 5. The agreement with the experimental data is good. Each ion experiences a 'pull' or 'push', depending on the direction of $c_i z_i(\mathcal{F}/RT)\nabla\Phi$ where $\nabla\Phi$ is the diffusion potential which can be calculated using eq. (69):

$$(\mathcal{F}/RT)\nabla\Phi = B_{41}^{-1}\nabla c_{H^+} + B_{42}^{-1}\nabla c_{Cl^-} + B_{43}^{-1}\nabla c_{Ba^{2+}}. \tag{71}$$

The Nernst–Planck model calculations anticipate negative values of $D_{Ba^{2+}}$ for $\sqrt{c_{H^+}/c_{Ba^{2+}}} > 2$ due to a strong electrostatic 'push'; see Fig. 5. In view of the fact that the effective ionic diffusivities can assume negative values, calculations of liquid-phase mass transfer coefficients in multicomponent ion exchange using these lead to unsatisfactory results (Frey, 1986).

It should also be clear from eq. (71) that the sign of diffusion potential is dictated by the concentration gradients of the individual ions and is therefore dependent on the signs (i.e. directions) of the concentration gradients. This directional influence of the diffusion potential is illustrated clearly by the experiments of Kraaijeveld and Wesselingh (1993a) for external mass transfer limited ion exchange. Exchanging Na^+ within the ion exchange bead with H^+ from the bulk chloride solution proceeds at a significantly higher rate than for the reverse exchange process; see Fig. 35. Smith and Dranoff (1964) report similar results. Analogous asymmetric exchange kinetics is found for the $Ca^{2+}/H^+/Cl^-$ system (Kraaijeveld and Wesselingh, 1993a).

The influence of the electrostatic potential created by ionic diffusion on mass transfer in liquid–liquid ion exchange operations is discussed by Van Brocklin and David (1972) and Tunison and Chapman (1976). The effect of ionic interactions is indicated qualitatively in Fig. 36 for the case of metals extraction. The difference in the mobilities of M^{2+} and H^+ gives rise to a net gradient of positive charge density which must be balanced by a non-uniform distribution of the counterion, for example SO_4^{2-}. The counterion must have a zero flux at the interface, however, so that an electric field ϕ, or a diffusion potential, must be established in the diffusion layer to balance this concentration gradient of the counterion. This potential gradient will have two effects on the metal transfer

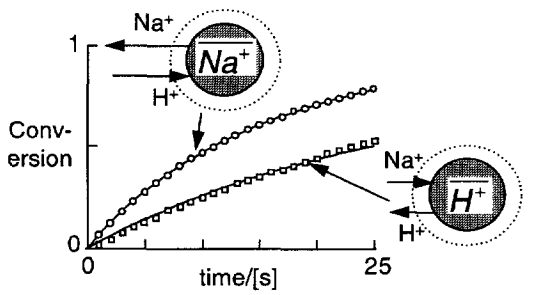

Fig. 35. External mass transfer limited transfer rates to and from ion-exchange particles are direction dependent. Experimental data of Kraaijeveld and Wesselingh (1993a).

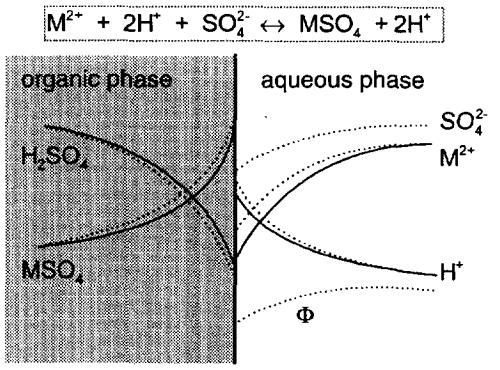

Fig. 36. Schematic indication of the concentration profile distortions caused by ionic interactions during metals extraction. Dashed profiles indicate corrected profiles taking the influence of ionic transport and the induced diffusion potential. Adapted from Tunison and Chapman (1976).

process: it will alter the metal flux directly by causing metal ion migration, and it will distort ionic concentration profiles, thus changing the surface concentrations, and hence the individual driving forces. Yoshida and Kataoka (1985) have analysed the entire fabrication process of an optical waveguide in soda-lime glass substrate by giving due consideration to differences in ionic mobilities and the engendered diffusion potential; see also Kapila and Plawsky (1995). Strictly speaking, the absorption of CO_2 and H_2S in alkanolamine solutions requires consideration of diffusion and reaction between ionic species (Glasscock and Rochelle, 1989) but Littel *et al.* (1991) have concluded that conventional approaches ignoring the influence of electric field on ion transport is not likely to lead to serious errors.

Deliberate use of electric fields can enhance mass transfer rates across liquid–liquid interfaces. This technique can be used for the recovery of fuchsine acid (a dye) or citric acid from water by extraction with *n*-butanol and applying an electric field across the two phases to enhance interphase mass transport (Stichlmair *et al.*, 1992). A survey of the use of electric fields to enhance separations is given by Muralidhara (1994) and Ptasinski and Kerkhof (1992).

Extension of the Maxwell–Stefan formulation to include thermoelectric effects is developed by Newman (1995).

Diffusion under the influence of a centrifugal force field

Consider a cylindrical centrifuge rotated subject to an angular velocity Ω. The centrifugal force experience per unit mass of each component i is

$$\tilde{\mathbf{F}}_i = \Omega^2 \mathbf{r} \tag{72}$$

and so

$$\sum_{k=1}^{n} \omega_k \tilde{\mathbf{F}}_k = \sum_{k=1}^{n} \omega_k \Omega^2 \mathbf{r} = \Omega^2 \mathbf{r}. \tag{73}$$

The pressure gradient caused by the centrifugal force is [cf. eq. (48)]

$$\nabla p = -\rho \sum_{i-1}^{n} \omega_i \tilde{\mathbf{F}}_i = -\rho \Omega^2 \mathbf{r} \tag{74}$$

and the generalized driving force simplifies for non-electrolyte systems to [cf. eq. (52)]

$$\mathbf{d}_i \equiv -\frac{x_i}{RT} \nabla_{T,p} \mu_i - (c_i \bar{V}_i - \omega_i) \frac{\rho}{c_t RT} \Omega^2 \mathbf{r}. \tag{75}$$

We note that the contribution of the centrifugal force to the overall driving force is effective only when there is a difference between the volume fraction of component i, $c_i \bar{V}_i$, and its mass fraction, ω_i; for a mixture where these differ the centrifugal force will cause relative motion of species. Components with a higher molar mass and mass density will experience a greater force and will therefore tend to congregate towards the periphery; this will cause a composition gradient $\nabla_{T,p} \mu_i$ directed inwards tending to cause redistribution; see Fig. 37. At equilibrium the net driving force on the system will vanish:

$$\frac{x_i}{RT} \nabla_{T,p} \mu_i = -(c_i \bar{V}_i - \omega_i) \frac{\rho}{c_t RT} \Omega^2 \mathbf{r} \quad \text{(equilibrium)}. \tag{76}$$

For separation of an equimolar gaseous mixture of $U^{235}F_6$ ($M_1 = 0.34915$ kg/mol) from $U^{238}F_6$ ($M_2 = 0.35215$ kg/mol) the difference between the mole fraction and mass fraction, $(c_i \bar{V}_i - \omega_i)$, is only 0.0021. In order to achieve a reasonable separation high rotational speeds, of the order of 700 rotations per second, will be required. Even so the separation achieved per stage is small and a few million centrifuges are required on a commercial scale (Van Halle, 1980; Voight, 1982)! Centrifugation techniques are also used in practice for separation of proteins from dilute aqueous solutions for which there is a large difference between the volume fraction and mass fractions of the protein molecule $(c_i \bar{V}_i - \omega_i) \approx -1000 x_1$ (Lee *et al.*, 1977).

An interesting alternative for effective separation by creating high-pressure gradients is the use of axisymmetric supersonic gaseous jets and this technique has

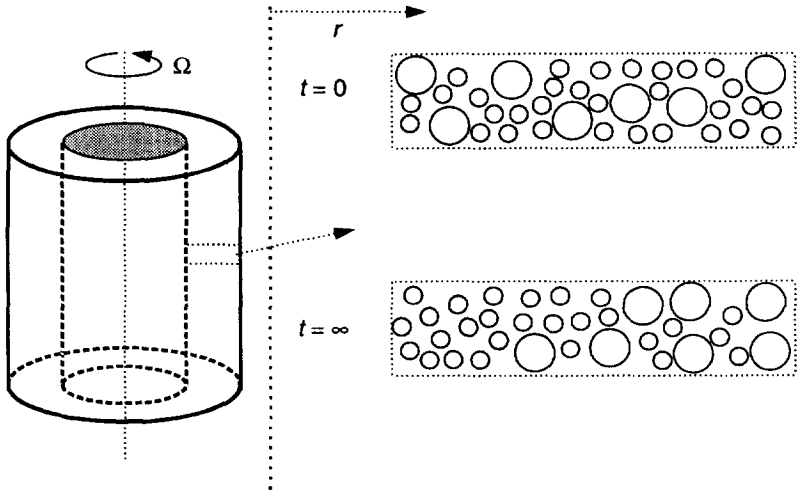

Fig. 37. Ultracentrifugal separation of a binary mixture.

been suggested for the separation of uranium isotopes (Mikami, 1970).

DIFFUSION INSIDE POROUS STRUCTURES

Diffusion mechanisms

Diffusion of fluid mixtures inside a porous matrix is important in catalysis, adsorption and membrane separations. Let us consider the example of gas adsorption. Most commercial adsorbents consist of small microporous crystals (e.g. zeolites) formed into a macroporous pellet (Ruthven, 1984). The molecular species constituting the fluid mixture have first to be transported from the bulk fluid phase to the external surface of the adsorbent. Within the particle there are two distinct diffusional resistances to mass transfer: the macropore (inter-crystalline) diffusional resistance of the pellet and the micropore (intra-crystalline) diffusion resistance. A schematic of a catalyst or adsorbent particle is given in Fig. 38. The relative importance of macropore and micropore diffusion resistances depend *inter alia* on the pore size distribution within the catalyst or adsorbent particle. *Micro*pores have diameters smaller than 2 nm; *macro*pores have sizes greater than 50 nm and *meso*pores are in the size range 2–50 nm. Figure 39 shows typical pore size distributions for three common adsorbent particles.

Within a pore we may, in general, distinguish three fundamentally different types of diffusion mechanisms, as depicted pictorially in Fig. 40:

- Bulk, 'free space' or free molecular diffusion that are significant for large pore sizes and high system pressures; here molecule–molecule collisions dominate over molecule–wall collisions.
- Knudsen diffusion becomes predominant when the mean-free path of the molecular species is much larger than the pore diameter and hence molecule-wall collisions become important.

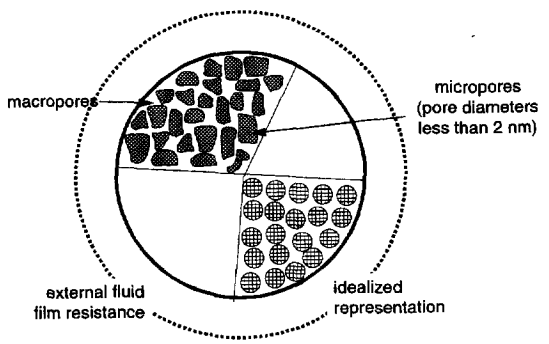

Fig. 38. Schematic diagram of adsorbent or catalyst particle depicting the three main diffusion resistances. Adapted from Ruthven (1984).

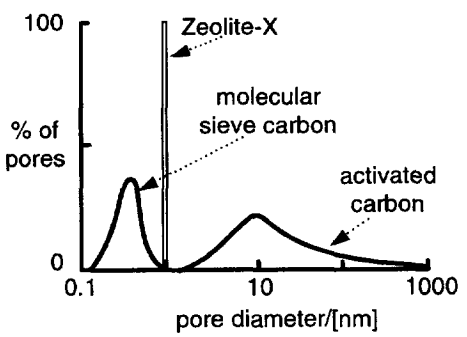

Fig. 39. Pore size distribution of zeolite-X, molecular sieve carbon and activated carbon. Adapted from Yang (1987).

- Surface diffusion of adsorbed molecular species along the pore wall surface; this mechanism of transport becomes dominant for micropores and for strongly adsorbed species.

Bulk and Knudsen diffusion mechanisms occur together and it is prudent to take both mechanisms into

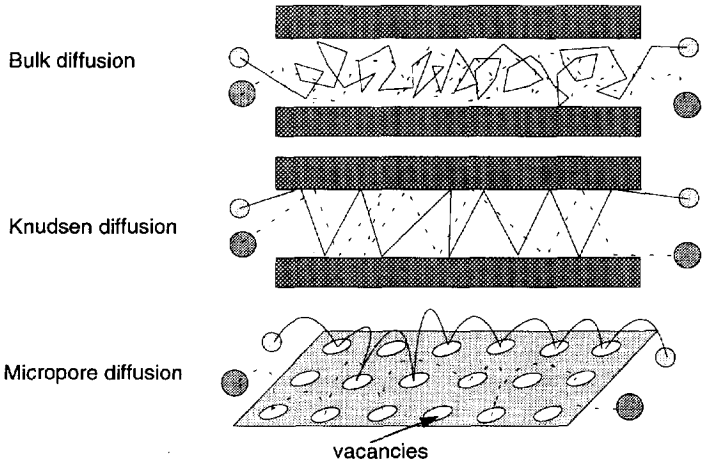

Fig. 40. Three distinct mechanisms by which molecular species get transported within an adsorbent or catalyst particle; (a) bulk diffusion; (b) Knudsen diffusion; and (c) surface diffusion of adsorbed species along the surface of the pores.

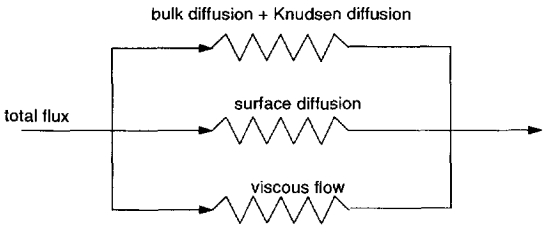

Fig. 41. Electric analogue circuit picturing the flux of the diffusing species within a porous medium. Adapted from Mason and Malinauskas (1983).

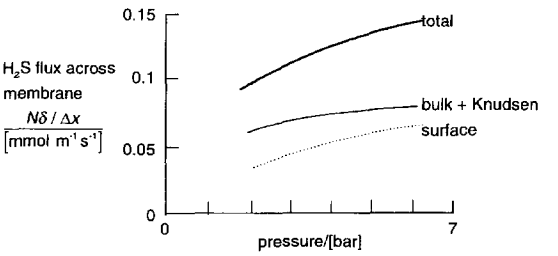

Fig. 42. Contributions of bulk, Knudsen and surface diffusion for transfer of H_2S across a catalytic membrane carrying the Claus reaction: $2\,H_2S + SO_2 \rightleftharpoons \frac{3}{8}\,S_8 + 2\,H_2O$. After Sloot (1991).

account rather than assume that one or other mechanism is 'controlling'. Surface diffusion occurs in parallel to the other two mechanisms and its contribution to the total species flux may be quite significant in many cases, as we shall see later in this paper. Within the micropores the dominant mechanism is surface diffusion. It is for this reason that surface diffusion is also referred to as micropore diffusion in the literature (e.g. Ruthven, 1984). For zeolitic structures micropore diffusion is also referred to as configurational diffusion. The pressure gradient inside the particle is not always negligible and this pressure gradient gives rise to viscous, or Darcy flow. Figure 41 shows the various contributions to the flux of the species inside the particle. The surface diffusion contribution can be important for components with high adsorption strength. Sloot (1991) has shown that the surface diffusion contribution to the total flux of H_2S through a membrane can be quite significant even though the pore size was as large as 350 nm; see Fig. 42. For separation of $H_2/CH_4/CO_2$ by pressure swing adsorption using activated carbon, Doong and Yang (1986) determined the contribution of the surface diffusion flux to be comparable in magnitude to the Knudsen flux.

Keil (1996) presents an up-to-date review of the modelling techniques used in practice for describing transport in porous media.

We first develop the Maxwell–Stefan formulation for combined bulk and Knudsen diffusion.

The dusty gas model

It is now generally agreed that the most convenient approach to modelling combined bulk and Knudsen diffusion is the *dusty gas model*; see Jackson (1977), Mason and Malinauskas (1983) and Wesselingh and Krishna (1990). The principle behind the *dusty gas model* is quite simple indeed and is really a straightforward application of the Maxwell–Stefan diffusion equations developed earlier. What we do is to consider the pore wall ('medium') as consisting of giant molecules ('dust') uniformly distributed in space. These dust molecules are considered to be a dummy, or pseudo, species in the mixture; see Fig. 43. To develop the transport relations we adopt the Maxwell–Stefan approach and use eq. (56) as a starting point and apply it for a $(n+1)$-component

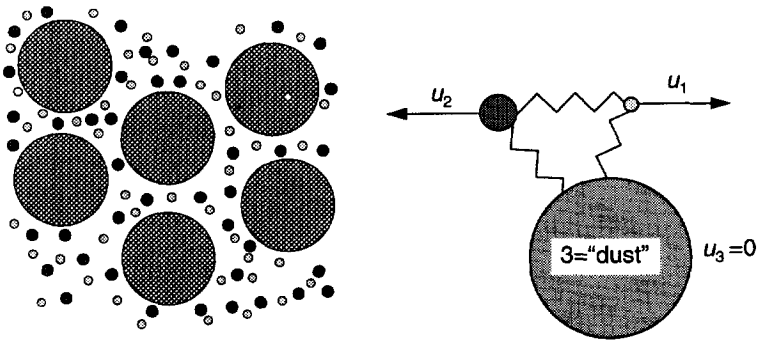

Fig. 43. Schematic picture of the dusty gas model in which the pore wall is modelled as giant dust molecules held motionless in space.

mixture:

$$-\nabla x_i' - \frac{(x_i' - \omega_i')}{p'}\nabla p' + \frac{1}{p'}\left(c_i\mathbf{F}_i - \omega_i' \sum_{i=1}^{n+1} c_i\mathbf{F}_i\right)$$

$$= \sum_{j=1}^{n+1} \frac{x_j'\mathbf{N}_i - x_i'\mathbf{N}_j}{c_t'\mathcal{D}_{ij}'}, \quad i = 1,2, \ldots, n+1. \tag{77}$$

It is important to bear in mind that the pressure, total concentration, mole fractions and mass fractions appearing in eq. (77) will now refer to the pseudo-mixture which includes the dust molecules, and not to the gas itself. This distinction will be maintained by writing p', c_t', x_i' and ω_i' for the quantities referred to the pseudo-mixture and p, c_t, x_i and ω_i for the same quantities referred to the gas. The latter quantities are of physical interest. In the case of species concentrations c_i, partial pressures p_i and flux vectors $\mathbf{N}_i$ there is no distinction between the two. The Maxwell–Stefan diffusivities in the pseudo-mixture are also primed to emphasise that their values differ from their 'free gas' counterparts.

To obtain equations describing the dusty gas model, the following set of assumptions must be applied:

(a) the dust concentration c_M is spatially uniform
(b) the dust is motionless, so that $\mathbf{N}_{n+1} = 0$
(c) the molar mass of the dust particles $M_{n+1} \to \infty$.

In order to satisfy requirement (b) the dust molecules must be constrained by external forces $\mathbf{F}_{n+1}$. Physically, these represent the support forces exerted on the dust molecules by an external agency which 'clamp' the molecules preventing it from moving in response to gas pressure gradients, i.e.

$$\nabla p = c_{n+1}\mathbf{F}_{n+1}. \tag{78}$$

We assume that there are no external body forces on the species $i = 1, 2, \ldots, n$:

$$\mathbf{F}_i = 0, \quad i = 1, \ldots, n. \tag{79}$$

With the above assumptions we may write out the first n equations as

$$-\nabla x_i' - \frac{(x_i' - \omega_i')}{p'}\nabla p' - \frac{\omega_i'}{p'} c_{n+1}'\mathbf{F}_{n+1}$$

$$= \sum_{j=1}^{n} \frac{x_j'\mathbf{N}_i - x_i'\mathbf{N}_j}{c_t'\mathcal{D}_{ij}'} + \frac{x_{n+1}'\mathbf{N}_i}{c_t'\mathcal{D}_{i,n+1}'}, \quad i = 1,2, \ldots, n. \tag{80}$$

Translating from the primed variables associated with the pseudo-mixture to the unprimed variables associated with the gas and defining effective transport parameters:

$$\mathcal{D}_{ij}^e = c_t'\mathcal{D}_{ij}'/c_t, \quad \mathcal{D}_{iM}^e = \mathcal{D}_{i,n+1}'/x_{n+1}' \tag{81}$$

we obtain (see Jackson, 1977 for detailed derivations)

$$-\frac{1}{RT}\nabla p_i = \sum_{j=1}^{n} \frac{x_j\mathbf{N}_i - x_i\mathbf{N}_j}{\mathcal{D}_{ij}^e} + \frac{N_i}{\mathcal{D}_{iM}^e}; \quad i = 1,2, \ldots, n. \tag{82}$$

The $\mathcal{D}_{ij}^e$ represent the effective binary pair diffusion coefficients in the porous medium, while $\mathcal{D}_{iM}^e$ represent the effective Knudsen diffusion coefficients. The $\mathcal{D}_{ij}^e$ are related to the corresponding free space values by

$$\mathcal{D}_{ij} = (\varepsilon/\tau)\mathcal{D}_{ij} \tag{83}$$

where the porosity-to-tortuosity factor (ε/τ) characterizes the porous matrix and is best determined by experiment; for a proper interpretation of ε and τ see the paper by Epstein (1989). For a cylindrical pore we have

$$\tau = 1 \text{ (cylindrical pore)}. \tag{84}$$

The free space diffusivities $\mathcal{D}_{ij}$ can be estimated from the kinetic gas theory (see e.g. Reid *et al.*, 1987). The effective Knudsen diffusivities are (Jackson, 1977; Mason and Malinauskas, 1983)

$$\mathcal{D}_{iM}^e = (\varepsilon/\tau)\frac{d_0}{3}\sqrt{\frac{8RT}{\pi M_i}} \tag{85}$$

where d_0 is the pore diameter and the square-root term represents the velocity of motion. Burganos and Sotirchos (1987) and Sotirchos and Burganos (1988) have analysed gaseous diffusion in pore networks of distributed pore size and length and obtained expressions for the effective diffusivities.

Equations (82) can be cast into n-dimensional matrix notation to obtain the following explicit expression for the fluxes:

$$(\mathbf{N}) = -\frac{1}{RT}[B^e]^{-1}(\nabla p) \tag{86}$$

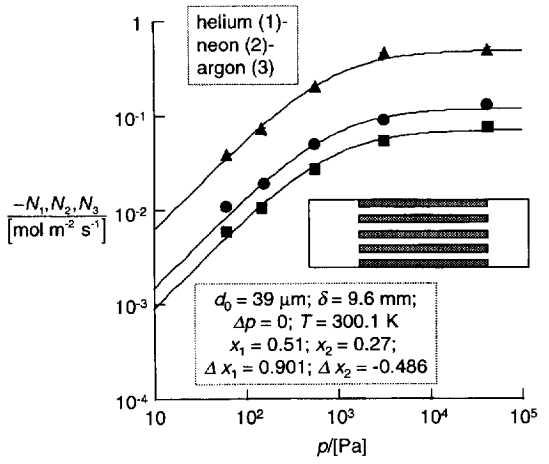

Fig. 44. Comparison of dusty gas model predictions with experimental data for diffusion of helium (1)–neon (2)–argon (3) through a bundle of capillaries. Data from Remick and Geankoplis (1974).

where the n-dimensional square matrix $[B^e]$ has the elements

$$B^e_{ii} = \frac{1}{\mathcal{D}^e_{iM}} + \sum_{\substack{k=1 \\ k \neq i}}^{n} \frac{x_k}{\mathcal{D}^e_{ik}}, \quad B^e_{ij(i \neq j)} = -\frac{x_i}{\mathcal{D}^e_{ij}},$$

$$i,j = 1,2, \ldots, n. \tag{87}$$

The diffusivities $\mathcal{D}^e_{ij}$ are inversely proportional to the pressure and independent of pore size and so in the bulk diffusion controlled regime the fluxes $\mathbf{N}_i$ are independent of system pressure and pore size. On the other hand, the Knudsen diffusivities $\mathcal{D}^e_{iM}$ are independent of the pressure and directly proportional to the pore size and so the fluxes $\mathbf{N}_i$ are directly proportional to the system pressure and pore size.

Figure 44 shows the calculation of the fluxes using eq. (86) for diffusion of helium (1)–neon (2) and argon (3) across a bundle of parallel capillaries with varying system pressures. With increasing pressure the system moves from Knudsen diffusion control to bulk diffusion control. The model calculations simulate the experimental results of Remick and Geankoplis (1974) very well. For a system at constant pressure, increasing the pore size produces analogous results; see Fig. 45.

Ofori and Sotirchos (1996) have presented simulation results to demonstrate the importance of using the complete form of the dusty-gas model in many applications.

Generalization to non-ideal fluid mixtures

The dusty gas model can be paralleled for diffusion of non-ideal fluid mixtures inside porous media following the treatment of Mason and Malinauskas

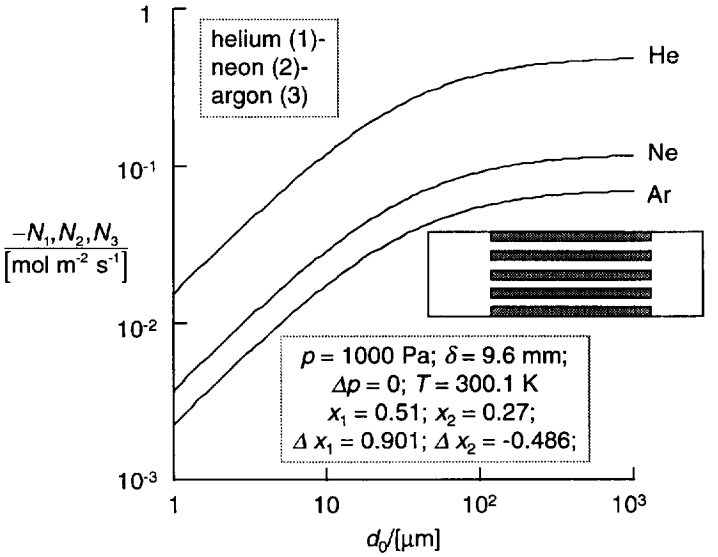

Fig. 45. Influence of pore size on the fluxes during diffusion of helium (1)–neon (2)–argon (3) through a bundle of capillaries; calculations using the dusty gas model.

(1983) to get

$$-\frac{x_i}{RT}\nabla_{T,p}\mu_i - \frac{x_i}{RT}\bar{V}_i\nabla p - \frac{x_i}{RT}z_i\mathscr{F}\nabla\Phi = \sum_{\substack{j=1\\ j\neq i}}^{n}\frac{x_j\mathbf{N}_i - x_i\mathbf{N}_j}{c_t\mathcal{D}_{ij}} + \frac{\mathbf{N}_i}{c_t\mathcal{D}^e_{iM}}, \quad i = 1,2,\ldots,n \quad (88)$$

which differs from its free-space counterpart, eq. (55), by the absence of the $\omega_i\nabla p$ term in the second left member. In deriving eq. (88) we have also assumed that both the solution and the matrix are electrically neutral and that the only external body force acting on the system is the electrostatic potential; these assumptions hold for the applications discussed in this paper. For high-pressure synthesis of ammonia the description of the transport processes within the catalyst particle requires that the chemical potential gradient be evaluated from a knowledge of the fugacity coefficients (Burghardt and Patzek, 1983).

An alternate form is to write eq. (88) in terms of the diffusion velocities $\mathbf{u}_i$ (Mason and del Castillo, 1985)

$$-\frac{1}{RT}\nabla_{T,p}\mu_i - \frac{1}{RT}\bar{V}_i\nabla p - \frac{1}{RT}z_i\mathscr{F}\nabla\Phi = \sum_{\substack{j=1\\ j\neq i}}^{n}\frac{x_j(\mathbf{u}_i - \mathbf{u}_j)}{\mathcal{D}^e_{ij}} + \frac{\mathbf{u}_i}{\mathcal{D}^e_{iM}}, \quad i = 1,2,\ldots,n. \quad (89)$$

The curious experimental results of Van Oers (1994) shown in Fig. 6 for the transport of PEG/dextran/water through an ultrafiltration membrane can be understood from the influence of the presence of dextran on the activity coefficient of PEG. High dextran concentrations upstream of the membrane results in a high chemical potential gradient driving force for PEG causing it to diffuse across the membrane reducing the rejection to even below zero. For ultrafiltration of mixtures of potassium phosphate and PEG, Vonk (1994) found that PEG at high concentrations tends to 'push' the phosphate through the membrane leading sometimes to negative rejections.

Heintz and Stephan (1994) have demonstrated that for pervaporation of ethanol and water across a poly (vinyl alcohol)–poly (acrylonitrile) composite membrane it is important to use the complete eqs (88) to calculate the fluxes. A typical result shown in Fig. 46 demonstrates the superiority of eq. (88) over an effective Fick diffusivity model for each component ignoring the mutual interaction between ethanol and water.

The intracatalyst transport during synthesis of methyl tert-butyl ether from isobutene and methanol has been modelled by Berg and Harris (1993) and Sundmacher and Hoffmann (1994a) using eq. (88) and taking proper account of thermodynamic non-ideality effects.

For the description of diffusion in ion exchange and electrodialysis we have to contend with at least five species, pictured in Fig. 47 for the case of a cation-exchange particle or membrane; these species are (i) the exchanger matrix with fixed charges (M), (ii) counterion initially present within membrane, (iii) counterion present in the adjacent bulk solution, (iv) solvent (usually water) and (v) co-ion (having the same charge as the fixed charge m). The co-ion, present in the bulk solution, is excluded from the membrane and for the description of transport within the particle or membrane we have to consider four species and the corresponding six Maxwell–Stefan diffusivities: (i) water-matrix: $\mathcal{D}^e_{wM}$, (ii) two water counterion diffusivities $\mathcal{D}^e_{w+}$, (iii) two matrix counterion diffusivities $\mathcal{D}^e_{M+}$ and (iv) the pair diffusivity of the two-counterions $\mathcal{D}^e_{++}$. Pinto and Graham (1987b) discuss estimations of the ionic diffusivities in ion-exchange resins, while some indications of the order of magnitudes of these coefficients are available in Wesselingh *et al.* (1995).

Since the behaviour of $\mathcal{D}^e_{++}$ is poorly understood it is usually ignored and eq. (88) reduces to the Nernst–Planck relation (68); see Graham and Dranoff (1982) and Helfferich (1962) for more detailed considerations. For ion exchange with particle diffusion controlling, the use of the Nernst–Planck equation predicts that the forward and reverse exchange of the

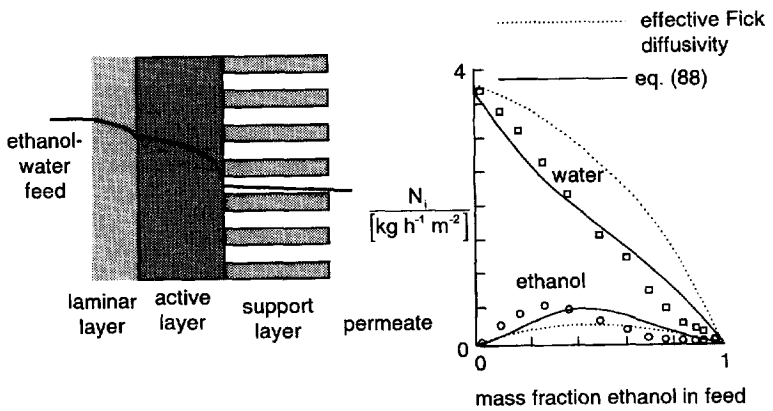

Fig. 46. Pervaporation of an ethanol–water mixture through a membrane. Comparison of Maxwell–Stefan and effective Fick formulations. Adapted from Heintz and Stephan (1994).

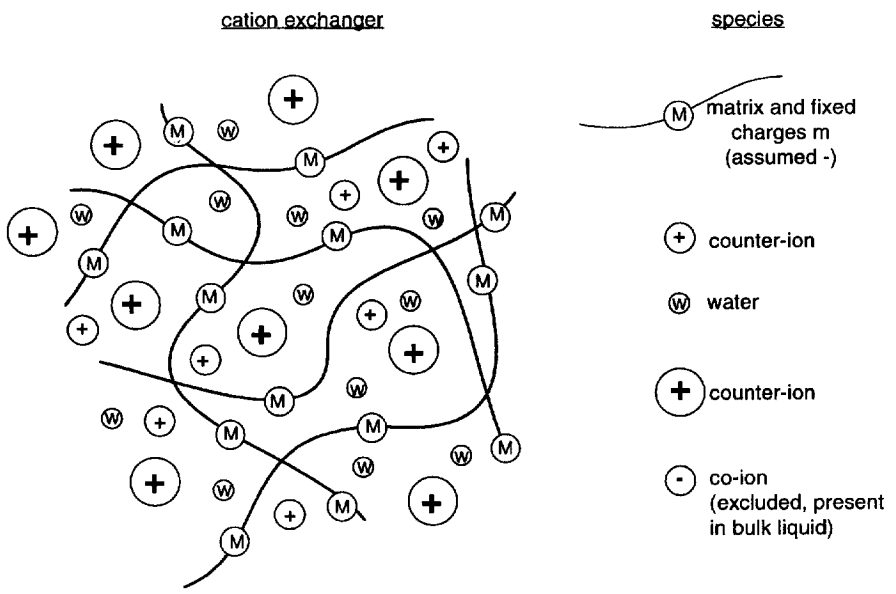

Fig. 47. Cation exchanger and the species involved in the transport process.

same counterions of different mobilities should occur at different rates. The exchange rate is higher if the counterion present initially in the ion exchanger is the faster of the two; see Fig. 48 (Helfferich, 1983). A further point to note is that when mass transfer external to the particle is limiting, the reverse trend is observed; compare Figs 35 and 48. Hu *et al.* (1992) consider both intraparticle and film diffusion in modelling the diffusion of bovine serum albumin in the presence of buffer electrolytes within a porous particle and emphasize the need for a proper modelling of ionic transport using the Nernst–Planck equations; a simple Fickian approach fails except for small protein concentrations. It is interesting to note that Anand *et al.* (1994) have analysed intraparticle diffusion in an acidic ion exchanger without any consideration being given to electrostatic potentials created by ion transport; it is small wonder that their effective Fick diffusivity values defy simple interpretation.

Kraaijeveld *et al.* (1995) have modelled electrodialysis of NaCl–HCl and amino acid mixtures using eq. (88) as a basis. Grimshaw *et al.* (1990) have demonstrated that protein transport across a polymethacrylic acid membrane can be enhanced significantly by the application of a transmembrane electric field.

Viscous flow

Under the action of fluid-phase pressure gradients viscous flow will occur within the porous matrix; see Fig. 49. If **v** represents the (mass-) average velocity of this flow it is usual to relate this to the pressure gradient by

$$\mathbf{v} = -\frac{B_0}{\eta}\nabla p \tag{90}$$

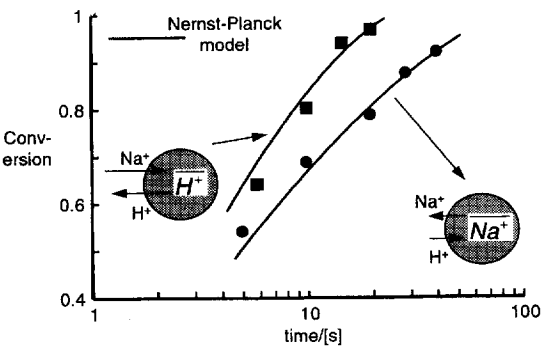

Fig. 48. Intra-particle diffusion limited ion-exchange rate asymmetry. Adapted from Helfferich (1983).

where the permeability B_0 is characteristic of the membrane structure and has to be determined experimentally, along with the porosity–tortuosity factor (ε/τ). The permeability coefficient B_0 can be calculated for some typical structures portrayed in Fig. 49. For a cylindrical pore the permeability is calculated from the Poiseuille flow relationship

$$B_0 = d_0^2/32. \tag{91}$$

For a suspension of spheres of diameter d_0, the Richardson–Zaki correlation gives

$$B_0 = (d_0^2/18)\varepsilon^{2.7} \tag{92}$$

where ε is the porosity of the suspension. The Carman–Kozeny relation for an aggregated bed of spheres is

$$B_0 = (d_0^2/180)(\varepsilon^2/(1-\varepsilon)^2) \tag{93}$$

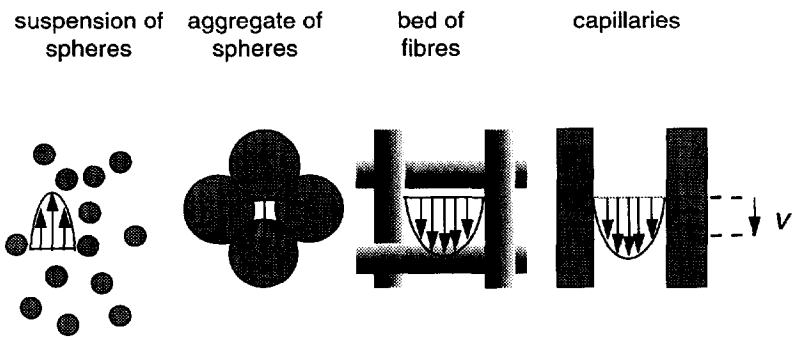

Fig. 49. Viscous flow of fluid through a suspension, bed of aggregated particles, bed of fibres and pores.

and for a corresponding bed of fibres

$$B_0 = (d_0^2/80)(\varepsilon^2/(1-\varepsilon)^2). \tag{94}$$

The viscous flow contribution is important for transport in membranes with open structures, such as in microfiltration and ultrafiltration. Viscous flow is relatively unimportant for transport in membranes with dense structures, such as present in gas permeation, pervaporation and reverse osmosis membranes.

Viscous flow tends to move the component species in the mixture along with it. In the original formulations of the dusty gas model (Mason and Malinauskas, 1983), this viscous flow has been assumed to non-separative. Thus, any viscous flow furnishes a permanent leak for *all* species and it is impossible to have the resulting transport equations describe semipermeable behaviour solely by the manipulation of the relative magnitudes of the transport coefficients $\mathcal{D}_{ij}^e$ and $\mathcal{D}_{iM}^e$. To overcome this dilemma we may allow viscous flow to have a separative character and introduce viscous selectivity factors α_i:

$$\mathbf{v}_i = \alpha_i \mathbf{v} = -\alpha_i \frac{B_0}{\eta} \nabla p. \tag{95}$$

The $\mathbf{v}_i$ represent the contribution of viscous flow to the velocity of species i. Relatively large molecules within narrow pores would tend to congregrate near the centre giving viscous selectivity factors exceeding unity, $\alpha_i > 1$, whereas for species which stick and slip at the pore walls we have $\alpha_i < 1$; see Fig. 50. Any species that cannot squeeze through the matrix of say a membrane by a viscous flow mechanism must have $\alpha_i = 0$. The viscous selectivity factors α_i must depend on the structure both of the matrix and the species.

In the presence of viscous flow the total species velocity is

$$\mathbf{w}_i = \mathbf{u}_i + \mathbf{v}_i \tag{96}$$

and the total species flux is therefore

$$\mathbf{N}_i = c_i(\mathbf{u}_i + \mathbf{v}_i) = c_i \mathbf{w}_i. \tag{97}$$

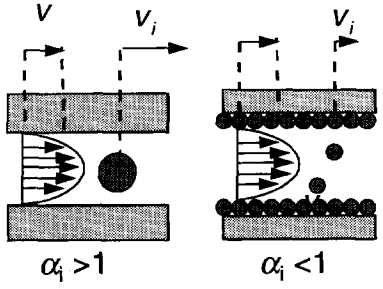

Fig. 50. Viscous selectivity effects for (a) large molecules moving close to the centreline and (b) strongly adsorbed species sticking to the walls.

Introducing

$$\mathbf{u}_i = \mathbf{w}_i + \alpha_i \frac{B_0}{\eta} \nabla p \tag{98}$$

into eq. (89) and rearranging we obtain

$$-\frac{1}{RT}\nabla_{T,p}\mu_i - \frac{1}{RT}\bar{V}_i \nabla p - \frac{\alpha_i' B_0}{\eta \mathcal{D}_{iM}} \nabla p - z_i \frac{\mathscr{F}}{RT} \nabla \Phi = \sum_{j=1}^{n} \frac{x_j(\mathbf{w}_i - \mathbf{w}_j)}{\mathcal{D}_{ij}^e} + \frac{\mathbf{w}_i}{\mathcal{D}_{iM}^e} \tag{99}$$

with the following modification of viscous selectivity factors

$$\alpha_i' = \alpha_i + \sum_{j=1}^{n} x_j \frac{\mathcal{D}_{iM}^e}{\mathcal{D}_{ij}^e} (\alpha_i - \alpha_j). \tag{100}$$

The final working form of the Mason formulation for intraparticle diffusion (Mason and del Castillo, 1985; Mason and Lonsdale, 1990) in terms of the fluxes is obtained by incorporating eq. (97) into eq. (99):

$$-\frac{c_i}{RT}\nabla_{T,p}\mu_i - \frac{c_i}{RT}\bar{V}_i \nabla p - \alpha_i' c_i \frac{B_0}{\eta \mathcal{D}_{iM}} \nabla p - c_i z_i \frac{F}{RT} \nabla \Phi = \sum_{j=1}^{n} \frac{x_j \mathbf{N}_i - x_i \mathbf{N}_j}{\mathcal{D}_{ij}^e} + \frac{\mathbf{N}_i}{\mathcal{D}_{iM}^e}. \tag{101}$$

Equation (101) has been derived from statistical–mechanical considerations by Mason and Viehland (1978) and is equally applicable for the description of aerosol transport (Mason and Malinauskas, 1983). By defining augmented species velocities according to eq. (46), we can extend eq. (101) to include thermal diffusion effects; this equation is then applicable for the description of thermophoresis. In the description of transport across membranes it is convenient to define further the total volumetric flux

$$\mathbf{N}_{\mathrm{vol}} = \sum_{i=1}^{n} \bar{V}_i \mathbf{N}_i. \tag{102}$$

Figure 51, adapted from Lakshminarayaniah (1969), summarizes the various transport mechanisms, driving forces and fluxes in membrane transport, and the importance of the individual terms in eq. (101) is indicated in Fig. 52.

Viscous selectivity effects are important for transport of large molecules such as proteins across e.g. ultrafiltration membranes. If these large molecules can be modelled as spheres, the theory of Deen (1987) when combined with that of Bungay and Brenner (1973) shows that α_i depends on the ratio of the sphere diameter to the pore diameter; see Fig. 53. We see that the convective selectivity tends to unity for very small

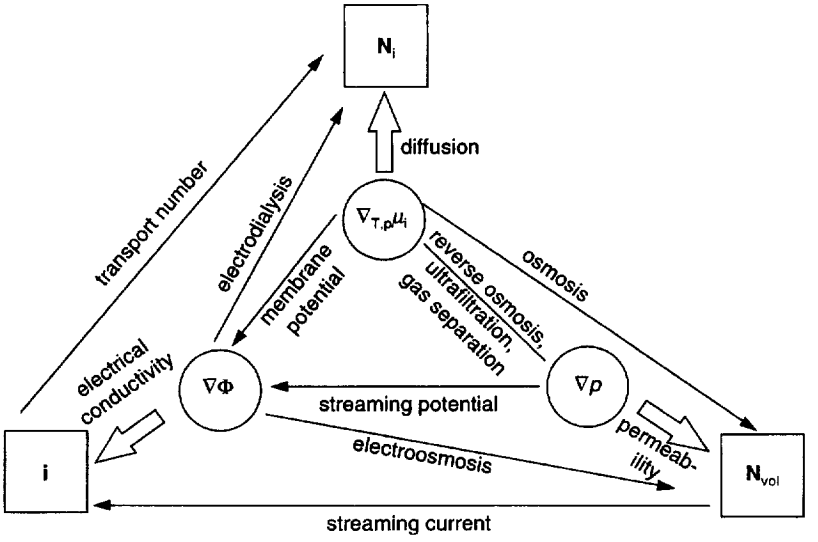

Fig. 51. Driving forces and fluxes in membrane transport. Adapted from Laksminarayanaiah (1969).

	$-\frac{c_i}{RT}\nabla_{T,p}\mu_i - \frac{c_i}{RT}\bar{V}_i\nabla p - \alpha_i' c_i \frac{B_0}{\eta \mathcal{D}_{iM}}\nabla p - c_i z_i \frac{\mathcal{F}}{RT}\nabla\Phi = \sum_{j=1}^{n} \frac{x_j\mathbf{N}_i - x_i\mathbf{N}_j}{\mathcal{D}_{ij}^e} + \frac{\mathbf{N}_i}{\mathcal{D}_{iM}^e}$						
Gas permeation	● ●	● ●					● ●
Reverse osmosis							
- *salt*	● ●	●					● ●
- *water*	●	● ●					● ●
Electrodialysis							
- *ions*	●			● ●	● ●		● ●
- *water*					● ●		● ●
Dialysis	● ●					●	● ●
Ultrafiltration							
- *salt*			● ●				●
- *water*			● ●				●
Pervaporation	● ●	● ●				●	● ●

Fig. 52. Importance of individual contributions to fluxes in various membrane transport processes. Blanks indicate: not important; one black circle: moderately important; two black circles: very important.

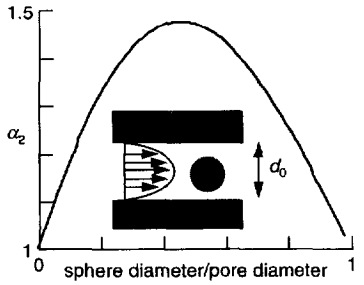

Fig. 53. Calculation of the viscous selectivity factor for spherical species moving inside a tube.

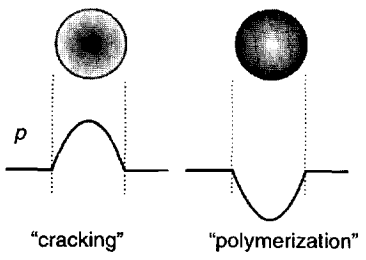

Fig. 54. Pressure profiles within porous catalyst particle for (a) cracking and (b) 'polymerization'-type reactions.

proteins (or large pores); this is as expected. The convective selectivity is also equal to unity in the case that the protein just fits into the pore. Then all of the fluid must move with the same velocity as the spheres. In the intermediate region, the convective selectivity of the protein has a maximum of about 1.5. For applications other than ultra- and nano-filtration convective selectivity effects can be ignored.

For the special case of single-component flow diffusion through medium the viscous selectivity coefficient $\alpha'_1 = 1$ and so

$$\mathbf{N}_1 = -\left(\frac{\mathcal{D}^e_{1M}}{RT} + c_1\frac{B_0}{\eta}\right)\nabla p \tag{103}$$

where the presence of the Knudsen term has the significance of a 'slip' flux, which is of significance for transport of gases at low pressures; see e.g. Cunningham and Williams (1980) and Mason and Malinauskas (1983). Within the framework of the dusty gas model, the condition of no-slip at the walls implies

$$\mathcal{D}^e_{1M} \to 0 \quad \text{(no slip of component 1)}. \tag{104}$$

Gaseous diffusion and heterogeneous chemical reactions

For diffusion with heterogeneous chemical reaction the flux ratios are governed by reaction stoichiometry [cf. eq. (34)]. Summing eqs (101) over the n species gives after introduction of the Gibbs–Duhem relationship (19) and the electroneutrality constraint (58):

$$\nabla p = -\frac{\sum_{i=1}^{n}\mathbf{N}_i/\mathcal{D}^e_{iM}}{\frac{1}{RT}\left(1 + \mathcal{D}_{\text{visc}}\sum_{i=1}^{n}\alpha'_i x_i/\mathcal{D}^e_{iM}\right)} = -\frac{\mathbf{N}_1\sum_{i=1}^{n}(v_i/v_1)1/\mathcal{D}^e_{iM}}{\frac{1}{RT}\left(1 + \mathcal{D}_{\text{visc}}\sum_{i=1}^{n}\alpha'_i x_i/\mathcal{D}^e_{iM}\right)} \tag{105}$$

where we have defined the 'viscous' diffusivity

$$\mathcal{D}_{\text{visc}} \equiv \frac{c_t B_0 RT}{\eta} \tag{106}$$

for convenience. For gaseous mixtures, imposing the constraint $\nabla p = 0$ places a special constraint on the fluxes [cf. eq. (85)]

$$\sum_{i=1}^{n}\mathbf{N}_i\sqrt{M_i} = 0, \quad (\nabla p = 0;\ \text{gaseous mixtures}) \tag{107}$$

which is Graham's law of diffusion in gaseous mixtures. Finite pressure gradients can be generated inside a porous catalyst when there is a net change in the number of moles, as illustrated in Fig. 54 for cracking and polymerization-type reactions. Sometimes the pressure build-up as a consequence of reaction stoichiometry is large enough to cause concerns on mechanical strengths of the catalyst. Burghardt and Aerts (1988) and Jackson (1977) present detailed discussions on influence of reaction stoichiometry on the developed pressure gradient. To give an illustration, taken from Jackson (1977), if the reaction is a simple irreversible one involving two species A and B: $A \to \nu_B B$ where ν_B is the stoichiometric coefficient for B, the pressure at the centre of the catalyst pellet, assuming complete conversion of A, is $p_0 = \sqrt{\nu_B}p$ where p is the pressure on the outside of the catalyst. Thus, for $\nu_B = 2$, we have a 40% increase in pressure as we proceed towards the centre of the pellet (Jackson, 1977). Neglect of internal pressure gradients can lead to inconsistencies for small pore catalysts (Hite and Jackson, 1977; Schneider, 1975). Also, internal pressure gradients will cause viscous flow (Ünal, 1987).

If the effective diffusivity of component i in the mixture is defined by

$$\mathbf{N}_i = -D_i\left(\frac{c_i}{RT}\nabla_{T,p}\mu_i + \frac{c_i}{RT}\bar{V}_i\nabla p + c_i z_i\frac{\mathcal{F}}{RT}\nabla\Phi\right)$$
$$i = 1, 2, \ldots, n \tag{108}$$

its value say for component 1 can be calculated from eqs (101) and (105):

$$\frac{1}{D_1} = \frac{1}{\mathcal{D}^e_{1M}} + \sum_{\substack{j=2\\ i}}^{n}\frac{x_j}{\mathcal{D}^e_{1j}}\left(1 - \frac{x_1 v_j}{x_j v_{1i}}\right) - \alpha'_1 x_1\frac{\mathcal{D}_{\text{visc}}}{\mathcal{D}_{1M}}\frac{\sum_{i=1}^{n}(v_i/v_1)/\mathcal{D}^e_{iM}}{\left(1 + \mathcal{D}_{\text{visc}}\sum_{i=1}^{n}\alpha'_i x_i/\mathcal{D}^e_{iM}\right)}. \tag{109}$$

The effective diffusivity thus defined will be a strong function of the composition and also the flux ratios of all the species participating in say a chemical reaction within the pellet. Schnitzlein and Hofmann (1988) have presented calculations for the effective diffusivity for hydrogen in a gaseous mixture undergoing catalytic reforming; see Fig. 55. Use of the dusty gas model and the classic Wilke formula [cf. eq. (32)] lead to significantly different effective diffusivity values for hydrogen. We also note that neglect of the viscous flow contribution [the third term on the right-hand side of eq. (109)] is not very serious; this result is typical (Haynes, 1978).

For the special case of a (i) binary mixture, (ii) with no net change in the number of moles, and (iii) satisfying eq. (107), eq. (109) simplifies to

$$\frac{1}{D_1} = \frac{1}{\mathcal{D}^e_{1M}} + \frac{1}{\mathcal{D}^e_{12}}, \tag{110}$$

a relation usually referred to as the Bosanquet formula. As noted above this formula is very restricted in its applicability. Elnashaie and Abasher (1993) and Reddy and Murty (1995) have explored the consequences of using approximate forms of eq. (109) for the calculation of effectiveness factors and chemical reaction rates in catalytic processes.

Kaza and Jackson (1980) demonstrate the possibility of uphill diffusion within a catalyst particle, a phenomena impossible to explain with say the Bosanquet formula (110) and Reinhardt and Dialer (1981) have investigated several interesting features of diffusion–reaction coupling. Veldsink *et al.* (1995) have shown the importance of using the dusty gas model in favour of the simpler Fick effective diffusivity formulation for modelling of catalytic membrane reactors. Sotirchos (1991), in a study of the deposition of SiC via decomposition of methyltrichlorosilane in a porous medium, concludes that simplified mass transport flux models can lead to significantly different results from the Dusty Gas model even if the concentration of the reactants are low. In the hydropyrolysis of coal particles, Ward and Russel (1981) have shown that it is necessary to take account of the differences in the component pair diffusivities $\mathcal{D}^e_{ij}$.

The computational issues involved in dynamic diffusion–reaction process simulations incorporating eq. (101), along with the proper energy balance, are addressed by Hindmarsh and Johnson (1988).

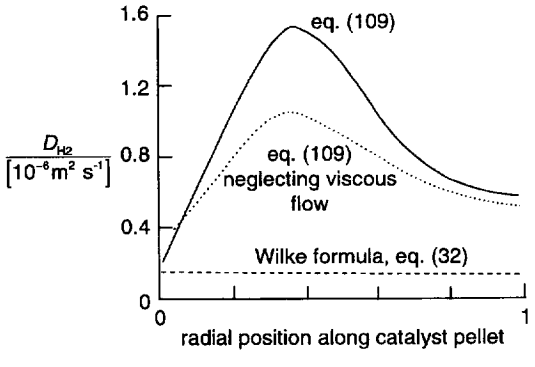

Fig. 55. Dependency of the effective diffusivity of hydrogen on the spatial position inside the catalyst particle for catalytic reforming of C_7 hydrocarbons. Adapted from Schnitzlein and Hofmann (1988).

The Lightfoot formulation

An alternative to the Mason formulation is to apply the Maxwell–Stefan equations in the form (cf. Lightfoot, 1974)

$$-\frac{c_i}{RT}\nabla_{T,p}\mu_i - \frac{c_i}{RT}\bar{V}_i\nabla p - \frac{c_i}{RT}z_i\mathcal{F}\nabla\Phi = \sum_{\substack{j=1\\ j\neq i}}^{n}\frac{x_j\mathbf{N}_i - x_i\mathbf{N}_j}{E_{ij}} + \frac{\mathbf{N}_i}{E_{iM}}, \quad i = 1,2,\ldots,n \tag{111}$$

for describing combined transport due to diffusion and viscous flow. The transport parameters E_{ij} and E_{iM} include the contribution due to viscous tranport and may be viewed as being 'apparent' transport coefficients. Written in terms of the velocities $\mathbf{w}_i$ [cf. eqs (96) and (97)]:

$$-\frac{1}{RT}\nabla_{T,p}\mu_i - \frac{1}{RT}\bar{V}_i\nabla p - z_i\frac{F}{RT}\nabla\Phi = \sum_{j=1}^{n}\frac{x_j(\mathbf{w}_i - \mathbf{w}_j)}{E_{ij}} + \frac{\mathbf{w}_i}{E_{iM}}, \quad i = 1,2,\ldots,n. \tag{112}$$

Equations (112) are equivalent to the frictional formulation (Kedem and Katchalsky, 1961; Smit *et al.*, 1975; Spiegler, 1958) with the frictional coefficients defined by

$$\zeta_{ij} \equiv \frac{RT}{E_{ij}}, \qquad \zeta_{iM} \equiv \frac{RT}{E_{iM}}. \tag{113}$$

The apparent, or Lightfoot coefficients, E may be related to the Mason coefficients $\mathcal{D}^e$ (Mason and del Castillo, 1985) as follows:

$$\frac{1}{E_{ij}} = \frac{1}{\mathcal{D}^e_{ij}} + \frac{\alpha'_i\mathcal{D}_{\text{visc}}}{\mathcal{D}^e_{iM}\mathcal{D}^e_{jM}}\frac{1}{(1 + \mathcal{D}_{\text{visc}}/\bar{\mathcal{D}}_M)} \tag{114}$$

and

$$\frac{1}{E_{iM}} = \frac{1}{\mathcal{D}^e_{iM}}\frac{1}{(1 + \mathcal{D}_{\text{visc}}/\bar{\mathcal{D}}_M)}\left[1 + (\mathcal{D}_{\text{visc}}/\bar{\mathcal{D}}_M)\left(1 - \frac{\alpha'_i\bar{\mathcal{D}}_M}{\bar{\mathcal{D}}^0_M}\right)\right] \tag{115}$$

with the following parameter definitions:

$$\frac{1}{\bar{\mathcal{D}}_M} \equiv \sum_{k=1}^{n}\frac{\alpha'_k x_k}{\mathcal{D}^e_{kM}}, \quad \frac{1}{\bar{\mathcal{D}}^0_M} \equiv \sum_{k=1}^{n}\frac{x_k}{\mathcal{D}^e_{kM}}. \tag{116}$$

Some methods for estimation of the E_{iM} for polymeric membranes are discussed by Peppas and Meadows (1983). We note from eq. (114) that the Lightfoot coefficients E_{ij} are not symmetric in general, whereas the Mason coefficients $\mathcal{D}^e_{ij}$ obey the Onsager reciprocal relations

$$\mathcal{D}^e_{ij} = \mathcal{D}^e_{ji}. \tag{117}$$

Inclusion of the viscous contribution into the E_{ij} destroys symmetry unless the viscous selectivity factors are all equal to unity.

For narrow pores $B_0 \to 0$ the viscous contributions vanish giving

$$E_{ij} = \mathcal{D}^e_{ij}, \quad E_{iM} = \mathcal{D}^e_{iM} \quad \text{(narrow pores)} \quad (118)$$

and there is no distinction between the Lightfoot and Mason coefficients. For a single component 1 diffusing through a suspension of 'dust' molecules (species M), we have

$$E_{1M} = \mathcal{D}^e_{iM} + \mathcal{D}_{\text{visc}}, \quad (119)$$

demonstrating clearly that the Lightfoot coefficient is a sum of diffusive and viscous contributions; cf. eqs (103) and (119). Wright (1972) further examines eq. (119) in the context of aerosol transport. For binary mixtures eqs (114)–(116) simplify to

$$E_{iM} = \mathcal{D}^e_{iM} \frac{\left[1 + \mathcal{D}_{\text{visc}}\left(\frac{\alpha'_1 x_1}{\mathcal{D}^e_{1M}} + \frac{\alpha'_2 x_2}{\mathcal{D}^e_{2iM}}\right)\right]}{\left[1 + \mathcal{D}_{\text{visc}}\left(\frac{\alpha'_1 x_1}{\mathcal{D}^e_{1M}} + \frac{\alpha'_2 x_2}{\mathcal{D}^e_{2M}}\right) - \alpha'_i \mathcal{D}_{\text{visc}}\left(\frac{x_1}{\mathcal{D}^e_{1M}} + \frac{x_2}{\mathcal{D}^e_{2M}}\right)\right]}, \quad i = 1,2 \quad (120)$$

$$E_{ij} = \frac{1}{\frac{1}{\mathcal{D}^e_{ij}} + \frac{\alpha'_i \mathcal{D}_{\text{visc}}}{\mathcal{D}^e_{iM}\mathcal{D}^e_{jM}} \frac{1}{\left[1 + \mathcal{D}_{\text{visc}}\left(\frac{\alpha'_1 x_1}{\mathcal{D}^e_{1M}} + \frac{\alpha'_2 x_2}{\mathcal{D}^e_{2M}}\right)\right]}}, \quad i,j = 1,2. \quad (121)$$

A lucid explanation of the differences in the behaviour of the E and $\mathcal{D}^e$ coefficients is given in Mehta *et al.* (1976). For dilute solutions of species 2 (say a protein) in which there is no slip of the solvent species 1 [say water; cf. eq. (104)] the relation between the Lightfoot and Mason coefficients further simplify to yield

$$\frac{1}{E_{12}} = \frac{1}{\mathcal{D}^e_{12}} + \frac{1}{\mathcal{D}^e_{2M}} \quad (122)$$

$$\frac{1}{E_{21}} = \alpha_2\left(\frac{1}{\mathcal{D}^e_{12}} + \frac{1}{\mathcal{D}^e_{2M}}\right) \quad (123)$$

$$E_{1M} = \mathcal{D}_{\text{visc}} \quad (124)$$

$$\frac{1}{E_{2M}} = (\alpha_2 - 1)\left(\frac{1}{\mathcal{D}^e_{12}} - \frac{1}{\mathcal{D}^e_{2M}}\right) \quad (125)$$

which shows that E_{1M} is purely viscous in nature and that there is a possibility of obtaining negative values for E_{2M}!

The Lightfoot formulation (111) has been used to model transport across ultrafiltration (Robertson and Zydney, 1988), dialysis (Keurentjes *et al.*, 1992) and ion-exchange membranes (Scattergood and Lightfoot, 1968; Wills and Lightfoot, 1966). The experimental data of Keurentjes *et al.* (1992) for transport of sodium oleate–isopropanol–water mixtures through a cellulose dialysis membrane into a aqueous solution of NaCl are particularly interesting because they found upwind diffusion and flux reversal occurred during the transient experiments. Scattergood and Lightfoot (1968) have shown that the drag between counterions and water for transport across an electrodialysis membrane could cause a significant flux of water even though there is a negligible pressure gradient (i.e. negligible viscous transport of water).

In a recent paper, Kerkhof (1996) criticizes the basis of the Mason formulation of intra-particle transport and presents arguments in favour of the Lightfoot formulation. In this context the reader's attention is drawn to the paper by MacElroy and Kelly (1985), who use the dense fluid kinetic theory as a basis for deriving the intraparticle transport relations.

The solution-diffusion model for intra-membrane transport (e.g. Wijmans and Baker, 1995) views the membrane as a pseudo-homogeneous phase. The Lightfoot formulation (111) is equally applicable to describe this model, and simplified forms of this equation are used in practice.

Diffusion within micropores

Within micropores, surface forces are dominant and an adsorbed molecule never escapes from the force field of the surface even when at the centre of the pore. Steric effects are important and diffusion is an activated process, proceeding by a sequence of jumps between regions of low potential energy (sites); see Fig. 56. Since the diffusing molecules never escape from the force field of the pore walls the fluid within the pore can be regarded as a single 'adsorbed' phase (Kärger and Ruthven, 1992). Diffusion within this regime is variously known as configurational diffusion, intra-crystalline diffusion, micropore diffusion or simply surface diffusion. In this section we consider the extension of the Maxwell–Stefan formulation, generally accepted for description of diffusion in bulk fluid phases to the description of diffusion inside micropores. The treatment here essentially follows the ideas and concepts developed first by Krishna (1990, 1993a, b).

Let us consider diffusion of n adsorbed molecular species along a surface within the pores of a catalyst, adsorbent or membrane. In developing our formulation for surface diffusion it is convenient to have a simple physical picture for surface diffusion in mind. Such a simple physical model is depicted in Fig. 56

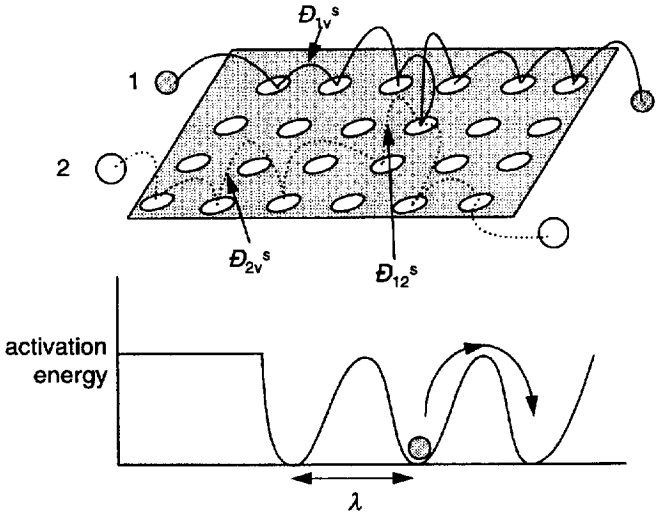

Fig. 56. A conceptual model for surface diffusion of adsorbed species 1 and 2. $Đ_{1V}^s$ and $Đ_{2V}^s$ are the Maxwell–Stefan surface diffusivities of components 1 and 2. $Đ_{12}^s$ represents the Maxwell–Stefan counter-sorption coefficient.

that shows molecules hopping from one adsorption site to another. One such description of the hopping model can be found in Gilliland *et al.* (1974). We can extend the dusty gas model approach (Mason and Malinauskas, 1983) to the description of surface diffusion by considering the vacant sites to be the $(n+1)$th pseudo-species in the (surface) system

$$-\nabla\mu_i = RT\sum_{j=1}^{n}\theta_j\frac{(\mathbf{u}_i-\mathbf{u}_j)}{Đ_{ij}^s} + RT\theta_{n+1}\frac{(\mathbf{u}_i-\mathbf{u}_{n+1})}{Đ_{i,n+1}^s}, \quad i=1,2,\ldots,n \tag{126}$$

where $-\nabla\mu_i$, the surface chemical potential gradient, is the force acting on species i tending to move it along the surface. The first term on the right-hand side of eq. (126) reflects the friction exerted by adsorbate j on the surface motion of adsorbed species i. The second right member reflects the friction experienced by the species i from the vacancies. The θ_i represents the fractional occupancy of the sites by the adsorbed species i and θ_{n+1} represents the fraction of unoccupied, vacant, sites

$$\theta_{n+1} = \theta_V = 1-\theta_1-\theta_2-\cdots-\theta_n = 1-\theta_t. \tag{127}$$

In analogy with the definition of the Knudsen diffusivity [cf. eq. (81)] we define the Maxwell–Stefan surface diffusivity as

$$Đ_{iV}^s \equiv \frac{Đ_{i,n+1}^s}{\theta_{n+1}} \tag{128}$$

The Maxwell–Stefan diffusivities $Đ_{iV}^s$ are entirely equivalent to the thermodynamically corrected diffusivities as defined by Ruthven (1984). Mechanistically, the Maxwell–Stefan surface diffusivity $Đ_{iV}^s$ may be related to the displacement of the adsorbed molecular species, λ, and the jump frequency, $\nu_i(\theta_t)$, which in general can be expected to be dependent on the total surface coverage (Aust *et al.*, 1989; Reed and Ehrlich, 1981a, b; Riekert, 1971; Zhdanov, 1985)

$$Đ_{iV}^s = \frac{1}{z}\lambda^2\,\nu_i(\theta_t) \tag{129}$$

where z represent the number of nearest neighbour sites. If the jump frequency remains constant, independent of surface coverage, i.e. $\nu_i(\theta_i) = \nu_i(0)$, the Maxwell–Stefan surface diffusivity $Đ_{iV}^s$ is also independent of surface coverage

$$\nu_i(\theta_t) = \nu_i(0), \quad Đ_{iV}^s = \frac{1}{z}\lambda^2\nu_i(0). \tag{130}$$

Another possibility is that due to interactions between adsorbed species the jump frequency decreases with surface coverage. If we assume that a molecule can migrate from one site to another only when the receiving site is vacant (Barrer, 1978; Riekert, 1971); the chance of this is proportional to $\theta_V \equiv (1-\theta_1-\theta_2\cdots-\theta_n)$ so that

$$\nu_i(\theta_t) = \nu_i(0)\theta_V, \quad Đ_{iV}^s = \frac{1}{z}\lambda^2\nu_i(0)\theta_V. \tag{131}$$

Okubo and Inoue (1988) demonstrate the possibility of enhancing the diffusivity $Đ_{iV}^s$ by modification of the properties of the surface, for example, by covering with hydrophilic groups which interact with the adsorbed molecules.

For zeolitic structures with interconnected cages, such as zeolite A or X, eq. (129) can be modified to the form

$$Đ_{iV}^s = \frac{1}{mz}\lambda^2\nu_i(\theta) = \frac{1}{mz}\lambda^2\nu_i(0)(1-\theta^{mz}) = Đ_{iV}^s(0)(1-\theta^{mz}) \tag{132}$$

where m represents the maximum number of molecules per cage and the factor mz represents the maximum number of nearest-neighbour sites per cage and $(1-\theta^{mz})$ is the probability that at least one of the nearest neighbour sites is vacant. For pore-type structures such as ZSM-5 we may take $m = 1$ and $z = 1$. For zeolites with three-dimensional cage structures, such as zeolite A and X, we may take $m = 2$ and $z = 4$ (Van den Broeke, 1995).

The coefficients $Đ^s_{ij}$ express the adsorbate i– adsorbate j interactions. We can consider this coefficient as representing the facility for counterexchange, i.e. at an adsorption site the sorbed species j is replaced by the species i; see Fig. 56. The countersorption coefficient $Đ^s_{ij}$ may therefore be expected to be related to the jump frequency of the species i and j. As a simple (limiting case) model we can imagine that the countersorption diffusivity will be dictated by the lower of the two frequencies ν_i and ν_j, i.e.

$$Đ^s_{ij} = \frac{1}{z}\lambda^2 \nu_j(\theta_t), \quad \nu_j < \nu_i. \tag{133}$$

Within a single narrow pore of zeolite crystals the mechanism of countersorption cannot prevail because there is room for only one type of molecular species at any given time; we refer to this situation as single file diffusion mechanism. Strictly speaking the term single file diffusion has to be reserved for the case in which the molecules are too large to pass one another. If we take into account the contribution of a bank of parallel pores along with cages, the possibility of countersorption cannot be ruled out; see Fig. 57.

An alternative procedure for the estimation of the countersorption diffusivity has been suggested by Krishna (1990) based on the generalization of Vignes (1966) relationship for diffusion in bulk liquid mixtures

$$Đ^s_{ij} = [Đ^s_{iV}(0)]^{\theta_i/(\theta_i+\theta_j)}[Đ^s_{jV}(0)]^{\theta_j/(\theta_i+\theta_j)}. \tag{134}$$

Micropore diffusion is an activated process and this is evidenced by the fact that the Maxwell–Stefan micropore diffusivity follows an Arrhenius temperature dependence, as illustrated for the diffusion on n-butane in silicalite-1 (Kapteijn *et al.*, 1994); see Fig. 58.

Assuming equilibrium between the surface and the bulk fluid we have the following relationship for the surface chemical potential μ_i of species i:

$$\mu_i = \mu_i^0 + RT\ln(f_i) \tag{135}$$

where μ_i^0 is the chemical potential in the chosen standard state and f_i is the fugacity of species i in the bulk fluid mixture. For not too high system pressures the component partial pressures, p_i, can be used in place of the component fugacities, f_i, i.e. $f_i = p_i$. The surface chemical potential gradients may be expressed in terms of the gradients of the surface occupancies by introduction of the matrix of thermodynamic factors

$$\frac{\theta_i}{RT}\nabla\mu_i = \sum_{j=1}^{n}\Gamma_{ij}\nabla\theta_j, \quad \Gamma_{ij} \equiv \theta_i\frac{\partial \ln p_i}{\partial\theta_j}, \quad i,j = 1,2\cdots,n. \tag{136}$$

For the Langmuir isotherm,

$$\theta_i = \frac{q_i^*}{q_{sat}} = \frac{b_i p_i}{1+\sum_{j=1}^{n} b_j p_j}, \quad b_i p_i = \frac{\theta_i}{1-\theta_t} \tag{137}$$

the elements of $[\Gamma]$ are

$$\Gamma_{ij} = \delta_{ij} + \frac{\theta_i}{\theta_V}, \quad i,j = 1,2,\ldots,n. \tag{138}$$

The surface concentration of component i, q_i^*, and the saturation surface concentration, q_{sat}, are commonly expressed in mol/kg of material (this is equivalent to expressing these in mmol/g as is commonly done in the literature) and the parameters b_i are usually expressed in the units Pa^{-1}.

The surface fluxes $\mathbf{N}_i^s$ of the diffusing adsorbed species are defined as

$$\mathbf{N}_i^s = \rho_p \varepsilon q_{sat}\theta_i \mathbf{u}_i \tag{139}$$

where ρ_p is the particle density usually expressed in kg/m^3 and ε is the porosity of the material. If the surface concentrations expressed in mol/kg, the fluxes $\mathbf{N}_i^s$ are obtained in the units of $mol\,m^{-2}s^{-1}$. The

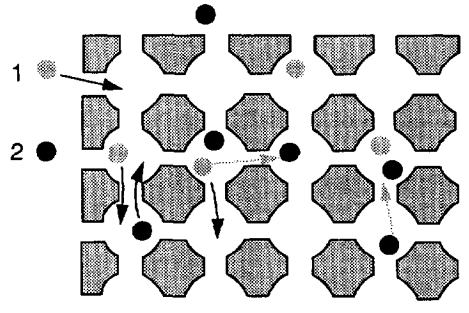

Fig. 57. Zeolitic diffusion in cage-type structures. The jump frequency of any molecule depends on the number of vacant nearest neighbour sites.

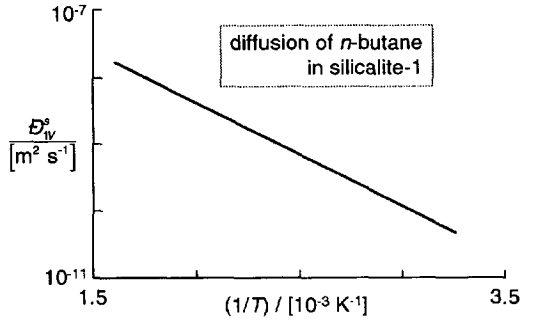

Fig. 58. Maxwell–Stefan micropore diffusivity of n-butane in silicalite-1. Adapted from Kapteijn *et al.* (1994).

vacant sites can be considered to be stationary, so

$$\mathbf{u}_{n+1} = 0. \tag{140}$$

Combining eqs (126), (139), and (140) we obtain

$$-\frac{\theta_i}{RT}\nabla\mu_i = \sum_{\substack{j=1\\ j\neq 1}}^{n} \frac{\theta_j \mathbf{N}_i^s - \theta_i \mathbf{N}_j^s}{\rho_p \varepsilon q_{sat} Đ_{ij}^s} + \frac{\mathbf{N}_i^s}{\rho_p \varepsilon q_{sat} Đ_i^s},$$

$$i = 1, 2, \ldots, n \tag{141}$$

which equation may be cast into n-dimensional matrix notation

$$-\rho\varepsilon q_{sat}[\Gamma](\nabla\theta) = [B^s](\mathbf{N}^s) \tag{142}$$

where the matrix $[B^s]$ has the elements

$$B_{ii}^s = \frac{1}{Đ_i^s} + \sum_{\substack{j=1\\ j\neq 1}}^{n} \frac{\theta_j}{Đ_{ij}^s}, \quad B_{ij}^s = -\frac{\theta_i}{Đ_{ij}^s}, \quad i,j = 1, 2, \ldots, n. \tag{143}$$

If we define a matrix of Fick surface diffusivities $[D^s]$ by

$$(\mathbf{N}^s) = -\rho_p \varepsilon q_{sat}[D^s](\nabla\theta) \tag{144}$$

we can obtain the following explicit expression for $[D^s]$:

$$[D^s] = [B^s]^{-1}[\Gamma]. \tag{145}$$

For single file diffusion mechanism, with no possibility of counterexchange between the adsorbed species i and j, the above equations simplify to give the following expressions for the Fick surface diffusivity matrix $[D^s]$:

$$[D^s] = \begin{bmatrix} Đ_{1V}^s & 0 & 0 & 0 \\ 0 & Đ_{2V}^s & 0 & 0 \\ 0 & 0 & \ddots & 0 \\ 0 & 0 & 0 & Đ_{nV}^s \end{bmatrix} [\Gamma]. \tag{146}$$

The Fick surface diffusivity matrix $[D^s]$ portrays a conglomerate of these two effects, namely, (i) the surface mobilities embodied in the $Đ_{iV}^s$, which can be determined from single-component sorption kinetic data, and (ii) the fluid–solid adsorption equilibrium ('isotherm') embodied in the thermodynamic matrix $[\Gamma]$.

For single component diffusion, eq. (144) reduces to the scalar form

$$\mathbf{N}_1^s = -\rho_p \varepsilon q_{sat} D_1^s \nabla\theta_1 \tag{147}$$

where the Fick surface diffusivity is [cf. eq. (145)]

$$D_1^s = Đ_{1V}^s \Gamma. \tag{148}$$

For the Langmuir adsorption isotherm the thermodynamic factor Γ is

$$\Gamma = \frac{1}{1-\theta_1} \tag{149}$$

and so

$$D_1^s = \frac{Đ_{1V}^s}{(1-\theta_1)}. \tag{150}$$

In the vast literature on micropore diffusion (Ruthven, 1984; Yang, 1987) the Maxwell–Stefan surface diffusivity $Đ_{1V}^s$ is also referred as the 'corrected diffusivity'. If $Đ_{1V}^s$ decreases with surface coverage following eq. (131), then the Fick surface diffusivity D_1^s must be independent of surface coverage. On the other hand, if $Đ_{1V}^s$ is independent of surface coverage [cf. eq. (130)], D_i^s should exhibit a sharp increase with θ_1. Such behaviour has been experimentally observed, for example, for the diffusion of oxygen and nitrogen in carbon molecular sieve (Chen *et al.*, 1994); see Fig. 59. The overall effect of the surface coverage dependence of D_i^s is to enhance the uptake during *ad*sorption and reduce it during *de*sorption (Garg and Ruthven, 1972; Kapoor and Yang, 1991). Figure 60 illustrates this asymmetry, which is reminiscent of the asymmetry observed in ion exchange (cf. Figs 35 and 48).

Use of other adsorption isotherms such as Freundlich, Dubinin–Radushkevich, Toth, Langmuir–Freundlich result in different correction factors as illustrated by Seidel and Carl (1989) for diffusion of phenol and indole from aqueous solution in activated carbon. Modification of eq. (150) to account for surface heterogeneity is developed by Kapoor and Yang (1989, 1990). Connectivity effects for surface diffusion on heterogeneous surfaces are analysed by Zgrablich

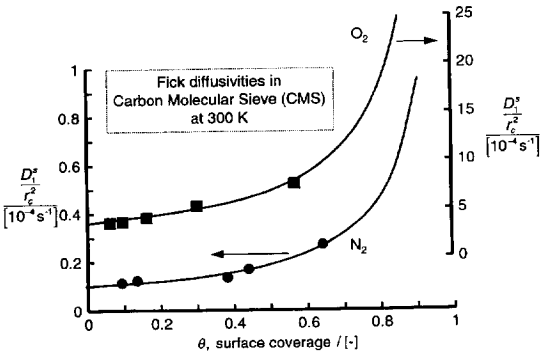

Fig. 59. Variation of Fick micropore diffusivity with surface coverage. Data for oxygen and nitrogen in carbon molecular sieve. Data from Chen *et al.* (1994).

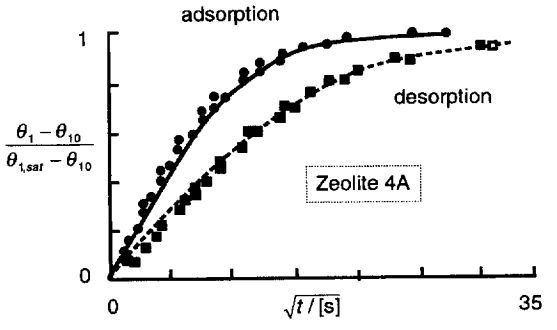

Fig. 60. Transient uptake profiles during adsorption and desorption of ethane in zeolite 4A. Adapted from Garg and Ruthven (1972).

et al. (1986). Multilayer surface adsorption is considered by Chen and Yang (1993).

Chen and Yang (1991) have developed a model for describing the surface coverage dependence of the Fick diffusivity in zeolitic structures by introducing a parameter Λ to account for pore blockage:

$$\frac{D_1^s}{\mathcal{D}_{1V}^s(0)} = \frac{1-\theta+\frac{\Lambda}{2}\theta(2-\theta)+H(1-\Lambda)(1-\Lambda)\frac{\Lambda}{2}\theta^2}{(1-\theta+\frac{1}{2}\Lambda\theta)^2} \tag{151}$$

This function is plotted as a function of the surface coverage θ for a variety of pore blockage parameters Λ in Fig. 61(a). Shown alongside in Fig. 61(b) is a plot of $D_1^s/\mathcal{D}_{1V}^s(0)$ for various assumed dependencies of the jump frequency on the surface occupancy $v_i(\theta_i)$. Inserting the value $\Lambda = 0$ results in eq. (150), which is representative of surface diffusion. Gutsche (1993) in a study of the diffusion of ammonia in A-type zeolite crystals have used eq. (148) taking $\mathcal{D}_{1V}^s$ to be constant; this is tantamount to assuming $\Lambda = 0$. Chen and Yang (1991) fitted the data for diffusion in zeolite A to obtain values of $\Lambda \approx 0.3$. Such a behaviour is perhaps typical of zeolites A and X which have interconnected cages and the results with $\Lambda \approx 0.3$ correspond closely to those of eq. (132) using $m = 2$ and $z = 4$. For $\Lambda = 2$, we note that the Fick diffusivity is practically independent of the surface coverage. This is equivalent to assuming that the jump frequency decreases with surface coverage following eq. (131), a scenario typical of pore-type zeolites such as ZSM-5; here we can take $m = 1$ and $z = 1$ (Van den Broeke, 1995). Indeed, Chen and Yang (1991) could fit the Qureshi and Wei (1990) data for diffusion in ZSM-5 taking $\Lambda = 2.11$.

Pore-blocking effects in ZSM-5 have been modelled by Theodorou and Wei (1983) using Monte-Carlo techniques. Tsikoyiannis and Wei (1991) use the theory of Markov jump processes to model zeolitic diffusion and reaction as a sequence of elementary jump events taking place in a finite periodic lattice. The estimation of $\mathcal{D}_{iV}^s$ for zeolitic structures is still an active area of research (Chen *et al.*, 1994; Wei, 1994).

For single file diffusion (SFD) involving two components, eqs (144)–(146) reduce to the two-dimensional form

$$(\mathbf{N}^s) = -\rho_p \varepsilon q_{sat} \begin{bmatrix} \mathcal{D}_{1V}^s & 0 \\ 0 & \mathcal{D}_{2V}^s \end{bmatrix} [\Gamma](\nabla\theta). \tag{152}$$

If we use the Langmuir isotherm to calculate $[\Gamma]$, we obtain

$$(\mathbf{N}^s) = -\rho_p \varepsilon q_{sat} [D^s](\nabla\theta),$$

$$[D^s] = \begin{bmatrix} \mathcal{D}_{1V}^s & 0 \\ 0 & \mathcal{D}_{2V}^s \end{bmatrix} \frac{\begin{bmatrix} 1-\theta_2 & \theta_1 \\ \theta_2 & 1-\theta_1 \end{bmatrix}}{1-\theta_1-\theta_2}. \tag{153}$$

An important extension of the approach discussed above is due to Chen and Yang (1992), Chen *et al.* (1993) and Sikavitsas and Yang (1995), who have derived a more general expression for the thermodynamic factor $[\Gamma]$ taking interaction between sorbed species into account. When such interactions are neglected their model reduces to eq. (153).

The effective Fick surface diffusivities D_i^s defined by

$$D_i^s \equiv \frac{-\mathbf{N}_i^s}{\rho_p \varepsilon q_{sat} \nabla\theta_i} \tag{154}$$

can be obtained by comparing eqs (153) and (154):

$$D_1^s = \frac{\mathcal{D}_{1V}^s}{(1-\theta_1-\theta_2)}\left((1-\theta_2)+\theta_1\frac{|\nabla\theta_2|}{|\nabla\theta_1|}\right) \tag{155}$$

$$D_2^s = \frac{\mathcal{D}_{2V}^s}{(1-\theta_1-\theta_2)}\left((1-\theta_1)+\theta_2\frac{|\nabla\theta_1|}{|\nabla\theta_2|}\right)$$

which coincide with those given by Habgood (1958) and Round *et al.* (1966). While Habgood and Round

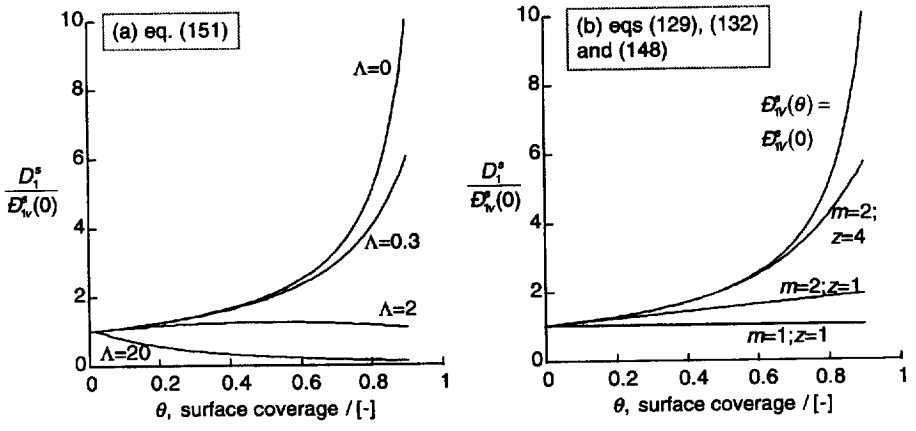

Fig. 61. Influence of the surface coverage and zeolite structural parameters on the Fick micropore diffusivity. Adapted from (a) Chen and Yang (1991) and (b) Van den Broeke (1995).

derived the above expressions specifically for a two-component system our approach can be easily extended to the general multicomponent case. Srinivasan *et al.* (1995) have shown that eqs (155) can also be derived assuming Langmuir kinetics for the sorption process. From eqs (155) we see that the effective surface diffusivities are strong functions of surface concentrations and surface concentration gradients. Further the effective diffusivity of component 1 is affected by the surface concentration gradient of component 2.

In order to illustrate the coupling effect, let us consider the example of the uptake of a mixture of *n*-heptane(1) and benzene (2) by NaX zeolite. The zeolite crystals are exposed to a bulk vapour mixture maintaining a constant composition environment of benzene and *n*-heptane and the uptake of these components by the zeolite is monitored as a function of time. The observed transient uptake profiles as measured experimentally by Kärger and Bülow (1975) are shown in Fig. 62. The profile for *n*-heptane exhibits a remarkable maximum at $t = 50$ min ($Fo = 0.015$) with the surface concentration reaching a value significantly higher than the final (low) equilibrium surface concentration value. The results can be explained physically as follows. The Maxwell–Stefan surface mobility of *n*-heptane $Đ^s_{1V}$ is about 50 times larger than the corresponding mobility of benzene $Đ^s_{2V}$; this is because of differences in the molecular configurations. Initially, beginning with fresh zeolite crystals, *n*-heptane quickly penetrates the pores of the zeolite occupying the sorption sites. The sorption strength of *n*-heptane is, however, considerably lower than that of benzene due *inter alia* to differences in polarity. The adsorbed *n*-heptane eventually gets displaced from the sorption sites by benzene and the surface concentration of *n*-heptane decreases from its maximum value to reach its final low saturation value. At equilibrium, achieved after about 5 h ($Fo = 0.09$), the pores of the zeolite are occupied predominantly by the strongly adsorbed benzene.

The transient uptake process can be simulated by solving the equations of continuity

$$\frac{\partial \theta_i}{\partial t} = \nabla \cdot (D_i^s \nabla \theta_i), \quad i = 1, 2 \tag{156}$$

together with eq. (155) and are also shown in Fig. 62 (for details of the calculations see Krishna, 1990; 1993a, b). The curious maximum in the *n*-heptane uptake is properly simulated. That the coupling effects are to be attributed to the thermodynamic matrix $[\Gamma]$ can be demonstrated by performing the simulations taking $[\Gamma]$ to be identity matrix, i.e.

$$[D^s] = \begin{bmatrix} Đ^s_{1V}(0) & 0 \\ 0 & Đ^s_{2V}(0) \end{bmatrix}. \tag{157}$$

The simulations using eq. (157), shown in Fig. 63 as dotted lines, predict monotonic approaches to equilibrium for both species, which deviates qualitatively from the experimental observations (cf. Fig. 62). Put another way, the observed non-monotonic behaviour observed experimentally in Fig. 62 for the uptake profile of *n*-heptane is due to the presence of non-diagonal elements in the Fick surface diffusivity matrix $[D^s]$. A further consequence is that counterdiffusion of binary mixtures in zeolite crystals can exhibit asymmetric behaviour (Krishna, 1990; Moore and Katzer, 1972).

Krishna and van den Broeke (1995) have shown that the curious maximum in the flux of hydrogen for transfer across a zeolite membrane in Fig. 6 can be predicted by the Maxwell–Stefan model (153); see Fig. 64. At steady state the more strongly adsorbed species has the higher flux. Use of eq. (157) with a composition-independent Fick diffusivity matrix yields a monotonous approach to steady state. Srinivasan *et al.* (1994) present another neat example of selectivity reversal with microporous membranes.

Rao and Sircar (1993) have shown the separation possibilities offered by microporous carbon membranes for separating hydrocarbons from a gaseous mixture containing hydrogen (Fig. 65). The hydrocarbons are much more strongly adsorbed than

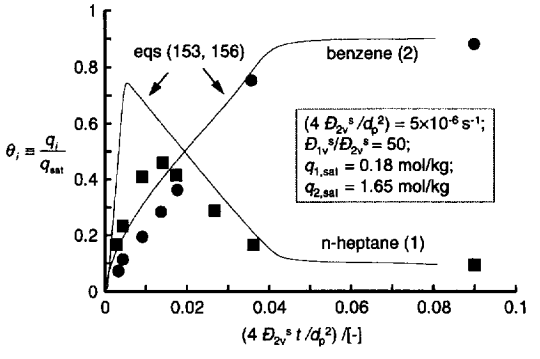

Fig. 62. Transient uptake of benzene and *n*-heptane by zeolite-X. Comparison of experimental results of Kärger and Bülow (1975) with simulations using the Maxwell–Stefan surface diffusion model.

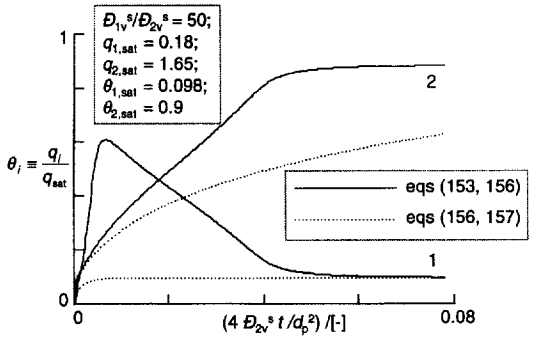

Fig. 63. Transient uptake of benzene and *n*-heptane by zeolite-X. Comparison of the Maxwell–Stefan model with a model assuming constant Fick surface diffusivities.

hydrogen and they move across the thickness of the membrane by surface diffusion. The adsorbed components then desorb at the low pressure side. In the process for recovery of hydrogen from refinery gases, the desired product hydrogen is 'rejected' at the high-pressure side of the membrane and can therefore be produced at feed pressure, eliminating the need for further product compression.

The use of the complete Maxwell–Stefan formulation including countersorption, eqs (143) together with say eq. (134), in place of the single file diffusion approximation, eq. (153) does not lead to significantly different results; see the simulation results of Fig. 66. This is a happy situation in view of the uncertainty in the prediction of the countersorption diffusivities $Đ_{ij}^s$.

For the prediction of breakthroughs in a packed bed of microporous adsorbents, Van den Broeke and Krishna (1995) have experimentally verified the superiority of the Maxwell–Stefan model (153) over the conventionally used linear driving force approximations; see Fig. 67.

Diffusional selectivity is the basis of an industrial process for the separation of nitrogen and oxygen. Despite a very small difference in the kinetic diameters of these two molecules, there is a significant difference in the Maxwell–Stefan diffusivities (cf. Fig. 59). Farooq *et al.* (1991, 1993) have shown that for simulation of a pressure swing adsorption process for air separation the use of the Maxwell–Stefan formulation (153) is essential. The simulations using the conventionally used LDF (linear driving force model) appear to be only slightly different from the Maxwell–Stefan model (cf. Fig. 68), but such small differences are apparently vital for the simulation of commercial units (Ruthven *et al.*, 1994). Micropore diffusion selectivity is also the basis of the separation of carbon dioxide from hydrocarbons using pressure swing adsorption with carbon molecular sieve sorbents (Kapoor *et al.*, 1993).

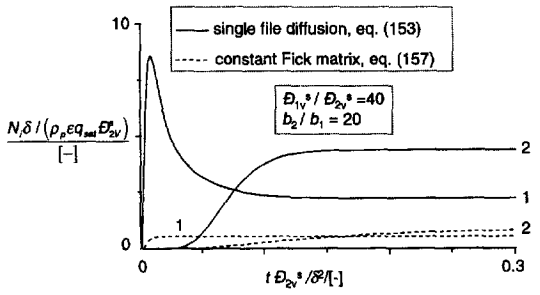

Fig. 64. Simulations for transport of hydrogen (1)– *n*-butane (2) across silicalite membrane. Comparison of the Maxwell–Stefan model with a Fick model with constant surface diffusivities. Details of model parameters and simulations are given by Krishna and van den Broeke (1995).

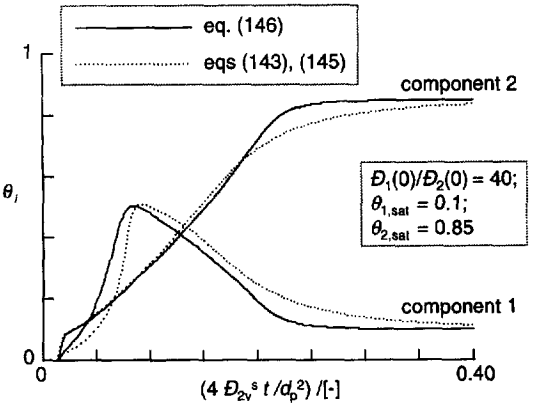

Fig. 66. Transient uptake profiles of a binary mixture inside a single spherical particle. The single file diffusion model is compared with the complete Maxwell–Stefan model including counter-sorption, with $Đ_{12}^s$ given by eq. (134).

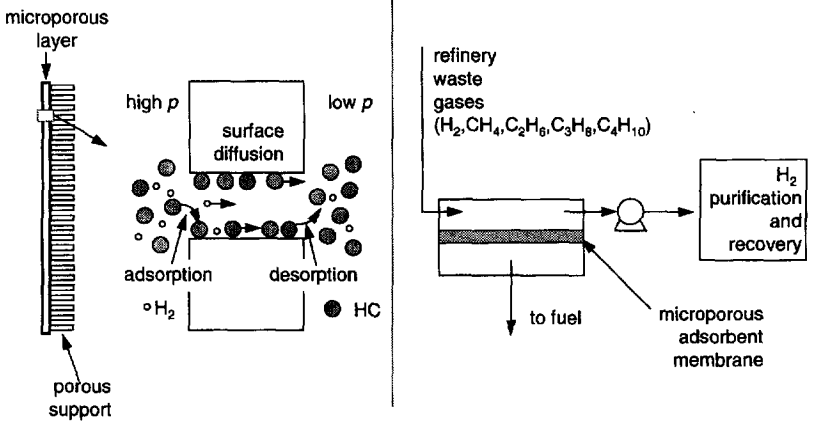

Fig. 65. A microporous carbon membrane can be used for separation of hydrocarbons from a gaseous mixture containing hydrogen. The hydrocarbons are more strongly adsorbed inside the micropores and are transported across the membrane much faster than hydrogen. Adapted from Rao and Sircar (1994).

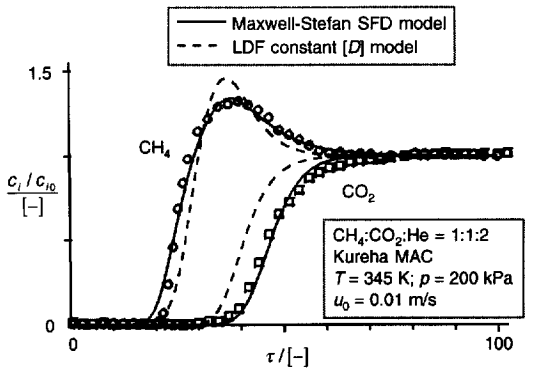

Fig. 67. Breakthrough curves for the system $CH_4/CO_2/He$ in the ratio of 1:1:2 with Kureha microporous carbon adsorbent particles. The effluent concentration is plotted on the y-axis and this is normalized with respect to the inlet concentration. On the x-axis is plotted the dimensionless time. The markers are experimental results and the solid lines are numerical fits with the single file diffusion model taking the Maxwell–Stefan diffusion coefficients $Đ^s_{1V}$ and $Đ^s_{2V}$ to be constant. Also shown are the simulations with the LDF model. Details of experimental conditions and simulations are given in Van den Broeke and Krishna (1995).

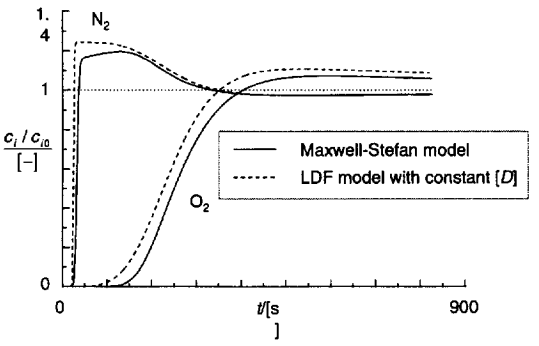

Fig. 68. Breakthrough curves for oxygen (1) and nitrogen (2) on Bergbau–Forschung carbon molecular sieve. The effluent concentration is plotted on the y-axis and this is normalized with respect to the inlet concentration c_0. The feed composition is O_2:21%; N_2:79%. Other parameters in the simulation are as follows. Packed bed length 0.7 m; column diameter = 0.035 m; inlet gas velocity = 0.038 m/s; bed porosity $\varepsilon_b = 0.4$; temperature, assumed isothermal, T = 294 K; pressure, p = 100 kPa. The Maxwell–Stefan diffusivities given as: $4\,Đ^s_{1V}/d_p^2 = 0.0027\ s^{-1}$; $4\,Đ^s_{2V}/d_p^2 = 0.000059\ s^{-1}$. The Langmuir adsorption isotherm parameters are $\rho q_{1,sat} = 2640\ mol\,m^{-3}$; $\rho q_{2,sat} = 2640\ mol\,m^{-3}$; $(b_1 RT) = 0.0035\ m^3\,mol^{-1}$; $(b_2 RT) = 0.00337\ m^3\,mol^{-1}$. Further details of simulations in Van den Broeke (1994).

In some zeolitic structures such as ZSM-5 the Maxwell–Stefan diffusivities $Đ^s_{iV}$ decrease with surface coverage following eq. (131) and so we obtain the following expression for the Fick surface diffusivity matrix:

$$[D^s] = \begin{bmatrix} Đ^s_{1V}(0) & 0 \\ 0 & Đ^s_{2V}(0) \end{bmatrix} \begin{bmatrix} 1-\theta_2 & \theta_1 \\ \theta_2 & 1-\theta_1 \end{bmatrix} \qquad (158)$$

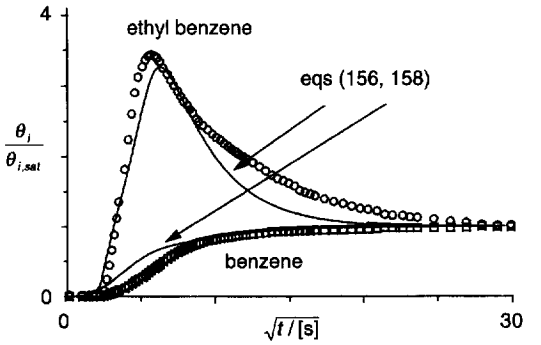

Fig. 69. Transient uptake profiles for benzene (1) and ethyl benzene (2) inside ZSM-5 crystals. The Maxwell–Stefan diffusion model is compared with experimental data of Niessen (1991). Further details of simulations are available in Van den Broeke (1995).

where $Đ^s_{iV}(0)$ represent the Maxwell–Stefan diffusivities at zero coverage. Equation (158) coincides with the expression derived by Qureshi and Wei (1990), using a different reasoning. The experimental data of Niessen (1991) for codiffusion of benzene (1)–ethyl benzene (2) in ZSM-5 can be successfully simulated by eq. (158) using only pure component diffusivities $Đ^s_{iV}$; see Fig. 69.

Sundaresan and Hall (1986) have developed a model for estimation of the Fick matrix $[Đ]$ for zeolites taking account of non-idealities arising from interaction between sorbed species as well as the effect of pore and surface blocking.

For regular structures such as zeolites, with well-defined geometry, it is possible to use Monte-Carlo simulation techniques to describe the diffusion process (Van den Broeke *et al.*, 1992; Dahlke and Emig, 1991; Palekar and Rajadhyaksha, 1985, 1986). Figure 70 compares the Monte Carlo simulations of Van den Broeke *et al.* (1992) with simulations using eqs (131) and (153). It is also interesting to note both the Monte-Carlo and Maxwell–Stefan formulations predict a maximum in the surface occupancy of the faster-moving component 2 at the same relative time scale. Both approaches also predict multiple maxima for ternary mixtures; cf. Fig. 71.

Kouyoumdjiev *et al.* (1993) have analysed single and multicomponent adsorption on activated carbon from aqueous solutions, involving both macro- and micropore diffusion, and have shown that a combination of eqs (88) and (152) allows the prediction of multicomponent behaviour on the basis of single-component transport parameters along with multicomponent adsorption equilibria.

An alternative approach to surface diffusion is to use the Onsager formulation of irreversible thermodynamics (Kärger, 1973; Yang *et al.*, 1991); in this formulation the surface fluxes are written as linear functions of the chemical potential gradients. For n-component systems we write

$$(\mathbf{N}^s) = -\rho_p \varepsilon q_{sat} [L^s] \frac{1}{RT} (\nabla \mu) \qquad (159)$$

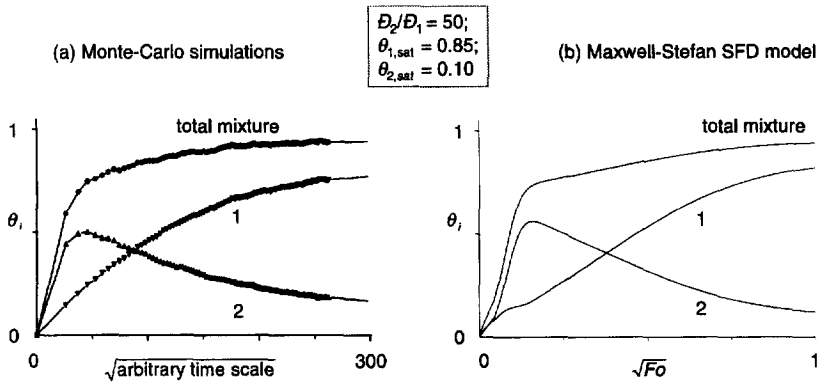

Fig. 70. Transient uptake profiles for binary diffusion in a square lattice of 25 × 25 sites. The Monte-Carlo simulations are compared with the Maxwell–Stefan single file diffusion model. Details of simulations are available in Van den Broeke *et al.* (1992).

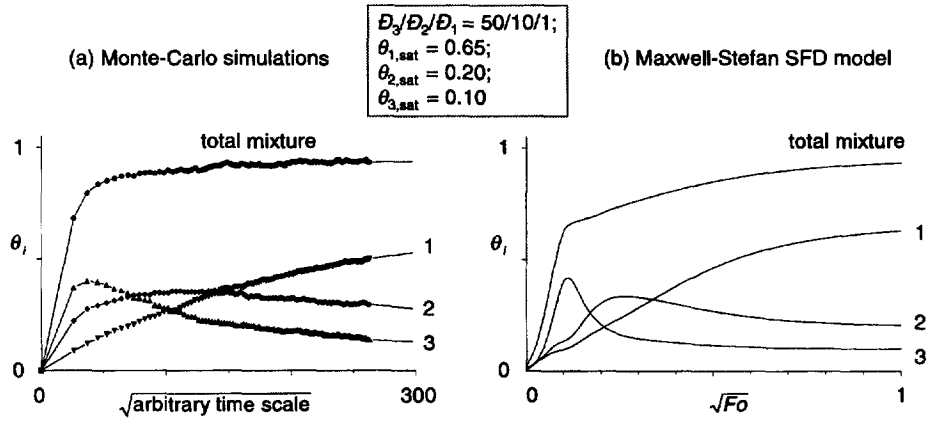

Fig. 71. Transient uptake profiles for ternary diffusion in a square lattice of 25 × 25 sites. The Monte-Carlo simulations are compared with the Maxwell–Stefan single file diffusion model. Details of simulations are available in Van den Broeke *et al.* (1992).

from the Onsager reciprocal relations we conclude that the matrix $[L^s]$ is symmetric, i.e.

$$L^s_{ik} = L^s_{ki}, \quad i,k = 1,2, \ldots, n. \tag{160}$$

The chemical potential gradients may be related to the gradient of the surface occupancies [cf. eq. (136)]

$$\frac{1}{RT}\nabla\mu_i = \sum_{j=1}^{n} \frac{1}{p_i}\frac{\partial p_i}{\partial \theta_j}\nabla\theta_j = \frac{1}{\theta_i}\sum_{j=1}^{n}\Gamma_{ij}\nabla\theta_j. \tag{161}$$

Combining eqs (160) and (161) we obtain

$$(\mathbf{N}^s) = -\rho_p \varepsilon q_{sat}[L^s]\begin{bmatrix} 1/\theta_1 & 0 & 0 \\ 0 & \ddots & 0 \\ 0 & 0 & 1/\theta_n \end{bmatrix}[\Gamma](\nabla\theta). \tag{162}$$

Comparison of eqs (144), (145) and (162) gives the relation between $[D^s]$, $[B^s]$ and $[L^s]$:

$$[B^s]^{-1} = [L^s]\begin{bmatrix} 1/\theta_1 & 0 & 0 \\ 0 & \ddots & 0 \\ 0 & 0 & 1/\theta_n \end{bmatrix},$$

$$[D^s] = [L^s]\begin{bmatrix} 1/\theta_1 & 0 & 0 \\ 0 & \ddots & 0 \\ 0 & 0 & 1/\theta_n \end{bmatrix}[\Gamma]. \tag{163}$$

The Onsager reciprocal relations

$$L^s_{ik} = L^s_{ki} \quad (i \neq k) \tag{164}$$

are equivalent to assuming symmetry of the counter-sorption diffusivities $Đ^s_{ik} = Đ^s_{ki}$. Though the Onsager formulation is equivalent to the Maxwell–Stefan formulation it is not as convenient for the prediction of the transport parameters.

CONCLUDING REMARKS

In this review we have attempted to develop a unified approach to mass transfer processes by using the Maxwell–Stefan formulation. This approach has been shown to be able to handle all processes of interest to chemical engineers and in many cases lead to superior predictions than the more conventionally used Fick formulation. In some cases where uphill diffusion can

occur the Fick approach fails even at the qualitative level to describe the mass transfer phenomena. With the availability of suitable text books (Cussler, 1976; Jackson, 1977; Lightfoot, 1974; Mason and Malinauskas, 1983; Taylor and Krishna, 1993; Wesselingh and Krishna, 1990; Zarzycki and Chacuk, 1993), the Maxwell–Stefan approach can be easily taught even at the undergraduate level.

Acknowledgements

The subject of this journal review is taught by the authors to university and industrial researchers in a one-week course entitled *A Unified Approach to Mass Transfer*, conducted regularly in The Netherlands under the auspices of the *Onderzoekschool Procestechnologie* (OSPT), the Dutch National Graduate Research School in Chemical Engineering. R. K. and J.A.W. acknowledge financial support from the OSPT for updating the course material; this has partly contributed to the preparation of this review.

The authors gratefully acknowledge comments, criticisms, suggestions and corrections received on the first draft of the manuscript from R. B. Bird (Wisconsin), D. W. F. Brilman (Twente), A. Gorak (Dortmund), A. Heintz (Rostock), H. Hofmann (Erlangen), F. J. Keil (Hamburg-Harburg), P. J. A. M. Kerkhof (Eindhoven), H. Martin (Karlsruhe), A. Rodrigues (Porto), E. U. Schlünder (Karlsruhe), R. Srinivasan (Air Products, Allentown), K. Sundmacher (Clausthal), D. Tondeur (Nancy) and J. W. Veldsink (Groningen).

NOTATION

b_i parameter in the Langmuir adsorption isotherm, kPa^{-1} or Pa^{-1}

B_0 permeability, m^2

$[B]$ square matrix of inverted Maxwell–Stefan diffusivities, eq. (26) or eq. (69), $m^{-2}\,s$

$[B^e]$ square matrix of inverted Maxwell–Stefan intrapore diffusivities, eq. (87), $m^{-2}\,s$

$[B^s]$ square matrix of inverted Maxwell–Stefan micropore diffusivities, eq. (143), $m^{-2}\,s$

c_0 inlet (at $z = 0$) molar concentration of the fluid mixture, $mol\,m^{-3}$

c_i molar concentration of species i, $mol\,m^{-3}$

c_t total molar concentration of the fluid mixture, $mol\,m^{-3}$

$\mathbf{d}_i$ generalized driving force, eq. (53), m^{-1}

d_p particle diameter, m

d_0 pore diameter, m

D Fick diffusivity in binary mixture, $m^2\,s^{-1}$

D_i effective Fick diffusivity of species i, $m^2\,s^{-1}$

D_i^s effective Fick micropore diffusivity of species i, $m^2\,s^{-1}$

$[D]$ square matrix of Fick diffusivities, eq. (27), $m^2\,s^{-1}$

$[D^s]$ square matrix of Fick micropore diffusivities, eq. (145), $m^2\,s^{-1}$

D_i^T thermal diffusion coefficient of component I, eq. (46), $kg^{-1}\,m^5\,s^{-1}$

$Đ_{ij}$ Maxwell–Stefan i–j pair diffusivity, $m^2\,s^{-1}$

$Đ_{ij}^e$ effective bulk diffusivity of binary pair i–j in porous medium, $m^2\,s^{-1}$

$Đ_{iM}^e$ effective Knudsen diffusivity of binary pair i–j in porous medium, $m^2\,s^{-1}$

$Đ_{iV}^s(0)$ Maxwell–Stefan diffusivity at zero coverage, $m^2\,s^{-1}$

$Đ_{iV}^s$ Maxwell–Stefan micropore diffusivity of component i, $m^2\,s^{-1}$

$Đ_{ij}^s$ Maxwell–Stefan micropore countersorption diffusivity, $m^2\,s^{-1}$

$Đ_{visc}$ 'viscous' diffusivity, defined by eq. (106), $m^2\,s^{-1}$

$\bar{Đ}_M$ parameter defined by eq. (116), $m^2\,s^{-1}$

$\bar{Đ}_M^0$ parameter defined by eq. (116), $m^2\,s^{-1}$

E_{ij} Lightfoot transport coefficients for i–j pair, see eq. (111), $m^2\,s^{-1}$

E_{iM} Lightfoot transport coefficients for i–M pair, see eq. (111), $m^2\,s^{-1}$

$\mathbf{E}$ energy flux, $W\,m^{-2}$

f_i fugacity of species i, $f_i = p_i$ for ideal gases, Pa

$\tilde{\mathbf{F}}_i$ the body force acting per kg of species i, $N\,kg^{-1}$

$\mathbf{F}_i$ the body force acting per mol of species i, $N\,mol^{-1}$

$\mathscr{F}$ Faraday constant, 96,500 $C\,mol^{-1}$

Fo Fourier number, $(= 4Đt/d_p^2)$ (single particle)

$H(x)$ Heavyside function

$\bar{H}_i$ partial molar enthalpy of species i, $J\,mol^{-1}$

$\mathbf{i}$ current, A

$[I]$ identity matrix, dimensionless

$(\mathbf{J})$ $(n-1)$-dimensional column vector of diffusion fluxes, $mol\,m^{-2}\,s^{-1}$

$\mathbf{J}_i$ molar diffusion flux of species i relative to the molar average reference velocity $\mathbf{u}$, $mol\,m^{-2}\,s^{-1}$

$[k]$ matrix of multicomponent mass transfer coefficients, eq. (40), $m\,s^{-1}$

ℓ length of diffusion path, e.g. capillary tube, m

$[L^s]$ matrix of Onsgager micropore diffusivities, eq. (162), $m^2\,s^{-1}$

m maximum number of molecules per cage, dimensionless

M_i molar mass of species i, $kg\,mol^{-1}$

n number of diffusing species

$\mathbf{N}_i$ molar flux of species i, $mol\,m^{-2}\,s^{-1}$

$\mathbf{N}_t$ mixture molar flux, $mol\,m^{-2}\,s^{-1}$

$\mathbf{N}_{vol}$ volume flux through matrix, $m^3\,m^{-2}\,s^{-1}$

p system pressure, Pa

p_i partial pressure of species i, Pa

p_{sat} saturation vapour pressure, Pa

$\mathbf{q}$ conductive heat flux, $W\,m^{-2}$

q_i adsorbed species concentration within micropores, $mol\,kg^{-1}$

q_{sat} total saturation concentration of adsorbed species, $mol\,kg^{-1}$

q^* equilibrium concentration of adsorbed species, $mol\,kg^{-1}$

r radial distance coordinate, m

r_c radius of crystal or particle, m

R gas constant, 8.314 $J\,mol^{-1}\,K^{-1}$

$[R]$ square matrix of inverted mass transfer coefficients, eq. (41), $m^{-1}\,s$

$\mathscr{R}_i$ rate of production of i due to chemical reaction, mol m^{-3} s^{-1}
t time, s
T absolute temperature, K
$\mathbf{u}_i$ velocity of the diffusing species i, m s^{-1}
$\mathbf{u}_i^T$ augmented species velocity including thermal diffusion, eq. (45), m s^{-1}
$\mathbf{u}$ molar average mixture velocity, m s^{-1}
$\mathbf{v}$ viscous velocity of mixture, m s^{-1}
$\mathbf{v}_i$ viscous velocity of species i, m s^{-1}
$\bar{V}_i$ partial molar volume of species i, m^3 mol^{-1}
$\mathbf{w}_i$ species velocity including viscous flow contribution , m s^{-1}
x_i mole fraction of species i, dimensionless
y_i mole fraction of species i, dimensionless
z direction coordinate, m
z number of nearest neighbour sites, dimensionless
z_i charge on species i, dimensionless

Greek letters

α_i viscous selectivity parameter, eq. (95), dimensionless
α_i' modified viscous selectivity parameter, eq. (100), dimensionless
γ_i activity coefficient of species i, dimensionless
Γ thermodynamic correction factor for binary mixture, dimensionless
$[\Gamma]$ matrix of thermodynamic factors, eq. (24) or (136), dimensionless
δ length of diffusion path or thickness of membrane, m
δ_{ij} Kronecker delta ($\delta_{ij} = 1$ for $i = j$, $\delta_{ij} = 0$ for $i \neq j$)
ε porosity of particle
ε_b void fraction of adsorbent bed
η viscosity of fluid mixture, Pa s
θ_i fractional surface occupancy of component i
θ_t total surface occupancy of n species
$\theta_{i,\mathrm{sat}}$ fractional surface occupancy of component i at saturation
θ_V fraction unoccupied sites
κ_{ij} Maxwell–Stefan mass transfer coefficient of binary pair i–j, m s^{-1}
λ lateral displacement, m
Λ pore blockage parameter, eq. (151), dimensionless
μ_i molar chemical potential, J mol^{-1}
ν_i jump frequency of component i, s^{-1}
ν_i stoichiometric coefficient, dimensionless
ξ_{ij} frictional coefficient for i–j pair, N mol^{-1} m^{-1} s
ξ_{ij} frictional coefficient for interaction of i with matrix, N mol^{-1} m^{-1} s
ρ fluid mixture density, kg m^{-3}
ρ_i species density, kg m^{-3}
ρ_p particle fluid density, kg m^{-3}
σ rate of entropy production, J m^{-3} s^{-1} K^{-1}
τ tortuosity of porous medium, dimensionless
τ shear stress, N m kg^{-1}
Φ electrostatic potential, V
ω_i mass fraction of species i, dimensionless
Ω angular velocity, rad s^{-1}

Subscripts

b bulk fluid phase
i,j components in mixture
eff effective parameter
I interface parameter
p derivative at constant pressure
p particle
s salt or solute
sat parameter value at saturation
t total mixture
T derivative at constant temperature
T,p derivative at constant temperature and pressure
V vacant site
w water
δ position $z = \delta$
0 initial value or value at position $z = 0$
$n+1$ pseudo-species

Superscripts

e effective parameter for intra-matrix diffusion
L liquid
n nth component or solvent
s surface or micropore parameter
V vapour
* equilibrium value
0 standard state
$-$ denotes averaged or partial parameter
$\cdot$ pseudo-mixture of $n+1$ species including dust molecule

Vector and matrix notation

( ) component vector
[ ] square matrix

Operators

∇ gradient or nabla
Δ difference
$|\ |$ determinant operator

List of abbreviations

CVD chemical vapour deposition
HETP height of a theoretical plate
HTU height of a transfer unit
LDF linear driving force
M–S Maxwell–Stefan
MTBE methyl tert-butyl ether
NTP number of theoretical plates
PEG polyethylene glycol
SFD single file diffusion

REFERENCES

Al-Ghawas, H. A. and Sandall, O. C. (1991) Simultaneous absorption of carbon dioxide, carbonyl sulfide and hydrogen sulfide in aqueous methyldiethanolamine. *Chem. Engng Sci.* **46**, 665–676.

Anand, N., Manoja, B. G. R. and Gupta, A. K. (1994) Kinetics of adsorption on biporous solids—for a system with rectangular equilibrium—reanalysed. *Chem. Engng Sci.* **49**, 3277–3290.

Aust, E., Dahlke, K. and Emig, G. (1989) Simulation of transport and self-diffusion in zeolites with the Monte Carlo method. *J. Catal.* **115**, 86–97.

Barrer, R. M. (1978) *Zeolites and Clay Minerals as Sorbents and Molecular Sieves.* Academic Press, London, U.K.

Berg, D. A. and Harris, T. J. (1993) Characterisation of multicomponent diffusion effects in MTBE synthesis. *Ind. Engng Chem. Res.* **32**, 2147–2158.

van den Berg, G. B. and Smolders, C. A. (1992) Diffusional phenomena in membrane separatin processes. *J. Membrane Sci.* **73**, 103–118.

Bird, R. B., Stewart, W. E. and Lightfoot, E. N. (1960) *Transport Phenomena.* Wiley, New York, U.S.A.

Bres, M. and Hatzfield, C. (1977) Three gas diffusion—Experimental and theoretical studies. *Pflügers Arch.* **371**, 227–233

van Brocklin, L. P. and David, M. M. (1972) Coupled ionic migration and diffusion during liquid phase controlled ion exchange. *Ind. Engng Chem. Fundam.* **11**, 91–99.

van den Broeke, L. J. P. (1995) Simulation of diffusion in zeolitic structures. *A.I.Ch.E. J.* **41**, 2399–2414.

van den Broeke, L. J. P. and Krishna, R. (1995) Experimental verification of the Maxwell–Stefan theory for micropore diffusion. *Chem. Engng Sci.* **50**, 2507–2522.

van den Broeke, L. J. P., Nijhuis, S. A. and Krishna, R. (1992) Monte Carlo Simulations of diffusion in zeolites and comparison with the Generalized Maxwell–Stefan theory. *J. Catal.* **136**, 463–477.

Bungay, P. M. and Brenner, H. (1973) The motion of a closely fitting sphere in a fluid-filled tube. *Int. J. Multiphase Flow* **1**, 25–26.

Burganos, V. N. and Sotirchos, S. V. (1987) Diffusion in pore networks: effective medium theory and smooth field approximation. *A.I.Ch.E. J.* **33**, 1678–1689.

Burghardt, A. and Aerts, J. (1988) Pressure changes during diffusion with chemical reaction in a porous pellet. *Chem. Engng Process.* **23**, 77–87.

Burghardt, A. and Patzek, T. W. (1983) Mass and energy transport in porous, granular catalysts in multicomponent and multireaction systems. *Int. Chem. Engng* **23**, 739–751.

Chandrasekaran, S. K. and King, C. J. (1972) Multicomponent diffusion and vapor–liquid equilibria of dilute organic components in aqueous sugar solutions. *A.I.Ch.E. J.* **18**, 513–526.

Chang, H.-K. and Farhi, L. E. (1973) On mathematical analysis of gas transport in the lung. *Respir. Physiol.* **18**, 370–385.

Chang, H.-K., Tai, R. C. and Farhi, L. E. (1975) Some implications of ternary diffusion in the lung. *Respir. Physiol.* **23**, 109–120.

Chang, Y. C. and Myerson, A. S. (1986) Diffusivity of glycine in concentrated saturated and supersaturated aqueous solutions. *A.I.Ch.E. J.* **32**, 1567–1569.

Chen, Y. D. and Yang, R. T. (1991) Concentration dependence of surface diffusion and zeolitic diffusion. *A.I.Ch.E. J.* **37**, 1579–1582.

Chen, Y. D. and Yang, R. T. (1992) Predicting binary Fickian diffusivities from pure-component Fickian diffusivities for surface diffusion. *Chem. Engng Sci.* **47**, 3895–3905.

Chen, Y. D. and Yang, R. T. (1993) Surface diffusion of multilayer adsorbed species. *A.I.Ch.E. J.* **39**, 599–606.

Chen, Y. D., Yang, R. T. and Sun, L. M. (1993) Further work on predicting multi-component diffusivities from pure-component diffusivities for surface diffusion and diffusion in zeolites. *Chem. Engng Sci.* **48**, 2815–2816.

Chen, Y. D., Yang, R. T. and Uawithya, P. (1994) Diffusion of oxygen, nitrogen and their binary mixtures in carbon molecular sieve. *A.I.Ch.E. J.* **40**, 577–585.

Chen, N. Y., Degnan, T. F. and Smith, C. M. (1994) *Molecular Transport and Reaction in Zeolites. Design and Application of Shape Selective Catalysts.* VCH Publishers, New York, U.S.A.

Christensen, N. H. (1977) Multiphase ternary diffusion couples. *J. Am. Chem. Soc.* **60**, 293–296.

Cichelli, M. T., Weatherford, W. D. and Bowman, J. R. (1951) Sweep diffusion gas separation process, Part I. *Chem. Engng Progress*, **47**, 63–74.

Clark, W. M. and Rowley, R. L. (1986) The mutual diffusion coefficient of methanol—*n*-hexane near the consolute point. *A.I.Ch.E. J.* **32**, 1125–1131.

Conlisk, A. T. (1996) Analytical solutions for falling film absorption of ternary mixtures—1. Theory. *Chem. Engng Sci.* **51**, 1157–1168.

Cooper, A. R. (1974) Vector space treatment of multicomponent diffusion. In *Geochemical Transport and Kinetics*, Papers Presented at a Conference, Airlie House, Warrenton, Virginia, June 1973, eds. A. W. Hofmann, B. J. Giletti, H. S. Yoder Jr and R. A. Yund, pp. 15–30 Carnegie Institute of Washington, Carnegie.

Coumans, W. J., Kerkhof, P. J. A. M. and Bruin, S. (1994) Theoretical and practical aspects of aroma retention in spray drying and freeze drying. *Drying Technol.* **12**, 99–149.

Cunningham, R. E. and Williams, R. J. J. (1980) *Diffusion in Gases and Porous Media.* Plenum Press, New York, U.S.A.

Curtiss, C. F. and Bird, R. B. (1996) Multicomponent diffusion in polymeric liquids. *Proc. Nat. Acad. Sci.* **93**, 7440–7445.

Cussler, E. L. (1976) *Multicomponent Diffusion.* Elsevier, Amsterdam, The Netherlands.

Cussler, E. L. (1984) *Diffusion: Mass Transfer in Fluid Systems.* Cambridge University Press, Cambridge, U.S.A.

Cussler, E. L. and Breuer, M. M. (1972) Accelerating diffusion with mixed solvents. *A.I.Ch.E. J.* **18**, 812–816.

Cussler, E. L. and Lightfoot, E. N. (1965) Multicomponent diffusion involving high polymers. III. Ternary diffusion in the system polystyrene 1–polystyrene 2–toluene. *J. Phys. Chem.* **69**, 2875–2879.

Dahlke, K. D. and Emig, G. (1991) Diffusion in zeolites—A random-walk approach. *Catal. Today* **8**, 439–450.

Deen, W. M. (1987) Hindered transport of large molecules in liquid-filled pores. *A.I.Ch.E. J.* **33**, 1409–1425.

Doong, S.-J. and Yang, R. T. (1986) Bulk separation of multicomponent gas mixtures by pressure swing adsorption: pore/surface diffusion and equilibrium models. *A.I.Ch.E. J.* **32**, 397–410.

Dribika, M. M. and Sandall, O. C. (1979) Simultaneous heat and mass transfer for multicomponent distillation in a wetted-wall column. *Chem. Engng Sci.* **34**, 733–739.

Duncan, J. B. and Toor, H. L. (1962) An experimental study of three component gas diffusion. *A.I.Ch.E. J.* **8**, 38–41.

Elnashaie, S. S., Abashar, M. E. and Al-Ubaid, A. S. (1989) Simulation and optimization of an industrial ammonia reactor. *Ind. Engng Chem. Res.* **27**, 2015–2022

Elnashaie, S. S. E. H. and Abasher, M. E. E. (1993) Steam reforming and methanation effectiveness factors using the dusty gas model under industrial conditions. *Chem. Engng Process.* **32**, 177–189.

Epstein, N. (1989) On the tortuosity and the tortuosity factor in flow and diffusion through porous media. *Chem. Engng Sci.* **44**, 777–779.

Etzel, M. R. (1993) Thermodynamic mechanisms for the retention of aroma compounds during drying of foods. *A.I.Ch.E. Symp. Ser. No. 297*, **89**, 32–38.

Farooq, S., Rathor, M. N. and Hidajat, K. (1993) A predictive model for a kinetically controlled pressure swing adsorption separation process. *Chem. Engng Sci.* **48**, 4129–4141.

Farooq, S. and Ruthven, D.M. (1991) Numerical simulation of kinetically controlled pressure swing adsorption bulk separation based on a diffusion model. *Chem. Engng Sci.* **46**, 2213–2224.

Frank, M. J. W., Kuipers, J. A. M., Krishna, R. and Van Swaaij, W. P. M. (1995b) Modelling of simultaneous mass and heat transfer with chemical reaction using the Maxwell–Stefan theory—II. Non-isothermal study. *Chem. Engng. Sci.* **50**, 1661–1671.

Frank, M. J. W., Kuipers, J. A. M.,Versteeg, G. F. and Van Swaaij, W. P. M. (1995a) Modelling of simultaneous mass and heat transfer with chemical reaction using the Maxwell–Stefan theory—I. Model development and isothermal study. *Chem. Engng Sci.* **50**, 1645–1659.

Frey, D. D. (1986) Prediction of liquid-phase mass transfer coefficients in multicomponent ion exchange: comparison of matrix, film-model, and effective diffusivity methods. *Chem. Engng Commun.* **47**, 273–293.

Fullarton, D. and Schlünder, E. (1986) Diffusion distillation—a new separation process for azeotropic mixtures. *Chem. Engng Process* **20**, 255–270.

Furno, J. S., Taylor, R. and Krishna, R. (1986) Condensation of vapor mixtures. II. Simulation of some test condensers. *Ind. Engng Chem. Process Des. Dev.* **25**, 98–101.

Garg, D. R. and Ruthven, D. M. (1972) The effect of the concentration dependence of diffusivity on zeolitic sorption curves. *Chem. Engng Sci.* **27**, 417–423.

Garside, J. (1985) Industrial crystallization from solution. *Chem. Engng Sci.* **40**, 3–26.

Gibbs, B. P., Smith, E. J. and Powers, S. R. (1973) A mathematical model of mass transport in the lung. *Int. J. Engng Sci.* **11**, 625–635.

Gilliland, E. R., Baddour, R. F., Perkinson, G. P. and Sladek, K. J. (1974) Diffusion on surfaces. I. Effect of concentration on the diffusivity of physically adsorbed gases. *Ind. Engng Chem. Fundam.* **13**, 95–100.

Glasscock, D. A. and Rochelle, G. T. (1989) Numerical simulation of theories for gas absorption with chemical reaction. *A.I.Ch.E. J.* **35**, 1271–1281.

Gorak, A. (1991) *Berechnungsmethoden der Mehrstoffrektifikation—Theorie und Anwendungen.* Habilitationsschrift, RWTH Aachen, Germany.

Gorak, A. (1995) Simulation thermischer Trennverfahren fluider Vielkomponentengemische. In *Prozeßsimulation*, ed. H. Schuler, pp. 349–408. VCH Verlagsgesellshaft mbH, Weinheim, Germany.

Graham, E. E. and Dranoff, J. S. (1982) Application of the Stefan–Maxwell equations to diffusion in ion exchangers. *Ind. Engng Chem. Fundam.* **21**, 360–369.

Grenier, P. (1966) Solvent counter-diffusion in gas absorption. *Canad. J. Chem. Engng* **44**, 213–216.

Grimshaw, P. E., Grodzinsky, A. J., Yarmushm, M. L. and Yarmush, D. M. (1990) Selective augmentation of macromolecular transport in gels by electrodiffusion and electrokinetics. *Chem. Engng Sci.* **45**, 2917–2929.

Gutsche, R. (1993) Concentration-dependent micropore diffusion analysed by measuring laboratory adsorber dynamics. *Chem. Engng Sci.* **48**, 3723–3742.

Haase, R. and Siry, M. (1968) Diffusion im kritischen Entmischungsgebiet binärer flüssiger Systeme. *Phys. Chem. Neue Folge* **57**, 56–73.

Habgood, H. W. (1958) The kinetics of molecular sieve action. Sorption of nitrogen–methane mixtures by Linde molecular sieve 4A. *Canad. J. Chem.* **36**, 1384–1397.

von Halle, E. (1980) The countercurrent gas centrifuge for the Enrichment of U-235, In *Recent Advances in Separation Techniques*—II. *A.I.Ch.E. Symp. Ser.* Vol. **76**, pp. 82–87. A.I.Ch.E., New York.

Haynes, H. W. (1978) Calculation of gas phase diffusion and reaction in heterogeneous catalysts. The importance of viscous flow. *Canad. J. Chem. Engng* **56**, 582–587.

Heintz, A. and Stephan, W. (1994) A generalized solution-diffusion model of the pervaporation process through composite membranes. *J. Membrane Sci.* **89**, 143–169.

Helfferich, F. (1962) Ion-exchange kinetics. III. Experimental test of the theory of particle-diffusion controlled ion exchange. *J. Phys. Chem.* **66**, 39–44.

Helfferich, F. (1983) Ion-exchange kinetics—Evolution of a theory. In *Mass Transfer and Kinetics of Ion Exchange*, eds. L. Liberti and F. G. Helfferich, NATO Advanced Study Institute Series E: Applied Sciences, No. 71. Martinus Nijhoff, The Hague.

Hindmarsh, A. C. and Johnson, S. H. (1988) Dynamic simulation of reversible solid–fluid reactions in nonisothermal porous spheres with Stefan–Maxwell diffusion. *Chem. Engng Sci.* **43**, 3235–3258.

Hirschfelder, J. O., Curtiss, C. F. and Bird, R. B. (1964) *Molecular Theory of Gases and Liquids* (2nd corrected printing). Wiley, New York, U.S.A.

Hite, R. H. and Jackson, R. (1977) Pressure gradients in porous catalyst pellets in the intermediate diffusion regime. *Chem. Engng Sci.* **32**, 703–709.

Hu, X., Do, D. D. and Yu, Q. (1992) Effects of supporting and buffer electrolytes (NaCl, CH_3COOH and NH_4OH) on the diffusion of BSA in porous media. *Chem. Engng Sci.* **47**, 151–164.

Jackson, R. (1977) *Transport in Porous Catalysts.* Elsevier, Amsterdam, The Netherlands.

Johansen, V., Jepsen, O. L., Christensen, N. H. and Gamborg Hansen, J. C. (1978) Ternary diffusion in cement clinker at 1500°C. *Cement Concrete Res.* **8**, 301–310.

Kapila, D. and Plawsky, J. L. (1995) Diffusion processes for integrated waveguide fabrication in glasses: a solid state electrochemical approach. *Chem. Engng Sci.* **50**, 2589–2600.

Kapoor, A., Krishnamurthy, K. R. and Shirley, A. (1993) Kinetic separation of carbon dioxide from hydrocarbons using carbon molecular sieve. *Gas Separation Purification* **7**, 259–263.

Kapoor, A. and Yang, R. T. (1989) Surface diffusion on energetically heterogeneous surfaces. *A.I.Ch.E. J.* **35**, 1735–1738.

Kapoor, A. and Yang, R. T. (1990) Surface diffusion on energetically heterogeneous surfaces. An effective medium approximation approach. *Chem. Engng Sci.* **45**, 3261–3270.

Kapoor, A. and Yang, R. T. (1991) Contribution of concentration-dependent surface diffusion to rate of adsorption. *Chem. Engng Sci.* **46**, 1995–2002.

Kapteijn, F., Bakker, W. J. W., van der Graaf, J., Zheng, G., Poppe, J. and Moulijn, J. A. (1995) Permeation and separation behaviour of a silicalite-1 membrane. *Catal. Today* **25**, 213–218.

Kapteijn, F., Bakker, W. J. W., Zheng, G., Poppe, J. and Moulijn, J. A. (1994) The temperature and occupancy dependent diffusion on *n*-butane through a silicalite membrane. *Microporous Mater.* **3**, 227–234.

Kärger, J. (1973) Some remarks on the straight and cross-coefficients in irreversible thermodynamics of surface flow and on the relation between diffusion and self diffusion. *Surf. Sci.* **36**, 797–801.

Kärger, J. and Bülow, M. (1975) Theoretical prediction of uptake behaviour in adsorption of binary gas mixtures using irreversible thermodynamics. *Chem. Engng Sci.* **30**, 893–896.

Kärger, J., Petzold, M., Pfeifer, H., Ernst, S. and Weitkamp, J. (1992) Single-file diffusion and reaction in zeolites. *J. Catal.* **136**, 283–299.

Kärger, J. and Ruthven, D. M. (1992) *Diffusion in Zeolites.* Wiley, New York, U.S.A.

Katti, S. (1995) Gas–liquid–solid systems: an industrial perspective. *Chem. Engng Res. Des. Trans. Ind Chem. Engng* Part A, **73**, 595–607.

Kaza, K. R. and Jackson, R. (1980) Diffusion and reaction of multicomponent gas mixtures in isothermal porous catalysts. *Chem. Engng Sci.* **35**, 1179–1197.

Kedem, O. and Katchalsky, A. (1961) A physical interpretation of the phenomenological coefficients in membrane permeability. *J. Gen. Physiol.* **45**, 143.

Keil, F. J. (1996) Modelling of phenomena within catalyst particles. *Chem. Engng Sci.* **51**, 1543–1567.

Kerkhof, P. J. A. M. (1996) A modified Maxwell–Stefan model for transport through inert membranes: the binary friction model. *Chem. Engng J.*

Keurentjes, J. T. F., Janssen, A. E. M., Broek, A. P., van der Padt, A., Wesselingh, J.A. and van "t Riet, K. (1992) Multicomponent diffusion in dialysis membrane. *Chem. Engng Sci.* **47**, 1963–1971.

King C. J. (1980) *Separation Processes*, 2nd Edn. McGraw-Hill, New York, U.S.A.

Kleijn, C. R. and Hoogendoorn, C. J. (1991) A study of 2- and 3-D transport phenomena in horizontal chemical vapor deposition reactors. *Chem. Engng Sci.* **46**, 321–334.

Kohl, A. L. and Riesenfeld, F. C. (1985) *Gas Purification.* 4th Edn, Gulf Publishing Co., TX, U.S.A.

Kouyoumdjiev, M. S., Vortsman, M. A. G. and Kerkhof, P. J. A. M. (1993) Single and multi-component adsorption from liquid phase on activated carbon in finite bath process. In *Precision Process Technology*, eds. M. P. C. Weijnen and A. A. H. Drinkenburg, pp. 257–266. Kluwer, Dordrecht, The Netherlands.

Kraaijeveld, G., Kuiken, G. D. C. and Wesselingh, J. A. (1994) Comments on "negative diffusion coefficients". *Ind. Engng Chem. Res.* **33**, 750–851.

Kraaijeveld, G., Sumberova, V., Kuindersma, S. and Wesselingh, J. A. (1995) Modelling electrodialysis using the Maxwell–Stefan description. *Chem. Engng J.* **57**, 163–176.

Kraaijeveld, G. and Wesselingh, J. A. (1993a) The kinetics of film diffusion limited ion exchange. *Chem. Engng Sci.* **48**, 467–473.

Kraaijeveld, G. and Wesselingh, J. A. (1993b) Negative Maxwell–Stefan diffusion coeffficients. *Ind. Engng Chem. Res.* **32**, 738–742.

Krishna, R. and Standart, G. (1976) A multicomponent film model incorporating an exact matrix method of solution to the Maxwell–Stefan equations. *A.I.Ch.E. J.* **22**, 383–389.

Krishna, R. (1977a) A generalized film model for mass transfer in non-ideal fluid mixtures. *Chem. Engng Sci.* **32**, 659–667.

Krishna, R. (1977b) A film model analysis of non-equimolar distillation of multicomponent mixtures. *Chem. Engng Sci.* **32**, 1197–1203.

Krishna, R. (1978a) A note on the film and penetration models for multicomponent mass transfer. *Chem. Engng Sci.* **33**, 765–767.

Krishna, R. (1978b) Penetration depths in multicomponent mass transfer. *Chem. Engng Sci.* **33**, 1495–1497.

Krishna, R. (1979) A simplified film model description of multicomponent interphase mass transfer. *Chem. Engng Commun.* **3**, 29–39.

Krishna, R. (1981a) Ternary mass transfer in a wetted-wall column—significance of diffusional interactions. I—Stefan diffusion. *Trans. Ind. Chem. Engng* **59**, 35–43.

Krishna, R. (1982) A turbulent film model for multicomponent mass transfer. *Chem. Engng J.* **24**, 163–172.

Krishna, R. (1987) Diffusion in multicomponent electrolyte systems. *Chem. Engng J.* **35**, 19–24.

Krishna, R. (1989) Comments on "Simulation and optimization of an industrial ammonia reactor". *Ind. Engng Chem. Res.* **28**, 1266.

Krishna, R. (1990) Multicomponent surface diffusion of adsorbed species. A description based on the generalized Maxwell–Stefan diffusion equations. *Chem. Engng Sci.* **45**, 1779–1791.

Krishna, R. (1993a) Problems and pitfalls in the use of the Fick formulation for intraparticle diffusion. *Chem. Engng Sci.* **48**, 845–861.

Krishna, R. (1993b) A unified approach to the modelling of intraparticle diffusion in adsorption processes. *Gas Separation Purification* **7**, 91–104.

Krishna, R. and van den Broeke, L. J. P. (1995) The Maxwell–Stefan description of mass transport across zeolite membranes. *Chem. Engng J.* **57**, 155–162.

Krishna, R., Low, C. Y., Newsham, D. M. T., Olivera-Fuentas, C. G. and Standart, G. L. (1985) Ternary mass transfer in liquid–liquid extraction. *Chem. Engng Sci.* **40**, 893–903.

Krishna, R., Salomo, R. M. and Rahman, M. A. (1981b) Ternary mass transfer in a wetted wall column. Significance of diffusional interactions. Part II. Equimolar diffusion. *Trans. Ind. Chem. Engng* **59**, 44–53.

Krishnamurthy, R. and Taylor, R. (1985a) Non-equilibrium stage model of multicomponent separation processes. *A.I.Ch.E. J.* **32**, 449–465.

Krishnamurthy, R. and Taylor, R. (1985b) Simulation of packed distillation and absorption columns. *Ind. Engng Chem. Process Des. Dev.* **24**, 513–524.

Kuijlaars, K. J., Kleijn, C. R. and van den Akker, H. E. A. (1995) Multicomponent diffusion phenomena in multiple wafer chemical vapour deposition reactors. *Chem. Engng J.* **57**, 127–136.

Kuijlaars, K. J. (1996) Modelling of transport phenomena and chemistry in chemical vapour deposition reactors. Ph.D. thesis, Delft University of Technology, Delft, The Netherlands.

Kuiken, G. D. C. (1994) *Thermodynamics of Irreversible Processes: Applications to Diffusion and Rheology.* Wiley, Chichester, U.K.

Lakshminarayaniah, N. (1969) *Transport Phenomena in Membranes.* Academic Press, New York, U.S.A.

Lao, M. and Taylor, R. (1994) Modelling mass transfer in three-phase distillation. *Ind. Engng Chem. Res.* **33**, 2637–2650.

Lee, H. L., Lightfoot, E. N., Reis, J. F. G. and Waissbluth, M. D. (1977) The systematic description and development of separations processes. In *Recent Developments in Separation Science*, Vol. III, Part A, ed. N. N. Li, pp. 1–69. CRC Press, Cleveland, OH, U.S.A.

Lightfoot, E. N. (1974) *Transport Phenomena and Living Systems.* McGraw-Hill, New York, U.S.A.

Littel, R. J., Filmer, B., Versteeg, G. F. and van Swaaij, W. P. M. (1991) Modelling of simultaneous absorption of H_2S and CO_2 in alkanolamine solutions: The influence of parallel and consecutive reversible reactions and the coupled diffusion of ionic species. *Chem. Engng Sci.* **46**, 2303–2313.

Lo, P. Y. and Myerson, A. S. (1989) Ternary diffusion coefficients in metastable solutions of glycine–valine–H_2O. *A.I.Ch.E. J.* **35**, 676–678.

Löwe, A. and Bub, G. (1976) Multiple steady states for isothermal catalytic gas–solid reactions with a positive reaction order. *Chem. Engng Sci.* **31**, 175–178.

McDowell, J. K. and Davis, J. F. (1988) A characterization of diffusion distillation for azeotropic separation. *Ind. Engng Chem. Res.* **27**, 2139–2148.

MacElroy, J. M. D. and Kelly, J. J. (1985) Hindered diffusion of gases in 'leaky' membranes using the dusty gas model. *A.I.Ch.E. J.* **31**, 35–44.

Martinez, J. and Setterwall, F. (1991) Gas-phase controlled convective drying of solids wetted with multicomponent liquid mixtures. *Chem. Engng Sci.* **46**, 2235–2252.

Mason, E. A. and del Castillo, L. F. (1985) The role of viscous flow in theories of membrane transport. *J. Membrane Sci.* **23**, 199–220.

Mason, E. A. and Lonsdale, H. K. (1990) Statistical mechanical theory of membrane transport. *J. Membrane Sci.* **51**, 1–81.

Mason, E. A. and Malinauskas, A. P. (1983) *Gas Transport in Porous Media: The Dusty Gas Model.* Elsevier, Amsterdam, The Netherlands.

Mason, E. A. and Viehland, L. A. (1978) Statistical mechanical theory of membrane transport for multicomponent systems: Passive transport through open membranes. *J. Chem. Phys.* **68**, 3562–3573.

Matsuoka, M. and Garside, J. (1991) Non-isothermal effectiveness factors and the role of heat transfer in crystal growth from solutions and melts. *Chem. Engng Sci.* **46**, 183–192.

Maxwell, J. C. 1866. On the dynamical theory of gases. *Phil. Trans. R. Soc.* **157**, 49–88.

Meerdink, G. and van 't Riet, K. (1993) Modeling segregation of solute material during drying of food liquids. *A.I.Ch.E. J.* **41**, 732–736.

Mehta, G. D., Morse, T. F., Mason, E. A. and Daneshpajooh, M. H. (1976) Generalized Nernst–Planck and Stefan–Maxwell equations for membrane transport. *J. Chem. Phys.* **64**, 3917–3923.

Mikami, H. (1970) Separation of a three-component gas mixture in an axisymmetric supersonic jet. *Ind. Engng Chem. Fundam.* **9**, 121–128.

Modell, H. I. and Farhi, L. E. (1976) Ternary gas diffusion—*in vitro* studies. *Respir. Physiol.* **27**, 65–71.

Modine, A. D. (1963) Ternary mass transfer. Ph.D. thesis, Carnegie Institute of Technology, Pittsburgh, PA, U.S.A.

Moore, R. M. and Katzer, J. R. (1972) Counterdiffusion of liquid hydrocarbons in Type Y zeolite: effect of molecular size, molecular type, and direction of diffusion. *A.I.Ch.E. J.* **18**, 816–824.

Mulder, M. (1991) *Basic Principles of Membrane Technology.* Kluwer Academic Press, Dordrecht, The Netherlands.

Muralidhara, H. S. (1994) Enhance separations with electricity. *Chemtech* **24**, 36–41.

Newman, J. (1991) *Electrochemical Systems.* 2nd Edn. Prentice-Hall, Englewood Cliffs, NJ, U.S.A.

Newman, J. (1995) Thermoelectric effects in electrochemical systems. *Ind. Engng Chem. Res.* **34**, 3208–3216.

Niessen, W. (1991) Untersuchungen zur Diffusion und Gegendiffusion in Zeolithen mit Hilfe der FTIR-Spectroskopie. Ph.D. thesis, Fritz Haber Institut der Max Planck Gesellschaft, Berlin, Germany.

van Oers, C. W. (1994) Solute rejection in multicomponent systems during ultrafiltration. Ph.D. thesis, Eindhoven University of Technology, Eindhoven, The Netherlands.

Ofori, J. Y. and Sotirchos, S. V. (1996) Multicomponent mass transport in chemical vapor infiltration. *Ind. Engng Chem. Res.* **35**, 1275–1287.

Okubo, T. and Inoue, H. (1988) Improvement of surface transport property by surface modification. *A.I.Ch.E. J.* **34**, 1031–1033.

Olano, S., Nagura, S., Kosuge, H. and Asano, K. (1995) Mass transfer in binary and ternary distillation by a packed column with structured packing. *J. Chem. Engng Japan* **28**, 750–757.

Othmer, H. G. and Scriven, L. E. (1969) Interactions of reaction and diffusion in open systems. *Ind. Engng Chem. Fundam.* **8**, 302–313.

Palekar, M. G. and Rajadhyaksha, R. A. (1985) Sorption in zeolites—I. Sorption of single component and binary sorbate systems. *Chem. Engng Sci.* **40**, 1085–1091.

Palekar, M. G. and Rajadhyaksha, R. A. (1986) Sorption in zeolites—III. Binary sorption. *Chem. Engng Sci.* **41**, 463–468.

Peppas, N. A. and Meadows, D. L. (1983) Macromolecular structure and solute diffusion in membranes: An overview of recent theories. *J. Membrane Sci.* **16**, 361–377.

Pertler, M., Blass, E. and Stevens, G. W. (1996) Fickian diffusion in binary mixtures that form two liquid phases. *A.I.Ch.E. J.* **42**, 910–920.

Pinto, N. G. and Graham, E. E. (1986) Estimation of diffusivities in electrolyte solutions using Stefan–Maxwell equations. *A.I.Ch.E. J.* **32**, 291–296.

Pinto, N. G. and Graham, E. E. (1987a) Multicomponent diffusion in concentrated electrolyte solutions: effect of solvation. *A.I.Ch.E. J.* **33**, 436–443.

Pinto, N. G. and Graham, E. E. (1987b) Characterization of ionic diffusivities in ion-exchange resins. *Ind. Engng Chem. Res.* **26**, 2331–2336.

Ptasinski, K. J. and Kerkhof, P. J. A. M. (1992) Electric field driven separations: phenomena and applications. *Sep. Sci. Technol.* **27**, 995–1021.

Qureshi, W. R. and Wei, J. (1990) One- and two-component diffusion in zeolite ZSM-5. *J. Catal.* **126**, 126–172.

Raal, J. D. and Khurana, M. K. (1973) Gas absorption with large heat effects in packed columns. *Canad. J. Chem. Eng.* **51**, 162–167.

Rao, M. B. and Sircar, S. (1993) Nanoporous carbon membrane for gas separation. *Gas Separation Purification* **7**, 279–284.

Reddy, K. V . and Murty, C. V. S. (1995) A methodology for the *a priori* selection of catalyst particle models. *Ind. Engng Chem. Res.* **34**, 468–473.

Reed, D. A. and Ehrlich, G. (1981a) Surface diffusion, atomic jump rates and thermodynamics. *Surf. Sci.* **102**, 588–609.

Reed, D. A. and Ehrlich, G. (1981b) Surface diffusivity and the time correlation of concentration fluctuations. *Surf. Sci.* **105**, 603–628.

Reid, R. C., Prausnitz, J. M. and Poling, B. (1987) *The Properties of Gases and Liquids.* 4th Edn. McGraw-Hill, New York, U.S.A.

Reinhardt, D. and Dialer, K. (1981) Geometrical relationships for ternary gas diffusion balances and criteria for multicomponent phenomena. *Chem. Engng Sci.* **36**, 1557–1566.

Remick, R. R. and Geankoplis, C. J. (1974) Ternary diffusion of gases in capillaries in the transition region between Knudsen and molecular diffusion. *Chem. Engng Sci.* **29**, 1447–1455.

Riede, Th. and Schlünder, E. U. (1990a) Selective evaporation of a binary mixture into dry or humidified air. *Chem. Engng Process.* **27**, 83–93.

Riede, Th. and Schlünder, E. U. (1990b) Selective evaporation of a ternary mixture containing one nonvolatile component with regard to drying processes. *Chem. Engng Process.* **28**, 151–163.

Riekert, L. (1971) Rates of sorption and diffusion of hydrocarbons in zeolites. *A.I.Ch.E. J.* **17**, 446–454.

Robertson, B. C. and Zydney, A. L. (1988) A Stefan–Maxwell analysis of protein transport in porous membranes. *Sep. Sci. Technol.* **23**, 1799–1811.

Ronge, G. (1995) Überprüfung unterschiedelicher Modelle für den Stoffaustausch bei der Rektifikation in Packungskolonnen. Fortschritt-Berichte VDI Verfahrenstechnik No. 390, Düsseldorf.

Round, G. F., Habgood, H. W. and Newton, R. (1966) A numerical analysis of surface diffusion in a binary adsorbed film. *Separ. Sci.* **1**, 219–244.

Ruthven, D. M. (1984) *Principles of Adsorption and Adsorption Processes.* Wiley, New York. U.S.A.

Ruthven, D. M., Farooq, S. and Knaebel, K. S. (1994) *Pressure Swing Adsorption*, VCH Publishers, New York, U.S.A.

Scattergood, E. M. and Lightfoot, E. N. (1968) Diffusional interaction in an ion-exchange membrane. *Trans. Faraday Soc.* **64**, 1135–1143.

Schneider, P. (1975) Intraparticle diffusion in multicomponent catalytic reactions. *Catal. Rev. — Sci. Engng* **12**, 201–278.

Schnitzlein, K. and Hofmann, H. (1988) Solving the pellet problem for multicomponent mass transport and complex reactions. *Comput. Chem. Engng* **12**, 1157–1161.

Seader, J. D. (1989) The rate-based approach for modeling staged separations. *Chem. Engng Prog.* **85**, 41–49.

Seidel, A. and Carl, P. S. (1989) The concentration dependence of surface diffusion for adsorption on energetically heterogeneous adsorbents. *Chem. Engng Sci.* **44**, 189–194.

Sentarli, I. and Hortaçsu, A. (1987) Solution of the linearized equations of multicomponent mass transfer with chemical reaction and convection for a film model, *Ind. Engng Chem. Res.* **26**, 2409–2413.

Shaeiwitz, J. A. (1984) Coupled boundary layer transport involving particles. *A.I.Ch.E. J.* **30**, 310–316.

Shaeiwitz, J. A. and Lechnick, W. J. (1984) Ternary diffusion formulation for diffusiophoresis. *Chem. Engng Sci.* **39**, 799–807.

Sherwood, T. K., Pigford, R. L. and Wilke, C. R. (1975) *Mass Transfer.* McGraw-Hill, New York, U.S.A.

Sikavitsas, V. I. and Yang, R. T. (1995) Predicting multicomponent diffusivities for diffusion on surfaces and in molecular sieves with energy heterogeneity. *Chem. Engng Sci.* **50**, 3057–3065.

Sloot, H. J. (1991) A non-permselective membrane reactor for catalytic gas phase reactions. Ph.D. thesis, University of Twente, Enschede, The Netherlands.

Smit, J. A. M, Eijsermans, J. C. and Staverman, A. J. (1975) Friction and partition in membranes. *J. Phys. Chem.* **79**, 2168–2175.

Smith, T. G. and Dranoff, J. S. (1964) Film diffusion-controlled kinetics in binary ion exchange. *Ind. Engng Chem. Fundam.* **3**, 195–200.

Spiegler, K. S. (1958) Transport processes in ionic membranes. *Trans. Faraday Soc.* **54**, 1408–1428.

Srinivasan, R., Auvil, S. R. and Burban, P. M. (1994) Eluciditating the mechanism(s) of gas transport in poly[1-(trimethylsilyl)-1-propyne] (PTMSP) membranes. *J. Membrane Sci.* **86**, 67–86.

Srinivasan, R., Auvil, S. R. and Schork, J. M. (1995) Mass transfer kinetic in carbon molecular sieves—an interpretation of "Langmuir kinetics". *Chem. Engng J.* **57**, 137–144.

Sotirchos, S. V. (1991) Dynamic modeling of chemical vapor infiltration. *A.I.Ch.E. J.* **37**, 1365–1378.

Sotirchos, S. V. and Burganos, V. N. (1988) Analysis of multicomponent diffusion in pore networks. *A.I.Ch.E. J.* **34**, 1106–1118.

Standart, G. L., Taylor, R. and Krishna, R. (1979) The Maxwell–Stefan formulation of irreversible thermodynamics for simultaneous heat and mass transfer. *Chem. Engng Commun.* **3**, 277–289.

Stefan, J. (1871) Über das Gleichgewicht und die Bewegung insbesondere die Diffusion von Gasgemengen. *Sitzber. Akad. Wiss. Wien.* **63**, 63–124.

Stichlmair, J., Schmidt, J. and Proplech, R. (1992) Electroextraction: a novel separation technique. *Chem. Engng Sci.* **47**, 3015–3022.

von Stockar, U. and Wilke, C. R. (1977) Rigorous and short-cut design calculations for gas absorption involving large heat effects. *Ind. Engng Chem. Fundam.* **16**, 88–103.

Sundaresan, S. and Hall, C. K. (1986) Mathematical modelling of diffusion and reaction in blocked zeolite catalysis. *Chem. Engng Sci.* **41**, 1631–1645.

Sundelöf, L.-O. (1979) Diffusion in macromolecular solutions. *Ber. Bunsenges. Phys. Chem.* **83**, 329–342.

Sundmacher, K. and Hoffmann, U. (1994a) Macrokinetic analysis of MTBE synthesis in chemical potentials. *Chem. Engng Sci.* **49**, 3077–3089.

Sundmacher, K. and Hoffmann, U. (1994b) Multicomponent mass and energy transport on different length scales in a packed distillation column for heterogeneously catalysed fuel ether production. *Chem. Engng Sci.* **49**, 4443–4464.

Tai, R. C. and Chang, H.-K. (1979) A mathematical study of non-equimolar ternary gas diffusion. *Bull. Math. Biol.* **41**, 591–606.

Theodorou, D. and Wei, J. (1983) Diffusion and reaction in blocked and high occupancy zeolite catalysis. *J. Catal.* **83**, 205–224.

Taylor, R. and Krishna, R. (1993) *Multicomponent Mass Transfer*. Wiley, New York, U.S.A.

Taylor, R., Krishnamurthy, R., Furno, J. S. and Krishna, R. (1986) Condensation of vapor mixtures. I. A mathematical model and a design method. *Ind. Engng Chem. Process Des. Dev.* **5**, 83–97.

Taylor, R. and Lucia, A. (1995) Modeling and analysis of multicomponent separation processes. *A.I.Ch.E. Symp. Ser. 304* **91**, 19–28. A.I.Ch.E., New York.

Toor, H. L. (1957) Diffusion in three component gas mixtures. *A.I.Ch.E. J.* **3**, 198–207.

Tsikoyiannis, J. G. and Wei, J. (1991) Diffusion and reaction in high-occupancy zeolite catalysts—I. A stochastic theory. *Chem. Engng Sci.* **46**, 233–253.

Tunison, M. E. and Chapman, T. W. (1976) The effect of a diffusion potential on the rate of liquid–liquid ion exchange. *Ind. Engng Chem. Fundam.* **15**, 196–201.

Tuohey, P. G., Pratt, H. R. C. and Yost, R. S. (1982) Binary and ternary distillation in a stirred mass transfer cell. *Chem. Engng Sci.* **37**, 1741–1750.

Umino, S. and Newman, J. (1993) Diffusion of sulfuric acid in concentrated solutions. *J. Electrochem. Soc.* **140**, 2217–2221.

Ünal, A. (1987) Gaseous mass transport in porous media through a stagnant gas. *Ind. Engng Chem. Res.* **26**, 72–77.

Valerio, S. and Vanni, M. (1994) Interfacial mass transfer and chemical reaction in non-ideal multicomponent systems. *Chem. Engng Sci.* **49**, 3297–3305.

Vanni, M., Valerio, S. and Baldi, G. (1995) The role of non-ideal phenomena in interfacial mass transfer with chemical reaction. *Chem. Engng J.* **57**, 205–217.

Varshneya, A. K. and Cooper, A. R. (1968) Diffusion in the system K_2O–SrO–SiO_2: III, interdiffusion coefficients. *J. Am. Chem. Soc.* **55**, 312–317.

Veldsink, J. W., van Damme, R. M. J., Versteeg, G. F. and van Swaaij, W. P. M. (1995) The use of the dusty gas model for the description of mass transport with chemical reaction in porous media. *Chem. Engng J.* **57**, 115–125.

Vignes, A. (1966) Diffusion in binary solutions. *Ind. Engng Chem. Fundam.* **5**, 189–199.

Vinograd, J. R. and McBain, J. W. (1941) Diffusion of electrolytes and ions in their mixtures. *J. Am. Chem. Soc.* **63**, 2008–2015.

Vitagliano, V., Sartorio, R., Scala, S. and Spaduzzi, D. (1978) Difffusion in a ternary system and the critical mixing point. *J. Solution Chem.* **7**, 605–621.

Vogelpohl, A. (1979) Murphree efficiencies in multicomponent systems. *Institution of Chem. Engng Symp. Ser. 56* **79**, 2.1, 25–31. I. Chem. E., Rugby, U.K.

Voight, W. (1982) Status and plans of the DOE uranium enrichment program. *A.I.Ch.E. Symp. Ser.* **78**, 1–9. A.I.Ch.E., New York.

Vonk, P. (1994) Diffusion of large molecules in porous structures. Ph. D. Thesis, University of Groningen, Groningen, The Netherlands.

Ward, C. E. and Russel, W. B. (1981) On the short-residence time hydropyrolysis of single coal particles: the effect of unequal diffusivities. *A.I.Ch.E. J.* **27**, 859–861.

Wei, J. (1994) Nonlinear phenomena in zeolite diffusion and reaction. *Ind. Engng Chem. Res.* **33**, 2467–2472.

Wesselingh, J. A., Kraaijeveld, G. and Vonk, P. (1995) Exploring the Maxwell–Stefan description of ion exchange. *Chem. Engng J.* **57**, 75–89.

Wesselingh, J. A. and Krishna, R. (1990. *Mass Transfer*. Ellis Horwood, Chichester, U.K.

Wijmans, J. G. and Baker, R. W. (1995) The solution-diffusion model: a review. *J. Membrane Sci.* **107**, 1–21.

Wilke, C. R. (1950) Diffusional properties of multicomponent gases. *Chem. Engng Prog.* **46**, 95–104.

Wills, G. B. and Lightfoot, E. N. (1966) Transport phenomena in ion exchange membranes. *Ind. Engng Chem. Fundam.* **5**, 114–120.

Wong, R. L. and Denny, V. E. (1975) Diffusion, flow and heterogeneous reaction of ternary mixtures in porous catalytic media. *Chem. Engng Sci.* **30**, 709–716.

Worth, H. and Piiper, J. (1978) Diffusion of helium, carbon dioxide, and sulfur hexafluoride in gas mixtures similar to alveolar gas. *Respir. Physiol.* **32**, 155–166.

Wright, P. G. (1972) Remarks on the Stefan–Maxwell equations for diffusion in a dusty gas. *J. Chem. Soc. Faraday. Trans.* **68**, 1951–1954.

Xiao, J. and Wei, J. (1992) Diffusion mechanism of hydrocarbons in zeolites. *Chem. Engng Sci.* **47**, 1123–1141.

Yang, R. T. (1987) *Gas Separation by Adsorption Processes*. Butterworth, Boston, U.S.A.

Yang, R. T., Chen, Y. D. and Yeh, Y. T. (1991) Predictions of cross-term coefficients in binary diffusion: diffusion in zeolite. *Chem. Engng Sci.* **46**, 3089–3099.

Yoshida, H. and Kataoka, T. (1985) Migration of two ions during electrolysis of glass wave guide. *J. Appl. Phys.* **58**, 1739–1743.

Yu, W.-C. and Astarita, G. (1987) Design of packed towers for selective chemical absorption. *Chem. Engng Sci.* **42**, 425–433.

Zarzycki, R. and Chacuk, A. (1993) *Absorption: Fundamentals and Applications.* Pergamon Press, Oxford, U.K.

Zhdanov, V. P. (1985) General equations for description of surface diffusion in the framework of the lattice gas model. *Surf. Sci.* **194**, L13–L17.

Zimmerman, A., Joulia, X., Gourdon, C. and Gorak, A. (1995) Maxwell–Stefan approach in extractor design. *Chem. Engng J.* **57**, 229–236.

Zgrablich, G., Pereyra, V., Ponzi, M. and Marchese, J. (1986) Connectivity effects for surface diffusion of adsorbed gases. *A.I.Ch.E. J.* **32**, 1158–1168.